Novel DyP-type Peroxidases from Actinobacteria: A Genome Mining Approach

Juandré Groep

UNIVERSITY *of the*
WESTERN CAPE

A thesis submitted in partial fulfilment of the requirements for the degree *Magister Scientiae* in the Department of Biotechnology, University of the Western Cape

Supervisors

Associate Professor Marilize Le Roes-Hill
Cape Peninsula University of Technology

Associate Professor Bronwyn Kirby-McCullough
University of the Western Cape

March 2024

ABSTRACT

Twenty-one whole genome actinobacterial sequences were obtained from strains previously isolated from various environments. A genome-mining approach was applied to identify the presence of Dye-decolourising (DyP-type or DyPs) peroxidases. From genome sequence annotation twenty-six DyP-type sequences were identified and through bioinformatic analysis for the presence of twin-arginine translocation (Tat) pathway signal peptides, was classified as belonging to class I (formerly class A) bacterial DyP-type peroxidases. Phylogenetic analysis of the DyP sequences showed that the *Streptomyces* derived DyPs were predominantly grouping together and the non-*Streptomyces* derived DyPs followed the same pattern. Eight DyP-type peroxidases were selected for cloning, with the majority being derived from *Streptomyces* spp., and primers were designed to amplify the DyP-type peroxidase genes. The PCR-amplicons were subjected to restriction digests and were ligated into pET20b(+). The constructs were transformed into *Escherichia coli* JM109. Only two of the constructs were successfully transformed: the DyP-type peroxidase genes from *Nocardia gamkensis* CZH20^{T} and *Micromonospora* sp. strain 30-1. Further analysis using T7-primers confirmed sequence identity of the constructs. The optimal expression host and media with the highest concentration of proteins detected was with ArcticExpress RP in Auto Induction media. The expressed proteins were purified using fast performance liquid chromatography and sizes confirmed via SDS-PAGE to be 44 kDa and 41 kDa, respectively for the CZH20-DyP and the 30-1-DyP. However, only purified and partially purified functional proteins were obtained for the CZH20-DyP transformant. Biochemical characterisation of the purified and partially purified CZH20-DyP showed that the enzyme shows functionality across a broad pH range, with a temperature optimum for the oxidation of the 2,4-dichlorophenol (2,4-DCP) substrate at 35 °C. The majority of the enzyme inhibitors, reducing agents and metal ions used in this study inhibited the oxidation of 2,4-DCP at low concentrations (≤2 mM), while the metal ions, copper and zinc, increased residual activity of the CZH20-DyP. Remarkably, the CZH20-DyP showed great tolerance to sodium azide and zinc which has not been reported in literature before. Enzyme kinetics parameters were determined for the purified and partially purified CZH20-DyP, with the K_m values determined as 29.17 and 36.44 mM, respectively and V_{max} values of 142 nmol/mg/protein.min and 155 nmol/mg/protein.min, respectively. Decolourisation of azo, anthraquinone and thiazine dyes was successful with, as literature suggests, the affinity to anthaquinone with the

highest rate of dye decolourisation at 39% and 42% for the purified and partially purified CZH20-DyP. Future studies will further explore the biochemical and structural properties of the enzyme, as well as other potential applications such as lignocellulose degradation and cross-coupling reactions.

Keywords: Actinobacteria, peroxidase, Dye-decolourising peroxidase, DyP-type, 2,4-DCP, decolourisation, anthraquinone dye

LIST OF ABBREVIATIONS

Terms/Acronyms/ Abbreviations	Definition/Explanation
ABTS	2,2'-azinobis (3-ethylbenzothiazoline-6-sulfonic acid)
ALA	5-aminolevulinic acid
BOD	Biological Oxidation Demand
BSA	Bovine serum albumin
$CaSO_4$	Calcium sufate
$CoSO_4$	Cobalt sulfate
$CuCl_2$	Copper chloride
dH_2O	Distilled water
DNA	Deoxyribonucleic Acid
2,4-DCP	2,4-Dichlorophenol
2,6-DMP	2,6-dimethoxyphenol
DMSO	Dimethyl sulfoxide
DyP/DyP-tye	Dye decoloursing peroxidases
E. coli	*Escherichia coli*
EtOH	Ethanol
EDTA	Ethylenediaminetetraacetic acid
$FeCl_2$	Iron chloride
FPLC	Fast performance liquid chromatography
HMM	Hidden Markov Model
HRP	Horseradish peroxidase
H_2O_2	Hydrogen peroxide
IPTG	Isopropyl-β-D-1-thiogalactopyranoside
kDa	Kilodalton
MeOH	Methanol
$MgCl_2$	Magnesium chloride
$MnCl_2$	Manganese chloride+
NGS	Next Generation Sequence
SDS-PAGE	Sodium dodecyl sulphate-polyacrylamide gel electrophoresis
SNF	Supernatant fluid
rpm	Revolutions per minute
$ZnCl_2$	Zinc chloride

DECLARATION

I declare that "*Novel DyP-type Peroxidases from Actinobacteria: A Genome Mining Approach*" is my own work, that it has not been submitted for any degree or examination in any other university, and that all the sources I have used or quoted have been indicated or acknowledged by complete references.

Full Name: Juandré Groep Date: March 2024

Signed: 

ACKNOWLEDGEMENTS

I would like to acknowledge the following persons:

- Prof. Marilize Le Roes-Hill – No words can describe how thankful I am to have l learned and grown as a scientist in your lab. Thank you for your patience, understanding and the ability to teach without even knowing that you're doing it. Your passion and dedication for science will always be inspiring.
- Prof. Bronwyn Kirby – thank you for peaking my interest in undergrad to the wonders of microbiology and marking my exam papers when I wrote just below the line. I am eternally grateful to you.
- To Mr Alaric Prins – Thank you for being an amazing colleague that has taught me so much in laboratories stretching continents. I am grateful that with all this time spent in the lab with you, you have become more than a colleague but a valued friend, I appreciate you.
- To my BTB Research group, thank you for accepting me and creating a space for growth and making every day exciting to come to the labs.
- To my mother, a self-sacrificing independent woman. I continue and will always look up to you and I hope I always make you proud. Thank you for unconditional love and support.
- To my family that always ask "how's classes going?" even though I have mentioned continuously that I do not have any with my master's studies. I appreciate the love and support you have given me through the years
- To my friends who root for me no matter how different our journeys have gone after undergrad, thank you always being there with unconditional love and support.
- To the Man above, every silent fear, prayer and hope through the throws of laboratory work, thank you for hearing me God.
- To the National Research Foundation for the financial assistance towards the research for this study.

Research Output(s)

2022

Annual AMHBI Biotechnology Research Symposium

07 September 2022, hosted by Prof JL Marnewick and A/Prof M Le Roes-Hill

Hybrid event – CPUT Hotel School/MS Teams

2020

Bioinformatics Workshop *sponsored by DIPLOMICS

Presented by Prof. David Tabb, Stellenbosch University

2019

Research Exchange – Fraunhofer Institute hosted by Prof. Dr. Volker Sieber

Straubing, Germany

Two-month NRF-funded Research Exchange working on the cloning of hybrid expansin constructs.

LIST OF FIGURES

LIST OF TABLES

TABLE OF CONTENTS

CHAPTER ONE
INTRODUCTION

1.1 Background

The textile industry remains one of the largest producers of polluted effluent due to the increasingly high quantity of water used in the dyeing process (Pagga and Brown, 1986). The wastewater, containing these dyes, present both an incredible health risk to the public as well as the ecosystems it is released into (Eaton and Clesceri, 1995). From the textile industries, the majority of the liquid effluent and solid waste have been treated by well-established physical and chemical methods and although these methods are applied across the industry, it remains difficult to treat and remediate these hazardous effluents due to high biological oxidation demand (BOD), pH and the difficulties associated with the post-production sludge, to mention a few (Asad *et al.*, 2007; Bell *et al.*, 2000). An alternative approach to alleviate these issues is through eco-friendly methods that remediate polluted environments by means of using various microbial species (Kidd *et al.*, 2009). This biological approach has better flexibility as they comprise of living systems that are able to perform intricate reactions relating to bioremediation through the degradation of organic pollutants and changing inorganic compounds into non-toxic products (Chen *et al.,* 2015b; Lui *et al.,* 2015).

Actinobacteria have been recognised for their diverse functions and the production of a plethora of extracellular enzymes (Chater *et al.,* 2010). Amongst microbial species, actinobacteria have also been widely described as possible bioremediation mediators (Nzila *et al.*, 2016). Actinobacteria isolated from various environments have the potential to be a resource for new enzymes and thus searching for actinobacterial enzymes from these environments, either through functional screening or data mining may be a practical approach in identifying novel enzymes (Lima and Porto, 2016; Suriya *et al.,* 2016). Recently, the data mining approach has become a prevalent method for enzyme discovery due to the increase in enzyme databases as well as the accessibility to computational tools (Wiltschi *et al.*, 2020; Lobb and Doxey, 2016). Furthermore, an advantage of using data mining is the identification of new enzymes through a large set

of genomic data without dealing with intensive and somewhat laborious functional screening processes (Lee *et al*., 2010).

One extracellular enzyme in particular produced by actinobacteria are dye-decolourising peroxidases, also known as DyP-type or DyPs (Savelli *et al.,* 2019). DyP-type peroxidases have been identified to oxidise numerous anthraquinone dyes in the presence of hydrogen peroxide, hence the name of dye-decolourising peroxidase was given. Originally, DyPs were identified from a culture of a basidiomycete (fungus), however more recently bacterial DyPs have been identified in species of Proteobacteria as well as Actinobacteria (Rahmanpour *et al.,* 2016; Faraco *et al.,* 2007; Kim and Shoda, 1999). DyP-type peroxidases were formerly classified into four subfamilies (A-D) according to their sequence alignment. However, advances made by Yoshida and Sugano have now classified DyPs according to their sequence-structure information which are now identified as class P (primitive), class I (intermediate) and class V (advanced) (Savelli *et al.,* 2019; Yoshida and Sugano, 2015). The main function of DyPs remain yet to be fully classified and understood, however these enzymes have the potential to be applied as biocatalysts, e.g., in the biotransformation of biomaterials in an environment due to their dye-decolourising and lignin degradation activities identified in some characterised DyPs, in particular those identified from Actinobacteria (Catucci *et al.,* 2020; Colpa *et al.,* 2014).

Thus, the aim of this study was to use a genome-mining approach to identify dye-decolourising peroxidases isolated from actinobacteria from various environments and to biochemically characterise this group of peroxidases. This was achieved through the following objectives:

- Identifying DyP-type genes from genome sequences of selected actinobacterial strains
- Designing primers which target the DyP-type genes, cloning of the genes and transforming the constructs into recombinant hosts followed by heterologous expression
- Purification of the expressed DyP-type peroxidases
- Biochemical characterisation of the DyP-type peroxidases

In the following chapters, the Literature Review, Chapter 2, will focus on previously described literature pertaining to genome mining for the identification of dye-decolourising peroxidases from actinobacteria and the need for their application in dye decolourisation, while Chapter 3 and Chapter 4 contain the Methodology and the Results respectively. Chapter 5 contains the Discussion and the culmination of the study will be in Chapter 6 with the Conclusion.

CHAPTER 2
LITERATURE REVIEW

In a time of increased public concern, social and ecological awareness as well as stringent legislative laws for the treatment of dye-contaminated wastewater, governments have fuelled the re-assessment of current wastewater treatment processes (Robinson *et al.,* 2001). Investigations into technologies that offer efficient, cost-effective, and viable alternative methods have become an imperative focus over recent years (Baban *et al.,* 2010). Within industries such as textile, paper, pharmaceutical and cosmetics an estimated 50% of applied reactive dye is wasted, which results in large effluent problems. Due to the recalcitrant nature of these dyes current methods used have become insufficient to alleviate the increased negative environmental effect of dye-containing wastewater (Baban *et al.,* 2010; Robinson *et al.,* 2001).

To address the growing concern, recent demands in biotechnological processes that are both novel and sustainable have been proposed. Among these, the use of industrially viable and novel microbial enzymes is being considered. Methods in identifying these particular enzymes include functional screening of microorganisms and (meta)genome mining techniques which are powerful strategies for the isolation and identification of promising enzymes (Subramaniyan and Prena, 2002).

2.1 Synthetic Dyes

Synthetic dyes are described as unsaturated poly-aromatic molecules that are soluble or dissoluble in water or solvents and have the ability to give permanent colour to materials such as fabrics (Singh *et al.,* 2015a). These dyes are classified according to colour, trade name, chemical structure, and their application. The most frequently used dyes are azo, anthraquinone, pthalocyanine and triarylmethane (Figure 2.1) (Berradi *et al.,* 2019). Amongst these synthetic dyes, azo dyes constitute more than a half of all dyestuffs produced and remain the most frequently utilized dye within the textile industry (Singh *et al.,* 2015b).

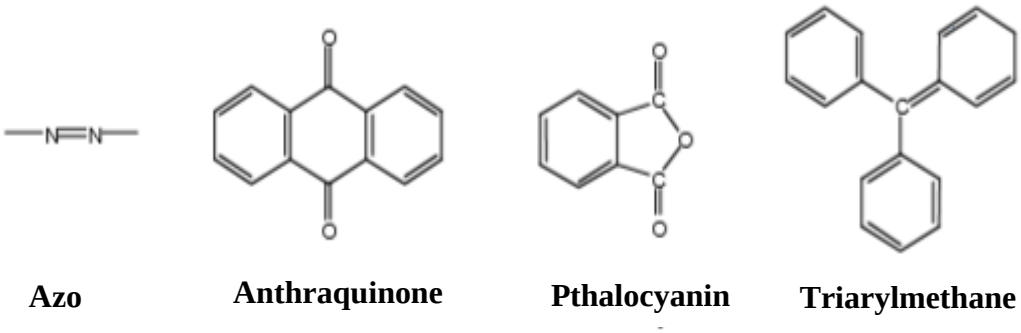

Figure 2.1: The chemical structures of the most frequently used synthetic dyes (structures obtained from Berradi *et al*., 2019).

Textile industries are one of the largest consumers of synthetic dyes worldwide whereby azo, anthraquinone and triphenylmethane dyes have been exploited on an industrial scale. Therefore, in relation to its consumption this industry is one of the main producers of dye-containing wastewater (Table 2.1) (Khadijah *et al.,* 2009; Bayoumi *et al.,* 2014). The dyeing processes used are inefficient as the dyes do not completely bind to the fabrics and the amount of dyes lost through textile wastewater is entirely dependent on the type of dye exploited which range from 2% for basic dyes to approximately 50% for reactive dyes. Furthermore, an estimation of 20% of unused dyes directly enter the environment through wastewater treatment as the conventional treatment processes are ineffective (Bayoumi *et al.,* 2014). By entering the environment these dyes impact a variety of areas in terms of their broad pH range (5-12) and the recalcitrance of organic compounds found within azo dyes to degradation (Kuberan *et al.,* 2011).

Table 2.1: Chemicals and effluents released during industrial textile processing (adapted from Mojsov *et al*., 2016).

Process	Chemicals-types used	Effluents
Dyeing	Urea, phosphates, ammonium salts, dyes	Nutrients (Nitrogen, Phosphates)
Dyeing, Scouring	Dyes, scoured wool impurities	Colour
Scouring, Desizing, Bleaching, Dyeing	NaOH, sodium chloride, sulphates, carbonate, silicate	Acids, Salts
Desizing, Bleaching, Dyeing, Finishing	Heavy metals, reducing agents, oxidising agents, biocides, quaternary ammonium salts	Toxic compounds

2.2 Toxicological Effects of Dyes

Wastewater treatment processes in the textile industry produce dye concentrations which range between 10-200 mg.litre^{-1} where in relation to the treatment, synthetic dyes remain exceedingly visible at concentrations less than 1 mg.litre^{-1}. Most dyes present remain toxic to all forms of life (Su and Horton, 1998). Initial exposure to these dyes causes allergic responses of the skin including but not limited to eczema and dermatoses whereby further exposure and possible digestion or adsorption of these dyes lead to damage of the lungs, liver, immune system, as well as the reproductive system of humans and animals (Su and Horton, 1998; Nikulina *et al.,* 1995). With the apparent industrial scale use of azo dyes and the current treatment processes, the degradation intermediates are highly poisonous and remain carcinogenic and mutagenic to all life forms (Singh *et al.,* 2014).

2.3 Present treatment processes for dye-containing wastewater

To achieve decolourization of dyes in wastewater, numerous methods have been devised in particular physiochemical processes namely, coagulation, adsorption, oxidation, filtration, and precipitation (Robinson *et al.,* 2001). With such a large extent of processes many drawbacks have occurred which include the expense of the process, the production of large quantities of sludge and the involvement of environmentally toxic chemical additives (Das *et al.,* 2016). A number of reports have identified the capability of microorganisms to decolourise synthetic dyes which are attributed to their production of enzymes which in turn could lead to a viable alternative method which is cost efficient for both the degradation and decolourisation of dyes within wastewater (Das *et al.,* 2016).

2.4 Biological approach to dye-containing wastewater treatment

The biological treatment processes of dye-containing wastewater may prove to be beneficial in terms of cost effectiveness, minimal production of sludge and an eco-friendly approach to the conventional and physicochemical treatments which are currently used (Asad *et al*., 2007; Bell *et al*., 2000). This process involves the use of a broad range of microorganisms such as fungi, yeast, algae, and bacteria to degrade and decolourise wastewater to overcome current limitations (Table 2.2) (Kalyani *et al.,* 2009). Research suggests that treatment systems constituted by a mixed microbial population accomplish a higher degree of biodegradation and mineralisation due to the synergism between a variety of microbial groups which further propels research into investigating a mixed microbial community over pure cultures to achieve this degree of degradation of synthetic azo dyes (Saratale *et al.,* 2011).

Table 2.2: Biological approaches to the treatment of wastewater through the application of microbial species in various industries (updated from Ahmad *et al*., 2018a).

Industry	Microbial Strain	Result	References
Paper and Pulp Industry	*Brevibacillus laterosporus* MTCC 2298	87% decolourisation according to the American Dye Manufacturing Institute (ADMI) within 24 hours	Kurade *et al*., 2011
Textile Industry	*Pseudomona putida*	Degradation of textile effluents observed at 25 °C	Babu *et al.,* 2011
Research Industry	*Bacillus licheniformis* LS04	More than 80% of colour removal of Reactive black 5, Reactive blue 19 and indigo carmine occurred in 1 hour at pH 6.6 or 9.0	Lu *et al*., 2012

The majority of synthetic dyes are xenobiotic compounds, chemical substances that are foreign to animal life, that are not effectively degraded through common biological treatments (Ahmed *et al.,* 2018a). Synthetic dyes such as azo dyes are characterised by aromatics substituted with one or more azo groups (-N=N-) (Singh *et al.,* 2015b). The primary step in the degradation of azo dyes by bacteria involve the reductive cleavage of the electrophilic azo bond under static, anoxic or anaerobic conditions which leads to the production of colourless aromatic amines. These products are further degraded into simpler non-toxic forms through a multiple-step bioconversion which can occur either aerobically or anaerobically (Singh *et al.,* 2015a; Singh *et al.,* 2014). Synthetic dyes, as mentioned are xenobiotic compounds, which are commonly not degraded effectively through an aerobic-treatment approach and in contrast microbial anaerobic reductions have been identified to produce aromatic amines which are essentially more toxic than the actual dyes themselves (Bafana *et al.,* 2008). Therefore, to further overcome the limitation of toxicity, the exploitation of enzymes from microorganisms are advantageous

due to their increased enzyme production which has the ability to remove and/or reduce the toxicity of synthetic dyes and in turn have greater stability and activity over a range of conditions and have proven to be cost effective through the use of recombinant DNA technology (Khan *et al.,* 2016).

Essentially, industrial waste, such as dye contaminated wastewater, contains a consortium of organic and inorganic substances whereby the former containing fatty acids, proteins and carbohydrates and the latter containing heavy metals, sulphites, and sulphides (Costa *et al.,* 2020). Despite microorganisms having the ability to express enzymes, the main limitation remains the rate of degradation for most recalcitrant pollutants in polluted sites which inhibit their widespread adoption (Brown and Hamburger, 1987).

2.5 Dye decolourisation through enzymatic approaches

Enzymes, primarily that of the oxidase-type, have been used as an alternative to the conventional treatment of effluents and white rot fungi such as *Phanerochaete* and *Trametes* species have been identified to successfully decolourise dyes in both aerobic and anaerobic treatment systems (Chander and Arora, 2007). Enzymes secreted by these organisms include manganese peroxidases, laccases, and lignin peroxidases which act by oxidative free radical cleavage of the azo bond. Furthermore, ligninolytic enzymes isolated from white rot fungi such as manganese peroxidase, phenol oxidase and lignin peroxidase are capable of oxidising a wide range of compounds when nutrients such as nitrogen, sulphur and carbon are limited. These enzymes in turn have various attributes which increase their viability to the conventional catalysts used namely, functionality over a broad pH, temperature and salinity range, biodegradability, and reduction in sludge formation. With specificity to the biotechnological field, they are capable of being designed with desired properties through genetic engineering and computational design (Nicell *et al.,* 1993; Barr and Aust, 1994).

To further understand enzymatic degradation, the focus of this review will be on three main lignin modifying enzymes, manganese peroxidase, laccases, and lignin peroxidases. Over recent years, the study and use of manganese peroxidases has increased due to their

high degradative potential. This enzyme functions by oxidising Mn^{2+} to Mn^{3+} which are highly reactive and in turn the products formed constitute a low molecular mass fragments, organic acids, and carbon dioxide to mention a few, which aid in a cascade of other reactions (Ziegenhagen and Hofrichter, 2000). Furthermore, laccases have been extensively studied for the treatment of a broad range of industrial effluents from industries ranging from the textile to tannery and other industrial effluents that contain phenolics or chloro-lignins. These studies aimed to assess degradation of tannery and textile waste as well as enzyme stability in these environments. These enzymes function through the removal of an H^+ atom from both hydroxyl and amino groups found within the ortho- and para- substituted mono- and polyphenolic substrates, as well as aromatic amines (Kahramann and Yasilada, 2001). The final enzyme, lignin peroxidase, functions through the oxidation of the phenolic group which results in the production of a radical at the carbon bearing the azo linkage which in turn degrades azo dyes (Rodriguez *et al.,* 1999). Furthermore, peroxidases from various sources are relatively nonspecific and in turn provide white rot fungi with the unique ability to degrade an extensive array of environmental pollutants such as polychlorinated biphenyls, industrial dye effluents, pesticides, and herbicides to mention a few (Marco-Urrea and Reddy, 2012). Bioremediation by this enzyme has potential application in treatmet of wastewater containing chlorinated phenols, cresols from the biopulping and biobleaching in the paper and pulp industry, and removal of peroxide from textile-dye. This is possible through extracellular peroxidases produced by white rot fungi which are capable of degrading lignin due to nonspecific free radical mediated reactions as mentioned previously (Lundell *et al*., 2010). Dye-decolourising peroxidases functions in a similar manner to the peroxidases mentioned and will be discussed more in detail in section 2.9.

2.6 Accessing enzymes of interest – A genome mining approach

Within microbial communities it is important to understand the structural and functional roles microbes play within the ecosystem to predict how the community responds to environmental changes (Allison and Martiny, 2008; Allison, 2012). Roughly 99% of bacteria in the environment cannot be cultured using conventional methods, therefore identifying the composition of unculturable microbial communities to identify functional

traits and in turn the functionality of the ecosystem, remains a challenge (Amann *et al.,* 1995; Handelsman *et al*., 1998; Cowan, 2000).

For decades metagenomics has been at the forefront of biotechnology and enzyme discovery, as it is able to access uncultured microbes by the construction of metagenome libraries (Handelsman *et al.*, 1998). Researchers have constructed metagenomic libraries to identify novel biocatalysts or molecules for pharmaceutical and biotechnological applications. Furthermore, outcomes from metagenomic research has identified an assortment of novel genes, such as small genes that translate to enzymes as well as complex gene clusters encoding proteins (Daniel, 2004). Metagenomics is an alternative method to conventional screening by directly cloning environmental DNA (metagenome) into a host. This is advantageous as one has the ability to thoroughly examine the metagenome regardless of the culturability of the original organism (Healy *et al.*, 1995). Current methods of metagenome screening technologies are conducted either by function (activity) or sequence-based screening (Schmeisser *et al.,* 2007; Iqbal *et al.,* 2012).

In the function-based screening approach, clones that express desired traits are selected from libraries and aspects of their molecular biology and biochemical make up are analysed. This approach allows for the rapid attainment of clones that may have prospective applications within industry (Yun and Ryu, 2005). This method is further able to detect genes with complete novel DNA sequences and the majority of metagenome-derived enzymes as well as biocatalysts, mainly glycoside hydrolases and esterases, have been obtained by this method (Ferrer *et al*., 2009; Simon and Daniel, 2009; Steele *et al.*, 2009; Tuffin *et al*., 2009). However, this approach does have several limitations, requires the expression of the function of interest within the host cell, usually *Escherichia coli*, as well as clustering of all the genes required for the particular function (Yun and Ryu, 2005). The probability of identifying a gene of interest depends on the factors above which are further intrinsically linked to multiple factors such as the host-vector system selected, the size of the gene of interest, the abundance of gene clustering, the assay method, and proficiency of heterologous gene expression in the host cell (Uchiyama and Miyazaki, 2009).

In contrast, the sequence-based screening approach does not depend on the expression of cloned genes in heterologous hosts. This method is focused on the conserved DNA sequences of target genes (Yun and Ryu, 2005). Sequence-based screening is conducted by either a PCR-based or hybridization-based processes, however the limitation to this is that the genes attained are restricted to those with similar homologies to the analysed sequence and thus obtaining novel genes is not always possible (Uchiyama and Miyazaki, 2009). Shotgun sequencing of metagenomic libraries, however, have derived a wide variety of data which include phylogenetic relationships, a plethora of novel genes and identified metabolic pathways of uncultured bacteria which have been rather promising compared to sequenced-based screening limitations (Venter *et al.,* 2004).

A study conducted by Ziemert *et al.* (2016) further highlights the benefits of genome mining for its ability to identify the biosynthetic pathways of bioactive products, as well as their probable functional and chemical interactions of these pathways. This approach exclusively depends on both computing technology and bioinformatics tools. When the complete set of genes within a genome is identified they can be assessed with those of known functions on public databases (Albarano *et al*., 2020). These databases assess both raw and annotated genomic data that aids in sequence comparison utilising various websites (Albarano *et al*., 2020). Genome-guided discovery has been aided in recent years by the advent of Next Generation Sequencing (NGS) technologies that have assisted researchers through its ability to sequence millions of DNA fragments at once. This is beneficial in providing information about the structure of genomes, gene activity, genetic variations as well as gene behaviour (Shendure *et al*., 2017). Additional benefits of NGS technologies are through its contribution to (meta)genomics, whereby it has assessed large quantities of sequences that have been used as identifiers for structural, diversity and possible functionality of microbial communities (Góngora-Castillo *et al*., 2020). Some drawbacks do come with this technology such as the requirement of specialised hardware infrastructure and understanding to be able to assess the copious amounts of sequences collected. Thus, tools such as EBI Metagenomics (Mitchell *et al*., 2018) as well as (MG-)RAST (Keegan *et al*., 2016) to mention a few, offers computational platforms to perform analysis of (meta)genomic samples for Quality Control (QC), filtering of sequences, taxonomic identification and much more (Góngora-Castillo *et al*., 2020).

A study conducted by Cordas *et al.* (2022), which has relevance to the current study, discovered and characterised a novel DyP-type peroxidase from a marine actinobacterium isolated from Trondheim fjord in Norway through a data mining approach. These researchers used this approach based on HMMER software and a profile Hidden Markov Model (HMM) to assess a dataset comprised of 1200 genomes from actinobacteria isolated from the Trondheim fjord. Hidden Markov Models have been recognised as a successful statistical model for the analysis of biological sequences and have applications within sequence analysis, especially that of predication-based analysis of exons and introns of genomic DNA, the identification of functional motifs (domains) in proteins and the alignment of two sequences (Franzese and Iuliano, 2019). This study (Cordas *et al*., 2022) further confirmed that data mining is a good accompaniment for identifying novel enzymes other than via high-throughput screening. Furthermore, with the addition of databases the identification of protein families is available, and the data mining approach allowed for screening of a very large set of genomes, 1200, that has assisted in the discovery of novel DyP-type peroxidases. Thus, the data mining approach will be selected for this study to access a variety of DyP-type peroxidases present in actinobacteria isolated from various environments.

2.7 Actinobacteria

Actinobacteria (phylum *Actinomycetota*), also referred to as actinomycetes, are one of the largest and most distinct bacterial groups that have been characterised throughout the years. This group of bacteria remains a source of interest for the discovery of novel biomolecules and enzyme activities (Tischler *et al.,* 2019). Their extraordinary diversity is noted by their various morphologies, broad spectrum of physiological and metabolic activities and their genetics.

Actinobacteria are Gram-positive bacteria which are characterised by a high GC-content of their genomic DNA of roughly between 50-70% (Lawson, 2018; Ventura *et al.,* 2007). These microorganisms are predominantly found in soil, where they constitute a substantial portion of the microbial population, but have also been identified in aquatic environments (Hong *et al.,* 2009; Macagnan *et al.,* 2006). Essentially, soil contains a multitude of ecological niches from which microbes produce various biologically active

natural compounds which have importance in many fields ranging from biotechnology to healthcare. Within actinobacteria, their ability to grow and adapt to a multitude of environments give these organisms great potential to produce antimicrobial compounds and enzymes (Goodfellow and Williams, 1983).

Morphological characteristics are typically used in the identification of actinobacterial isolates. This drove the identification of standard culture media for the proliferation of certain species of actinobacteria, for instance that of the International *Streptomyces* Project (ISP) medium. Actinobacteria identification over the years has included a variety of morphological observations such as spore germination, elongation and branching of vegetative mycelium, formation, and colour of either aerial or substrate mycelium and pigment production (Figure 2.2) (Holt *et al.*, 1994).

Figure 2.2: Colony morphology of a *Gordonia* sp. on International *Streptomyces* Project-2 medium (ISP-2) (A) and a Scanning electron micrograph (SEM) of a *Gordonia* sp. on ISP-2 medium indicating spore chain formation and spore surfaces (updated from Betancur *et al*., 2017).

Actinobacteria are generally comprised of a group of unicellular branching microorganisms which mostly are aerobic, mycelium-forming (aerial and/or substrate mycelium) (Ranjani *et al.,* 2016). Reproduction within these taxa occurs by spore production or conidia in which sporulation occurs through fragmentation and segmentation (Anandan *et al.,* 2016). The two predominant morphological appearances of actinobacteria are that of aerial mycelium and substrate mycelium. Aerial mycelium of actinobacteria exhibits abundant differentiation that allows a variety of isolates to be segregated into groups which share similarity in morphological characteristics under

fixed conditions, such as growth on the same culture media. Aerial mycelia are typically thicker than substrate mycelium. Substrate mycelium of actinobacteria differs in thickness, shape, and size. Furthermore, colour ranges from white a semi-colourless pink, yellow, brown, red, or black (Okoro *et al.,* 2010).

2.7.1 Niches of Actinobacteria

As aforementioned, actinobacteria are predominantly found in terrestrial environments such as soil and existing as the major component of the microbial population. Actinobacteria from the terrestrial environment play an important part within the rhizospheric microbial community in the turnover of recalcitrant plant matter, which has been suggested as the best habitats for the isolation of these microorganisms (Priyadharsini and Dhanasekaran, 2015).

Marine and freshwater environments have also been identified to contain actinobacterial species, such as *Micromonospora,* which, it has been proposed, are not true aquatic species, but rather washed in from terrestrial environments (Cross, 1981). Actinobacterial species isolated from these environments aid in the turnover of chitin, cellulose, and lignin, and therefore have the potential to produce novel enzymes needed for the breakdown of these materials. Marine environments contain the greatest biodiversity of species and therefore is an untapped source of novel actinobacterial diversity which in theory could also lead to novel antimicrobials, enzymes, and metabolites (Subramani and Aalbersberg, 2013). Actinobacteria isolated from these environments have adapted over the years to deal with extremely high pressure, anaerobic conditions, as well as temperatures ranging between 0-8 °C on the ocean floor and 8-100 °C close to hydrothermal vents (Jensen *et al.,* 2005). Although there are limitations for screening marine actinobacteria, there have been discoveries of novel secondary metabolites that have exceeded that of the terrestrial counterparts, which is evident by the isolation of a variety of chemical compounds from marine actinobacteria (Anandan *et al.,* 2016).

2.7.2 Applications of Actinobacteria

Actinobacteria are an extensively studied group of bacteria due to their production of both primary and secondary metabolites that remain important in a variety of fields. This group of bacteria serve as a promising source of diverse enzymes that continue to be produced on an industrial scale. In addition, a large fraction of antibiotics that are currently used are acquired from this group (Anandan *et al.,* 2016). Actinobacteria have the ability to degrade a broad range of hydrocarbons, aromatic compounds as well as pesticides (Chen *at al*., 2015b). Furthermore, they are used in the microbial transformation of organic compounds such as the conversion of lignocellulose to its various derivatives. One noticeable example is the nitrile hydratase from *Rhodococcus* species which is used in the production of acrylamide (Nagasawa *et al.,* 1993). Applications of actinobacteria include, but are not limited to, bioremediation, enzymes, antimicrobials, and probiotics.

2.7.2.1 Bioremediation

Actinobacteria contain abundant properties that make them crucial members for the bioremediation of soils which have been contaminated by organic pollutants. This group of bacteria have shown dominance over other groups in contaminated areas as the predominant degraders (Johnson *et al*., 2002). They also play an important role in the recycling of organic carbon and are further able to degrade complex polymers. Furthermore, actinobacterial strains are also known to possess the ability to solubilize lignin and degrade lignin-derivatives, thus producing hemicellulose and cellulose-degrading enzymes, as well as extracellular peroxidase (Mason *et al*., 2001). A study conducted by Saha *et al*. (2013) identified that an actinobacterial species with the ability to live in an oily environment and can in turn be used to bioremediate oil pollutants. Another example is *Nocardiopsis* sp. strain SD5 which was able to produce keratinase for the degradation of feather waste (Dhanasekaran and Latha, 2013).

2.7.2.2 Actinobacterial Enzymes

A consortium of biologically active enzymes is produced by actinobacteria isolated from both terrestrial and aquatic environments. The biological functions of these species are predominantly dependent on the sources from which the bacteria are isolated (Sharmin *et al.,* 2005). The reason(s) why actinobacteria produce peroxidases in nature are largely not understood however, their potential in industrial process have been suggested. These processes include the production of antibiotics, lignocellulosics degradation, as well as xenobiotic degradation (Le Roes-Hill *et al*., 2011).

2.8. Peroxidases

Peroxidases (EC 1.11.7) (Figure 2.3) are a large group of oxidoreductases that catalyse the oxidation of substrate molecules and use hydrogen peroxide as their electron acceptor. These enzymes are found in almost all forms of life ranging from microbes, plants, and animals. Furthermore, the broader variety of peroxidases contain haem as a cofactor, however, a small group of peroxidases are non-haem containing enzymes (Banci, 1997).

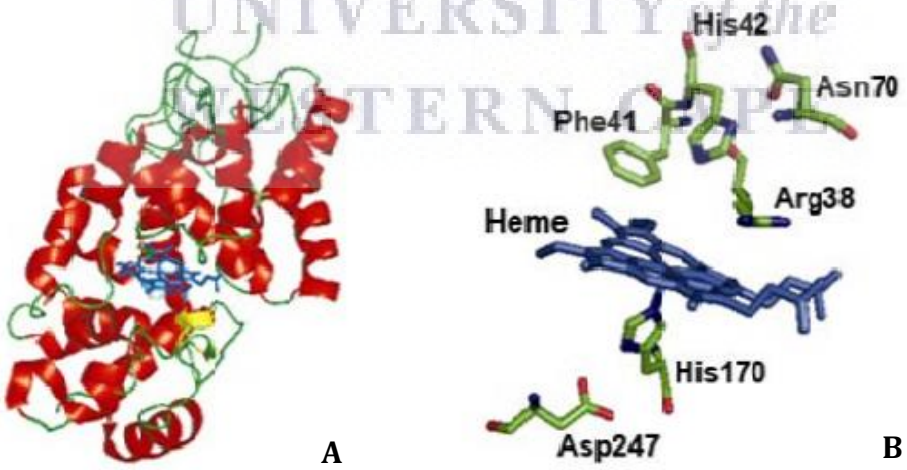

Figure 2.3: 3-D protein model of horseradish peroxidase from *Armoracia rusticana* (A) whereby α-helices are indicated in red, β-sheets indicated in yellow, haem cofactor indicated in blue and key amino acids in haem-surrounding regions (B) (PDB ID: 1ATJ).

Haem-containing enzymes are proteins which catalyse the oxidation of a variety of organic and inorganic compounds whilst reducing hydrogen peroxide (H_2O_2) to water (H_2O) (Danford, 1999). In a typical peroxidase reaction, one molecule hydrogen peroxide oxidises two equivalents of the reducing substrate. Furthermore, haem peroxidases are a prevalent and useful class of enzyme due to their ability to utilise a variety of reducing substrates. Some of the reactions catalysed by this enzyme include the oxidation of a number of organic and inorganic compounds, and the reduction of peroxides such as hydrogen peroxide. However, these enzymes play a broader role in all forms of life ranging from biosynthesis of cell wall material to immunological host-defense responses (Passardi *et al.,* 2005; Davies *et al.,* 2008).

Peroxidases have been identified in plant sources namely, horseradish, banana (*Musa paradisiacal*) and papaya (*Carica papaya*) (Twala *et al.,* 2020). The well-studied horseradish peroxidase (HRP) is used in diagnostic kits, in the formation of a wide variety of aromatic chemicals, and the removal of peroxides from foodstuffs and industrial waste. Peroxidases from microbial sources have also been identified from *Pseudomonas* species and *Bacillus subtilis*; fungal species such as *Phanerochaete chrysosporium* and other bacterial sources such as actinomycetes, namely the well-studied *Thermobifida fusca* and various *Streptomyces* species. These sources of peroxidases aid in a multitude of processes such as in the production of animal feedstock, textile dye degradation and sewage treatment, and have the potential to be used as biosensors (Lundell *et al.,* 2010; Hofrichter *et al.,* 2010). Notably, the peroxidase superfamily has been studied for many years, however, it was fascinating to find a newly discovered peroxidase superfamily in the late 1990s grouped as dye-decolourising peroxidases which presents promising biotechnological potential (Kim and Shoda, 1999).

2.9 Dye-decolourising Peroxidases

Dye-decolourising peroxidases (E.C. 1.11.1.19) (Figure 2.4), also commonly referred to as DyPs or DyP-type, denote a novel superfamily of haem-containing enzymes which have been characterised by their broad substrate range and functionality at low pH, remaining stable at a more neutral pH. Furthermore, this class of peroxidases do not share any substantial similarity in primary sequence and structure to other characterised peroxidase superfamilies (Colpa *et al.,* 2014; Lončar *et al.,* 2016). However, commonly shared with other peroxidases is their ability to use hydrogen peroxide as the electron acceptor which in turn has important use by their oxidation of a broad variety of industrialy-viable substrates which include but are not limited to anthraquinone dyes, aromatic sulphides as well as β-carotene (Liers *et al.,* 2010; Lindie *et al.,* 2015; Salvachua *et al.,* 2013; van Bloois *et al.,* 2010).

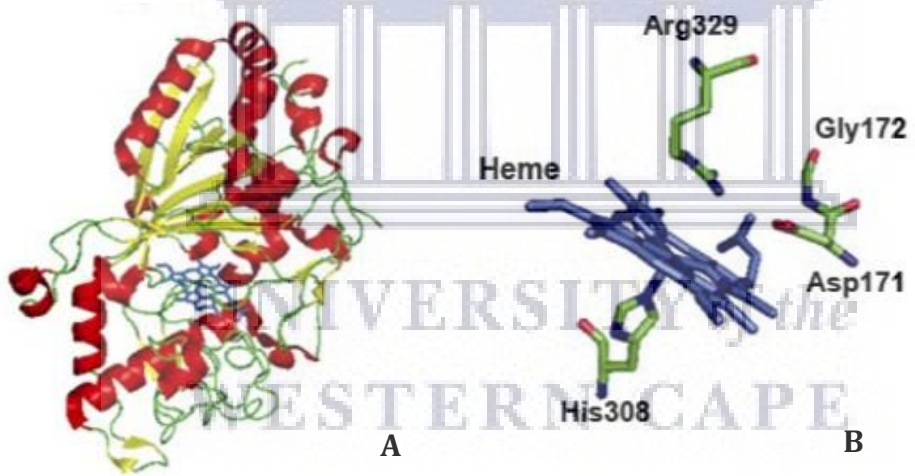

Figure 2.4: 3-D protein model of DyP from *Bjerkandera adusta* Dec 1 (A) whereby α-helices are indicated in red, β-sheets indicated in yellow, haem cofactor indicated in blue and key amino acids in haem-surrounding regions (B) (PDB ID: 2D3Q).

2.9.1 Phylogeny and Structure of DyPs

DyP-type peroxidades were originally discovered in white-rot fungi and subsequently named for their ability to degrade a variety of dyes (Kim and Shoda, 1999). They have been found in the proteomes of several fungi and bacteria (Sugano, 2009). Recently, genome analysis has identified that these enzymes are more prevalent in bacteria in comparison to fungi and higher eukaryotes. Furthermore, research compiled by using the

Interpro database have identified up to 4000 members of this superfamily of which 3707 members belonged to bacteria, 117 in eukaryotes and only 11 in archaea (Colpa *et al.,* 2014). With most putative DyP-type peroxidases identified in bacteria, researchers suggest that this superfamily be renamed as bacterial peroxidases (Adav *et al.,* 2010). In addition, information compiled by Peroxibase have further sub-classified DyP-types according to their phylogenetically distinct characteristics into classes namely, A, B, C and D. Class A contains enzymes that have a twin arginine translocation (TAT)-dependent signal sequence which suggest that they function extracellularly or outside of the cytoplasm. Classes B and C contains mainly bacterial enzymes which are putatively cytoplasmic, which indicates intracellular metabolism and the final class, Class D, primarily contains fungal variants (van Bloois *et al.,* 2010; Sturm *et al.,* 2006; Jongbloed *et al.,* 2004).

The physiological function of the majority of the DyPs remains largely unclear, however, further research has discovered some bacterial variants are involved in lignin degradation (van Bloois *et al.,* 2010; Adav *et al.,* 2010). Researchers have proposed that these lignolytic enzymes isolated from bacterial variants may be regarded as complements to fungal lignin degrading peroxidases. In contrast to plant and animal peroxidases, DyPs are dissimilar in primary sequence level and lack the characteristic haem-binding motif of plant peroxidases in which only one proximal histidine is included, this being the distal histidine and an essential arginine (Passardi *et al.,* 2005; Veitch, 2004; Sugano, 2009). DyPs contain a GXXDG motif in their primary sequence which forms part of its haem-binding region and plays a critical role in overall peroxidase activity. Any removal or replacement of the conserved aspartate by an asparagine or an alanine inactivates the enzyme though the haem-binding remains unaffected (van Bloois *et al.,* 2010; Sugano *et al.,* 2007).

Only a limited number of fungal and bacterial DyPs have been characterised which includes the elucidation of their crystal structures (Sugano *et al.,* 2007; Lui *et al.,* 2011; Zubieta *et al.,* 2007a; Zubieta *et al.,* 2007b). DyP-type peroxidases from the different subclasses regularly exhibit low sequence similarity although their overall structural topology remains conserved. Based on structure alone, DyPs are comprised of two domains that contain α-helices and anti-parallel β-sheets which contrasts with plant

peroxidases as they contain mostly α-helices. Both domains in DyPs assume a unique ferredoxin-like fold and form a crevice known as the active site where the haem cofactor is inserted between the two (Sugano *et al.,* 2007). The haem-binding motif inserted between the two domains contains a highly conserved histidine in the C-terminal of the enzyme and is similar to that of the proximal histidine of plant peroxidase based on functionality alone (Sugano *et al.,* 2007; Lui *et al.,* 2011; Zubieta *et al.,* 2007a, 2007b).

A study conducted by Yoshida and Sugano (2015) challenged the old classification system and henceforth renamed the classes of DyPs into three groups. The previous classification system used phylogenetic analysis based on amino acid sequence similarity to group DyP-type peroxidases, however, the definitions of each class remained ambiguous and the amino acid sequence similarity amongst them was low which ultimately resulted in inexact multiple sequence alignments and approximations of evolutionary relationships (Kawabata, 2003). Yoshida and Sugano readdressed the classification system by focusing on structure-based sequence alignments using the MATRAS program, which is a three-dimensional alignment tool, and ten structures were determined at a higher resolution (Kawabata, 2003). Sequence analyses identified three defining characteristics namely, (i) Significant residues were conserved which include a histidine which functions as the ligand for haem, four amino acid residues which form a hydrogen peroxide binding pocket in the distal side of haem and a GXXDG motif which contains the catalytic aspartic acid residue (Yoshida *et al.,* 2012; Yoshida *et al.,* 2011; Sugano *et al.,* 2009; Sugano, 2009); (ii) Haem-binding is perceived necessary for functionality within all classes of DyPs due to one α-helix containing a histidine residue coordinated to haem (α-helix 2) which together with another α-helix (α-helix 1) form one long α-helix. Granted the sequences for each helix are not successive, however, an important histidine residue is located near the center of the long α-helix and the amino acid residues that form this long chain remain well conserved. This suggests that the histidine residue serves as an integral function in each class of DyPs (Sugano *et al.,* 2009); (iii) Classes A, C and D contain extra sequences in comparison to Class B proteins which was deduced from their short amino acid sequence (Yoshida *et al.,* 2012). Furthermore, the four structures of class A proteins contain extra sequences in the same regions although the three structures of classes C and D proteins contain extra sequences in the exact same regions which could suggest a sequence-based relationship between these classes of proteins.

The MATRAS program identified only three key branches, whereby Classes C and D formed one large branch, which relates to the extra sequences shared in the same regions. The DyP structures exhibit both a dimeric α- as well as β-barrel structures, classes A, C and D proteins essentially contain extra sequences which make their structures larger in comparison to class B proteins. Therefore, these extra sequences may aid in the characterisation of functions for each class of these proteins (Yoshida *et al.,* 2012; Sugano, 2009). Classes C and D proteins have comparable structural features which also confirms higher peroxidase catalytic efficiency in comparison to that of class A and B proteins. Therefore, with the results obtained Yoshida and Sugano (2015) proposed a new classification system of only three classes. These were thus reclassified as: P (primitive), I (intermediate) and V (advanced). Class B has been reclassified as class P as their structures are most compact, classes C and D have thus been reclassified as class V as they share extra sequences in the same regions, and class A forms class I as they contain fewer extra sequences than those of class V.

2.9.2 Biochemical Properties of DyPs

Bacterial DyPs are known to catalyse the oxidation of a variety of substrates ranging from synthetic anthraquinones such as Reactive Blue, ABTS (2,2'-azino-bis(3-ethylbenzothiazoline-6-sulfonic acid)) and small phenolic compounds which include, but are not limited to, guaiacol, 2,6-dimethoxyphenol (DMP) and catechol (van Bloois *et al.,* 2010). The biochemical properties of only a small number of fungal and bacterial DyPs were studied over the years and researchers deduced that these enzymes are typically 50-60 kDa in size whereas in contrast several bacterial variants have been identified to be around 40 kDa (Kim and Shoda, 1999; van Bloois *et al.,* 2010; Sturm *et al.,* 2006; Ahmad *et al.,* 2011b). DyPs which have been characterised contain a non-covalently bound haem (proto haem IX) as the cofactor, which is comparable to that of animal and non-animal subfamilies of peroxidases. Furthermore, several oligomeric states have been identified varying from monomers to hexamers (Zubieta *et al.,* 2007a; Li *et al.,* 2012; Ogola *et al.,* 2009). Bacterial DyPs are primarily assembled in dimers whereas fungal DyPs are solely monomers due to numerous C-terminal insertion sequences which prevent enzyme dimerization (Zubieta *et al.,* 2007a, 2007b). In contrast, bacterial DyP dimerization is

caused by a hydrophobic interaction between monomers. A defining feature of DyPs is their catalytic properties which entail active enzyme functionality at a low pH. This could be relative to the aspartate of the GXXDG motif whereby it functions as an acid-base catalyst at a low pH, although this can only be said for subsets of DyP-type peroxidases (van Bloois *et al.,* 2010; Sugano *et al.,* 2007).

Research has identified the catalytic mechanism of both plant and animal peroxidases which proceeds by the formation of Compound I (also suggested for DyPs) (Fraaije and Van Bloois, 2012). Although the catalytic cycle for DyPs still remains unclear, studies have identified key differences between the catalytic mechanism of other peroxidases in comparison to that of DyPs. For instance, four novel structures of a well-studied fungal DyP were used to understand the biochemical properties whereby research proposed that the aspartate of the GXXDG motif moves into an alignment which allows for optimal interaction with hydrogen peroxide therefore enabling the formation of compound I (Yoshida *et al.*, 2011). The critical role of the conserved aspartate is further corroborated from the results deduced by mutagenesis studies completed on both fungal and bacterial DyPs. Plant peroxidases function differently whereby the formation of Compound I is aided by a crucial arginine residue and the acid-base catalyst of the distal histidine residue (Veitch, 2004). A study conducted by Singh *et al.* (2012) analysed the peroxidative cycle of DypB from *Rhodococcus jostii* RHA1 and acknowledged that its conserved aspartate was not required for peroxidase activity as a substitution of this residue with an alanine had an insignificant effect on reactivity towards hydrogen peroxide and the formation of Compound I. It was however found that a conserved arginine of DypB proved essential for peroxidase activity which suggest that DyPs utilize different residues as an acid-base catalyst throughout their catalytic cycle (Colpa *et al.*, 2014). One of the most synonymous catalytic features of DyPs are their unique ability to degrade a variety of dyes. These enzymes display an inimitable profile in the degradation of anthraquinone dyes however exhibit poor activity towards azo dyes and small non-phenolic compounds which cannot be said for plant and animal peroxidases (Kim and Shoda, 1999; van Bloois *et al.,* 2010; Burner *et al.,* 2000; Stolz, 2001; Reszka *et al.,* 2005; Reszka *et al.,* 2001; Chen, 2006).

2.9.3 Biotechnological Prospects of DyP-type peroxidases

Peroxidases, in particular plant peroxidases, are an appealing source of biocatalysts due to their broad substrate range, neutral pH optimum and their ability to catalyse a multitude of reactions (Regalado *et al.,* 2004). Although the use of these enzymes has produced good results, the use thereof is hindered by limited stability and difficulty of heterologous expression. Interestingly, DyP-type peroxidases exhibit robustness and through further characterization of the *T. fusca* DyP (TfuDyP) show exemplary heterologous expression in the recombinant host (van Bloois *et al.,* 2010; Liers *et al.,* 2013; Puhse *et al.,* 2009). The biotechnological potential of DyPs is further highlighted by their biocatalytic activity which may be used within industrial applications and their ability to degrade a wide range of synthetics which in turn lead to the remediation of dye-contaminated water (Marco-Urrea and Reddy, 2012). The ability of some fungal DyPs to degrade β-carotene has been exploited in the enzymatic whitening of food and beverages, which is extremely useful in the food industry. Furthermore, bacterial DyPs seem to offer promising biocatalytic activity over that of their fungal counterparts such as the fungal DyP from ascomycetous fungus *Xylaria grammica* (Kimani *et al.,* 2021). The advances in NGS as well as metagenome sequencing have identified an assortment of bacterial DyPs that may potentially possess novel activities (Bornscheuer *et al.,* 2012; Reetz, 2010). Currently, characterised enzymes have exhibited efficient activity towards a variety of substrates which include, lignin model compounds and recalcitrant dyes, as well as exhibiting favourable activities under acidic conditions (Reetz, 2013). An increase in antibiotic resistant pathogenic bacteria has fuelled the need for the discovery of novel antimicrobial targets. DyP-type peroxidases have the potential to assist in this endeavour as they are abundant in the proteomes of bacteria and not found within the proteomes of mammals. This suggests that DyPs may be promising novel anti-microbial (pro) drug targets (Kong *et al.,* 2010).

CHAPTER THREE
METHODS AND MATERIALS

All chemicals were purchased from Merck Millipore unless stated otherwise. Actinobacterial strains used in this study are listed in Table 3.1. Actinobacterial strains were isolated from diverse sampling sites ranging from Algoa Bay, Riversdale and the Gamka River (South Africa) and the Bwanda Hot Springs (Zambia), to mention a few, by researchers from the Biocatalysis and Technical Biology Lab (BTB), Cape Peninsula University of Technology (CPUT), and a sampling site in Clanwilliam, South Africa by the Institute of Microbial Biotechnology and Metagenomics (IMBM), University of the Western Cape (UWC).

Table 3.1 Information on the actinobacterial strains used in the study – full name, source of isolation, the sequencing technology employed in the whole genome sequencing, and the genome size.

Full name	Source	Sequencing Technology	Genome Size (Mbp)
SPR: *Streptomyces polyantibioticus* SPR^T	Soil – Umgeni River, South Africa	Roche 454	7.18
CZA14: *Streptomyces pharetrae* CZA14^T	Soil collected from the base of a giant quiver tree – Worcester, South Africa	Roche 454	8.14
30-1: *Micromonospora* sp. strain 30-1	Marine sponge (*Polysyncraton cf millipore*) – Algoa Bay, South Africa	Illumina Miseq	6.71
HMC10: *Nonomurea candida* HMC10^T	Soil – Gamka River, South Africa	Illumina Miseq	10.73

Full name	Source	Sequencing Technology	Genome Size (Mbp)
CZH20: *Nocardia gamkensis* CZH20^T	Soil – Gamka River, South Africa	Illumina Miseq	7.74
BSII#1: *Streptomyces* sp. strain BSII#1	Soil – Bwanda Hotsprings, Zambia	Illumina Miseq	7.00
BG1.3: *Gordonia* sp. strain BG1.3	Soil – Goukou River, South Africa	Illumina Miseq	5.57
BS2: *Gordonia lacunae* BS2^T	Estuary (soil) – Plettenberg Bay, South Africa	Illumina Miseq	5.75
TVU1: *Micromonospora tulbaghiae* sp. TVU1^T	Leaves of wild garlic (*Tulbaghia violacea*) – Wellington, South Africa	Illumina Miseq	6.46
M26: *Streptosporangium minitrum*	Soil (garden) – Roodepoort, South Africa	Illumina Miseq	9.58
SF1.2: *Actinomadura* sp. strain SF1.2	Soil (peatland) – Springfield, South Africa	Illumina Miseq	8.54
SF1.4: *Actinomadura* sp. strain SF1.4	Soil (peatland) – Springfield, South Africa	Illumina Miseq	10.49
HMC13: *Streptomyces swartbergensis* sp. nov. HMC13^T	Soil – Gamka River, South Africa	Illumina Miseq	9.20
151: *Streptomyces* sp.	Rooibos (soil) - Clanwilliam, South Africa	Illumina Miseq	6.17

Full name	Source	Sequencing Technology	Genome Size (Mbp)
385: *Streptomyces* sp.	Rooibos (soil) - Clanwilliam, South Africa	Illumina Miseq	6.78
163: *Streptomyces* sp.	Rooibos (soil) - Clanwilliam, South Africa	Illumina Miseq	4.96
85: *Streptomyces* sp.	Rooibos (soil) - Clanwilliam, South Africa	Illumina Miseq	5.87
S129: Streptomyces sp.	Cancer bush (*Sutherlandia frutescens*) - Clanwilliam, South Africa	Illumina Miseq	8.29
885: Streptomyces sp.	Rooibos (soil)- Clanwilliam, South Africa	Illumina Miseq	5.14
A159: Streptomyces sp.	Cape Aloe Plant (*Aloe ferox*) - Clanwilliam, South Africa	Illumina Miseq	3.97
A81: Streptomyces sp.	Cape Aloe Plant (*Aloe ferox*) - Clanwilliam, South Africa	Illumina Miseq	7.28

3.1 Genome mining

Twenty-one whole genome sequence fasta files were submitted to RAST (Rapid Annotations using Subsystems Technology; https://rast.nmpdr.org/). The annotated genome information was downloaded in Excel format and analysed for the presence of predicted DyP-type peroxidases. Potential DyP-type peroxidase amino acid sequences were submitted to NCBI, BLASTp to identify the nearest phylogenetic hit (https://blast.ncbi.nlm.nih.gov). Those identified as DyP-type peroxidases were submitted to PRED-TAT to further identify the presence of the twin arginine translocation

(TAT)-sequence (http://www.compgen.org/tools/PRED-TAT/submiT - accessed on 23 May 2018). Sequences of published DyP-type peroxidases were used in the construction of a phylogenetic tree with the use of the amino acid lengths that aids in the determination of a class within the DyP-type peroxidase group. The data was aligned to that of a well-established DyP-type peroxidase from *Thermobifida fusca* (accession no. NC_007333.1), and a non-actinobacterial DyP-type peroxidase from *Bacillus subtilis* (accession no. KFK78021.1), in order to construct a phylogenetic tree using MEGA 6 (www.megasoftware.com). Based on the analyses, a subset of eight strains were selected for primer design and gene cloning.

3.1.2 Cultivation of Strains for Genomic DNA Extraction

A modified version of the Genomic DNA Extraction method described by Mandel and Marmur (1968) was applied. All selected strains were grown in International *Streptomyces* Project-2 Medium (ISP-2) for one week (at 30 °C, 160 rpm) and 20% (v/v) glycerol stocks were made of each [For 1 L ISP-2: 4 g yeast powder, 10 g malt extract and 4 g glucose; to a final pH 7.2]. All buffers and solutions were made prior to DNA extraction unless stated otherwise.

The selected strains were centrifuged at 12 000 rpm for 2 minutes at room temperature (22 ± 3 °C) and the supernatant fluid was removed before the addition of 400 µL resuspension buffer and dry lysozyme (8 mg/mL), and allowed to incubate overnight at 4 °C. Four hundred µL (400 µL) of the 2× lysing solution (Appendix A) and 200 µL of 5 M $NaClO_4$ was added whereby cell precipitation occurred and cells were lysed overnight at 55 °C. Proteins were precipitated by the addition of 300 µL phenol:chloroform solution (2:1; v/v) and placed on a shaker for 20 minutes. Thereafter, centrifugation occurred at 12 000 rpm for 10 minutes at room temperature (22 ± 3 °C) and the aqueous layer was transferred to a sterile 1.5 mL Eppendorf tube. This step was repeated twice. Five hundred µL of 76% (v/v) ethanol was added to the aqueous layer and allowed to stand for 10 minutes and centrifuged again at 12 000 rpm for 10 minutes. The precipitate was dried at 37 °C for 15 minutes and resuspended in 400 µL 1× Tris-EDTA buffer (pH 7.0) overnight at 4 °C. The dissolved precipitate was supplemented with 5 µL of RNase mix (10 mg/mL in 90 µL 1× TE buffer, pH 7.0) and incubated at 37 °C for one hour before

extraction with 100 µL chloroform:isoamyl alcohol solution (24:1; v/v), centrifuged at 12 000 rpm for 10 minutes at room temperature (22 ± 3 °C) and the aqueous layer transferred to a sterile 1.5 mL Eppendorf tube. The aqueous layer was overlayed with 0.1 volumes of 3 M sodium acetate and mixed gently. This mixture was overlayed with 2 volumes of absolute ethanol and centrifuged at 12 000 rpm for 2 minutes to pellet the DNA. The remaining solution was removed, and the pelleted DNA dried at 37 °C and resuspended in 400 µL 1× TE buffer overnight at 4 °C.

3.1.3 16S rRNA gene sequencing

The 16S rRNA gene was amplified using the KAPA Taq ReadyMix Kit and the universal 16S rRNA primers F1 (5' – AGAGTTTGATCTGGCTAG-3') and R5 (5' – ACGGTACCTTGTTACGACTT-3') (Cook and Meyers, 2003). A PCR reaction was set up in 25 µL reaction volumes consisting of 12.5 µL 2× KAPA Taq ReadyMix, 9.5 µL PCR-grade H_2O, 1 µM forward primer, 1 µM reverse primer and 1 µL of template DNA. The BioRad T100 thermal cycler was used for the PCR amplification with the following cycling conditions: 2-minute initial denaturation at 96 °C, followed by 30 cycles of denaturation at 96 °C for 30 sec, annealing at 56 °C for 30 sec and extension at 72 °C for 2 min. Thereafter a 5-minute final extension at 72 °C was completed. The sample was held at 10 °C until analysis.

PCR products were analysed by electrophoresis on a 1% (w/v) agarose gel which contained 0.5 µg/mL of ethidium bromide to ensure that the fragments amplified were of the correct size. In each well 10 µL of amplified product with 1 µL of tracking dye was loaded. Five µL KAPA universal DNA ladder was included for size determination. This gel was viewed using the BIO RAD Molecular Imager® Gel DocTM XR+ Imaging System.

3.1.4 Amplicon purification and sequence analysis

Successful amplicons at small-scale (25 µL) PCR were subjected to large-scale PCR (50 µL) and verified by 1% (w/v) agarose gel electrophoresis (as described above). Amplicons were purified using an MSB® Spin PCRapace kit according to the manufacturer's instructions. DNA concentration was measured via Nanodrop (Jenway, Model: Genova Nano, manufactured by Bibby Scientific Ltd.). Sanger sequencing was performed by Inqaba Biotech on an ABI 3500XL Genetic Analyzer. Sequence information was returned as a chromatogram and edited using BioEdit Sequence Alignment Editor and submitted to NCBI BLAST and EzBioCloud for the determination of the closest phylogenetic neighbour.

3.2 Enzyme Production

I. Preparation of amplicons of interest for cloning

A gradient PCR was applied using the KAPA Taq ReadyMix Kit with the designed DyP-primers for each strain (Table 3.2). The initial PCR reaction was set up in 25 µL reaction volumes consisting of 12.5 µL 2× KAPA Taq ReadyMix, 8.7 µL PCR-grade H_2O, 1 µM forward primer, 1 µM reverse primer, 0.8 µL dimethyl sulfoxide (DMSO) and 1 µL of template DNA. The BioRad T100 thermal cycler was used for the PCR amplification with the following cycling conditions: 2-minute initial denaturation at 96 °C, followed by 30 cycles of denaturation at 96 °C for 30 sec, annealing at 56 °C-72 °C for 30 sec and extension at 72 °C for 2 min. Thereafter a 5-minute final extension at 72 °C was completed. The sample was held at 10 °C until analysis.

PCR products were analysed by electrophoresis on a 1% (w/v) agarose gel (as previously described). Successful amplification of amplicons at small scale PCR was subjected to large-scale PCR of 50 µL reactions. Amplicons were purified using an MSB® Spin PCRapace kit according to the manufacturer's instructions, and DNA concentration measured via Nanodrop (Jenway, Model: Genova Nano, manufactured by Bibby Scientific Ltd.) (Table 3.2).

Table 3.2: The strains, primers, and predicted size (base pairs, bp) for the amplification of genes annotated as DyP-type peroxidases.

Strains	Forward and Reverse Primers	Predicted amplicon size (bp)
151: ***Streptomyces sp.***	5' attcatatgatggaccgtacggtgagccgg 3' 5' attctcgagcagtgactccatgaggtcctg 3'	1209
88S: ***Streptomyces sp.***	5' attcatatgatggctgaacagaccgagatgac 3' 5' attctcgaggccctccagcagacgctgtc 3'	1239
30-1: ***Micromonospora* sp. 30-1**	5' attcatatgatgaccggcaggcgggtgagc 3' 5' attctcgaggccgagcagtggagagccga 3'	1218
HMC10: ***Nonomuraea candida* HMC10^T**	5' attcatatgatgatcacccgcagagggctct 3' 5' attctcgagggccagcagcgactccccg 3'	1131
CZH20: ***Nocardia gamkensis* CZH20^T**	5' attcatatggtggctgagcggaacggaccg 3' 5' attctcgagcgcctcgaacagtgattgccc 3'	1212
S129: ***Streptomyces sp.***	5' attcatatgatgcctgaccagtcccttcc 3' 5' attctcgagcccctccagcaacttctgcc 3'	1299
SPR: ***Streptomyces polyantibioticus* SPR^T**	5' attcatatgatgtctgagaaccacgacgcga 3' 5' attctcgagggccaggtcgaaccggtgg 3'	1284

II. Double digestion of amplicons of interest

A double digest was performed on DyP-type amplicons and pET20b(+) using *Nde*I and *Xho*I (New England BioLabs). Each 50 µL reaction contained the following components: 1 µg DNA, 5 µL 10× CutSmart Buffer (New England BioLabs), 1 µL *Nde*I, and made up to 50 µL with dH_2O adjusting for the *Xho*I to be added thereafter. The procedure commenced by activating the enzyme in a heating block (Hangzhou Allsheng Instruments Co., Ltd.) at 37

°C for 30 minutes and inactivating it at 65 °C for 20 minutes and placed on ice. The addition of 1 µL *Xho*I followed, and the enzyme was again activated in a heating block (Hangzhou Allsheng Instruments Co., Ltd.) at 37 °C for 30 minutes and inactivated at 65 °C for 20 minutes. The same procedure was followed for pET20b(+). Digests were analysed on a 1% (w/v) agarose gel and an undigested plasmid was run as control. Digests from both DyP-type genes and pET20b(+) were cut out of the agarose gel and purified via gel purification (NucleoSpin® Gel and PCR Clean Up, Macherey-Nagel) as per the manufacturer's instructions.

III. Ligation of vector with plasmid

For ligations, the LigaFast™ Rapid DNA Ligation System (New England Biolabs) was used as per the manufacturer's instruction and a 1:3 molar ratio of vector to insert was used. To calculate the amount of insert required the following formula was used:

$$\frac{\textbf{ng vector} \times \textbf{kb size of insert}}{\textbf{kb size of vector}} \times \frac{\textbf{molar ratio of insert}}{\textbf{vector}} = \textbf{ng of insert}$$

IV. Transformation of the ligated plasmid

The plasmid-insert ligations were transformed into *Escherichia coli* JM109 (Promega). Competent cells (*E. coli* JM109) were removed from the -80 °C freezer and allowed to thaw on ice for 5 minutes. Two µL of the ligation were mixed with 50 µL of competent cells and the tube was placed immediately on ice for 20 minutes. The cells were heat-shocked in a heating block (Hangzhou Allsheng Instruments Co., Ltd.) for 25 seconds at 42 °C and immediately placed on ice for 2 minutes. Four-hundred and fifty µL of Super Optimal broth with Catabolite repression (SOC) media [in 90 mL of dH_2O: 2.0 g Tryptone, 0.5 g Yeast Extract, 1 mL NaCl (1M), 0.25 ml KCl (1M), 1 mL Mg^{2+} (2M), 1 mL glucose (2M)] was added to each transformation reaction and allowed to incubate for 1 hour at 37 °C, shaking at 180 rpm. One hundred µL of the transformed mixture was spread-plated onto LB agar plates (for 300 mL: 1.5 g Tryptone, 1.5 g NaCl, 0.75 g Yeast Extract, 2.25 g Agar Bacteriological) supplemented with 100 µg/mL filter-sterilised ampicillin and incubated

overnight at 37 °C. Controls included SOC medium, *E. coli* JM109 (no plasmid), and *E. coli* JM109 with pET20b(+).

Colonies formed on the LB-agar plates overnight were subjected to colony PCR with their specific DyP-type primers to observe positive transformation. A small-scale colony PCR of 25 µL was conducted with the following components: 12.5 µL 2× KAPA Taq ReadyMix, 9.5 µL PCR-grade H_2O, 1 µM forward primer, 1 µM reverse primer and 1 µL of transformed DNA (single colony picked and mixed into 20 µL dH_2O). The BioRad T100 thermal cycler was used for the PCR amplification with the conditions set for each DyP-type containing strain as mentioned in preparation of amplicons of interest for cloning (3.2.*I*) as followed. PCR products were analysed by electrophoresis on a 1% (w/v) agarose gel which contained 0.5 µg/mL of ethidium bromide to ensure that the fragments amplified were of the correct size, and were viewed using the BIO RAD Molecular Imager® Gel DocTM XR+ Imaging System. Colonies which had been correctly transformed were grown overnight at 37 °C on fresh plates and plasmid purification followed as per manufacturer's instructions (NucleoSpin® Gel and PCR Clean Up, Macherey-Nagel). These purified plasmids were transformed into *E. coli* BL21 (DE3) (Novagen™), Rosetta™ (DE3) PLysS (Novagen™), SHuffle® T7 (NEB), and ArcticExpress RP (Agilent) following the same process as mentioned above.

IV. Production of DyP-type peroxidase on small scale

All successful constructs were subjected to protein expression on small scale. Protein expression was conducted with four different hosts within four different media: Luria Bertani (LB) broth, 2× YT, Terrific Broth, and Auto Induction media (Appendix C). Each medium was supplemented with 100 µg/mL ampicillin and an additional antibiotic was supplemented to each medium corresponding to the specific host; therefore, media for the growth of Rosetta™ (DE3) pLySs was supplemented with 34 µg/mL chloramphenicol, SHuffle® T7 was supplemented with 25 µg/mL spectinomycin, and for ArticExpress RP was supplemented with 20 µg/mL gentamycin.

Overnight cultures were prepared by inoculating 50 µL of expression hosts: pET-DyP-*E. coli* BL21 (DE3), pET-DyP-Rosseta™ (DE3) pLysS, pET-DyP-SHuffle® T7 and pET-DyP-ArcticExpress RP in 5 mL Luria Bertani (LB) broth, 2× YT, Terrific Broth and ZY – Auto

Induction media (pre-culture grown in ZY and main cultures grown in Auto Induction media). For the rest of this study, in the protein expression and purification section the protein expression hosts will be referred to as BL21 instead of *E. coli* BL21 (DE3), R instead of Rosseta™ (DE3) pLysS, ST7 instead of SHuffle® T7 and AE instead of ArcticExpress RP. Knowing that these constructs were transformed into *E. coli* JM109 therefore the cultures will be named Sample_DyP_Expression Host_Expression media, E.g. CZH20_DyP_BL21_LB (unless stated otherwise).

The cultures were incubated overnight at 37 °C, shaking at 160 rpm on an orbital shaker. Twenty µL of the overnight culture was transferred to 20 mL LB (containing 100 µg/mL ampicillin and their respective antibiotic dependent on the host) and allowed to grow until an OD600nm measurement of 0.6 was reached (monitored using a Rayleigh UV-9200 Spectrophotometer, Beijing Rayleigh Analytical Instrument Corp). Overexpression of the DyPs was induced by the addition of isopropyl β-D-1-thiogalactopyranoside (IPTG) to a final concentration of 1 mM once the OD600nm reached 0.6, except for the cultures growing in Auto Induction Medium. The culture was then incubated overnight at 22 °C, shaking at 160 rpm. Samples that exhibited the best expression in their host and the desired medium were scaled up to 200 mL of protein expression. Induction temperatures were also tested, which ranged from 15 °C, 25 °C, 30 °C and 37 °C.

V. SDS-PAGE Analysis

A 12.5% (w/v) resolving gel and 5% (w/v) stacking gel was used for the separation of the proteins of interest. Gels were prepared and poured according to the Laemmli SDS-PAGE protocol (Laemmli, 1970) (Appendix C).

Twenty µL of each crude DyP-type peroxidase sample was mixed with 5 µL of 5× sample buffer containing dithiothriotol (DTT) [3.1 mL 1 M Tris-HCl (pH 6.8), 5 mL glycerol, 0.5 mL bromophenol blue, 5 mM DDT, and 1.4 mL water]. The 25 µL samples were boiled for 10 minutes and loaded onto the gel. To the first well of the gel, 10 µL of a Colour Prestained Protein Standard, Broad Range (New England BioLabs Inc.) was loaded and 20 µL of the samples were subsequently loaded into the other wells. The gel was run at 180 V for 45 minutes in electrophoresis buffer [mix 3.0 g Tris (25 mM), 14.4 g glycine

(192 mM) and 1 g SDS in 1 litre water; final pH should be 8.8] at room temperature (22 °C). The gel was stained overnight with Coomassie Brilliant Blue R-250 solution (2.5 g Coomassie Brilliant Blue R-250, 450 mL methanol, 100 mL acetic acid and 450 mL distilled water) on a rocking shaker. Destaining was performed with the same solution with the omission of Coomassie Brilliant Blue R-250 for 1 hour on a rocking shaker and placed in distilled water for 30 minutes before visualization on the BIO RAD Molecular Imager® Gel DocTM XR+ Imaging System.

VI. Production of DyP-type peroxidase on larger scale (200 mL)

Overnight cultures were prepared by inoculating 100 µL of *E. coli* BL21 containing pET_DyP_desired host (the optimal expression occurred in ArcticExpress RP (Agilent) in Auto Induction media) in 25 mL ZY medium. The cultures were incubated overnight at 37 °C, shaking at 160 rpm on an orbital shaker. Two mL of the overnight culture was transferred to 200 mL Auto Induction media (containing 100 µg/mL ampicillin and 20 µg/mL gentamycin) and allowed to proliferate until an OD600nm measurement of 0.6 on a spectrophotometer (Rayleigh UV-9200 Spectrophotometer, Beijing Rayleigh Analytical Instrument Corp) was reached. An uninduced control was also prepared in the same manner with the omission of 50× 5052 for each enzyme variant.

Cells were harvested by an updated Cell Lysis by Freeze-Thaw treatment (Promega). Cells were harvested by centrifugation at 5000 rpm for 10 minutes using a Multifuge 3SR+ centrifuge (Thermo Scientific). The soluble fraction was discarded, followed by the addition of 10% (v/v) culture-volume of 0.1 M potassium phosphate buffer (pH 7.3). The cell suspension was supplemented with 1 mg/mL lysozyme from chicken egg (Sigma-Aldrich) and vortexed till the mixture was homogenised. The cell suspension was freeze-thawed for five 15-minute cycles at -80 °C and 37 °C in a waterbath. After these cycles, the cell suspension was sonicated on ice for 5 minutes (15 seconds bursts, 15 second rest) (VirSonc Ultrasonic Cell Disrupter 100, United Scientific (Pty) Ltd.). The now sonicated cell suspension was further centrifuged at 13 500 g for 45 minutes (Multifuge 3SR+ centrifuge, Thermofisher Scientific) after which the soluble fraction was transferred to a clean 50 mL sterile Greiner tube and the insoluble fraction was supplemented with 2 mL Urea (8M). Both the soluble and insoluble fraction was supplemented with 0.2 U/mL

RNAse1 (Thermofisher Scientific) and 0.3 U/mL DNase1 (Thermofisher Scientific). These fractions were subjected to SDS-PAGE analysis as described above and thus characterisation of successful expression followed.

VII. Enzyme Characterisation

a. Protein quantification using Bradford's Assay

A 1 mg/mL stock solution of bovine serum albumin (BSA) was prepared by dissolving 10 mg crystalline BSA in 10 mL 10 mM potassium sulphate buffer (pH 7.3). Working standards for the standard curve were prepared from 100 µg/mL BSA, as seen in Table 1E (Appendix E).

The Bradford Assay was performed in a 96-well microtitre plate. Twenty µL of either the relevant standard or sample was aliquoted into individual empty wells (in triplicate) and 180 µL of Bradford's Reagent (Sigma-Aldrich) was aliquoted to these wells containing either the relevant standard or sample. The reaction was left to stand for 2 minutes, and the absorbance measured at 595 nm using a Molecular Devices SpectroMax M2. A standard curve was constructed by plotting absorbance of standards versus their respective concentrations. The concentration of each sample was estimated by using the regression line equation from the standard curve.

b. Enzyme activity using the 2,4-Dichlorophenol (DCP) assay

All solutions and buffers were made prior to experimentation and the reagents used were supplied by Sigma-Aldrich unless stated otherwise. Five mL of each reagent (25 mM 2,4-DCP, 16 mM 4-aminoantipyrine, 100 mM potassium phosphate buffer (pH 7.3), 50 mM hydrogen peroxidase) was placed into a reservoir to make up the reaction mixture using 2,4-DCP as a substrate. Five hundred µL of each enzyme test sample (including controls, expression media without transformed plasmid) were pipetted into 1.5 mL tubes respectively and centrifuged at 10 000 rpm for 5 minutes. Fifty µL of each supernatant (from samples) was pipetted into a microtitre plate and 200 µL of the substrate reaction mixture added using a digital micropipette into the wells containing the 50 µL of test samples. The absorbance was read at 492 nm over a 5-minute period and at room temperature (22 ± 3°C) using a Molecular Devices SpectroMax M2. Horseradish

peroxidase (HRP) served as a positive control (1:100 dilution with 100 mM potassium phosphate buffer (pH 7.3)).

Additionally, protein concentration (mg/mL) and activity (U/mL) of the enzyme sample was used to calculate the specific activity (U/mg), which was calculated as follows:

$$\text{Activity} = \frac{\Delta Abs/min}{\varepsilon \text{ in } mM^{-1}\ cm^{-1}} \times \frac{\text{assay volume (mL)}}{\text{enzyme volume (mL)}} \times \text{dilution}$$

Specific activity (U/mg) = activity (U/mL)/protein concentration (mg/mL)

The extinction coefficient used for the 2,4-DCP substrate, took into account the shorter pathlength in microtiter plate readers vs that of standard spectrophotometers. One unit was defined as the amount of enzyme required to oxidize 1 μmol of substrate in one minute under the conditions used in this study. Specific activity is defined here as the amount of enzyme required to convert 1 micromole of substrate per minute per milligram of protein (μmol/min/mg) at the conditions of the experiment.

3.3 Purification of DyP-type Peroxidases

Size-exclusion chromatography was used for the purification of the enzymes of interest whereby a 75 mL size-exclusion column was prepared by heating 8.5 g of Sephadex G-75 beads in 50 mM potassium buffer (pH 7.0) at 90 °C for 2 hours to allow the beads to swell. A glass chromatography column was pre-rinsed with 10 mM potassium phosphate buffer (pH 7.0) and once the bead-slurry was cooled, poured into the glass column. Beads were allowed to settle, and the column was equilibrated with three column volumes of 10 mM potassium phosphate, 300 mM NaCl (pH 7.5). Furthermore, the DyP-samples were purified via fast performance liquid chromatography (FPLC) using an AKTAprime™ system (Amersham-Biosciences). Four mL of enzyme sample was applied to a 120 mL HiLoad 16/60 Superdex 75 chromatography column (Sigma-Aldrich). Separation of the samples was performed using a flowrate of 0.800 mL/min and 50 mM potassium phosphate buffer (pH 7.5) as the mobile phase. Fractions of 2 mL were collected and subjected to SDS-PAGE analysis as previously described. Identification of purified

fractions were pooled together and incubated with trace salts (per litre: 1 g $FeSO_4.7H_20$; 0.9 g $ZnSO_4$; 0.2 g $MnSO_4.7H_2O$) overnight at 4 °C. These fractions collected were analysed for protein concentration (Bradford's Protein Assay) and peroxidase activity [2,4-dichlorophenol (DCP)]. Fractions with the highest activity were pooled together and final specific activity was determined.

3.4 Biochemical Characterisation

All characterisation studies were performed using the FPLC-partially purified and purified DyP-fractions using the SpectraMax-I3 and the SoftMax® Pro 7 Data Acquisition and Analysis Software (Molecular Devices).

3.4.1 Optimum pH

The optimum pH for the oxidation of 2,4-DCP was determined from pH 3 to 9, in increments of 0.5 pH units for each buffer (50 mM) and tested at room temperature (25±2 °C). *Legionella* Acid Buffer (KCl-HCl) pH 2.0, potassium dihydrogen phosphate-hydrochloric acid buffer pH 3.0, sodium acetate buffer pH 3.0-5.5; potassium phosphate buffer pH 6.0-7.5, and Tris-HCl buffer pH 8.0-9.0, were used in this study.

3.4.2 Optimum Temperature

The optimum temperature for the oxidation of 2,4-DCP was determined by varying temperatures ranging from 25 °C to 45 °C in 5 °C intervals. The partially purified and purified DyP fractions were evaluated for optimum temperature in their respective optimum pH buffers from the previous assay.

3.4.3 Effect of Inhibitors, Reducing Agents, and Metal Ions

The effect of the following compounds on the enzyme's ability to oxidise 2,4-DCP were evaluated: NaCl, L-cysteine, sodium dodecylsulphate (SDS), sodium metabisulphite, EDTA, L-ascorbic acid, hydrogen peroxide, and sodium azide (0 to 50 mM). The effect of the following metal ions was also assessed: $CaSO_4$, $CoSO_4$, CuCl, FeCl, MgCl, MnCl and ZnCl each at 0.1, 0.5, 1, 2, and 5 mM concentrations. The enzymes were incubated in the presence of the compound or metal ion for 1 hour before being assayed for DyP activity at optimum temperature and pH.

3.4.4 Effects of Organic Solvents on Enzyme Activity

The effect of the following organic solvents on the ability of dye decolourising peroxidase to oxidise 2,4-DCP was assessed: ethanol, methanol, acetone, acetonitrile, dimethylsulfoxide (DMSO), and 2-propanol. The organic solvent was added to the 2,4-DCP assay mix (at 10, 20, 30 and 40%, v/v, concentration) prior to running the assay (35 °C, pH 7.5 for purified and pH 7.0 for partially purified dye-decolourising peroxidase). The control sample did not contain any organic solvent for the duration of the characterisation.

3.4.5 Enzyme Kinetics

The kinetic parameters V_{max}, K_m, K_{cat} were determined for the oxidation of 2,4-DCP by the use of non-linear regression analysis (Michaelis-Menton). Data was analysed using GraphPad version 10 (www.graphpad.com – Accessed on 22 September 2023).

3.4.6 Spectral Characteristics

A complete wavelength scan, 200 nm to 700 nm, of the partially purified and purified *Nocardia gamkensis* strain CZH20^T DyP was acquired.

3.4.7 Dye Decolourisation Assays

To identify the ability of the partially purified and purified CZH20^T DyP to decolourise dyes, 100, 75, 25, 10 and 1 µM solutions of each dye were prepared in 50 mM sodium acetate buffer (pH 3.5), 50 mM sodium acetate buffer (pH 5.5), 50 mM potassium phosphate buffer (pH 7.5), and 50 mM Tris-HCl buffer (pH 9.5). Two hundred µL of dye solution and 50 µL 50 mM H_2O_2 (prepared in respective buffers) were aliquoted into a 96 well microtitre plate in triplicate and 50 µL of a 1 U/mL enzyme solution was added to each well. The decrease in absorbance was monitored over a 6-hour period, scanning at 30 minute increments, as well as 24 hours at ambient temperature (25±2 °C). Oxidation of Reactive Blue 4 (anthraquinone dye) was monitored at 597 nm (ε = 4200 M^{-1} cm^{-1}), Reactive Black 5 (azo dye) at 598 nm (ε = 37 200 M^{-1} cm^{-1}), and Azure B (thiazine dye) at 605 nm (ε = 8700 M^{-1} cm^{-1}).

CHAPTER FOUR
RESULTS

4.1. Actinobacterial genomes

Twenty-one actinobacterial strains from various sources such as soil, wild garlic as well as rooibos were isolated from sampling sites ranging from South Africa to Zambia (Table 3.1). These strains were cultivated as previously described and their genomic DNA extracted using the method described by Mandel and Marmur (1968). Different sequencing technologies, including Illumina MiSeq, as well as Roche 454 were used to sequence the genomes (NGS Facility, University of the Western Cape (UWC)). These genomes were assembled using the A5-miseq pipeline (Coil *et al.*, 2015) and annotated using the online server RAST (Rapid Annotations using Subsystems Technology) (Aziz *et al*., 2008).

4.1.1 Genome mining and peroxidase sequence analyses

The annotated genomes were analysed for the presence of genes encoding for peroxidases, specifically those annotated as DyP-type peroxidases. The predicted amino acid sequences were analysed by BLASTp (NCBI) to identify related peroxidase sequences (Passardi *et al.,* 2007), while SnapGene® Viewer 5.1.7 was used to determine the amino acid content of the genome-mined peroxidases. Furthermore, for the DyP-type peroxidase class assignment/grouping the protein sequences were submitted to PRED-TAT for the identification of the signal peptide sequence typically associated with the twin arginine translocation (TAT)-pathway (Melén *et al.,* 2003). Twenty-six DyP-type peroxidase sequences were identified from the 21 genomes analysed. These sequences were used in a multiple-sequence alignment with the sequence of the well-established industrial DyP-type peroxidase from *Thermobifida fusca* (accession no. NC_007333.1). The amino acid sequences were aligned using the alignment function of MEGA 6 (Tamura *et al.,* 2013) and was used to generate a Neighbour-Joining tree with the DyP-type peroxidase from *Bacillus subtilis* (accession no. KFK78021.1) as a non-actinomycete representative. The resulting genome mining and phylogenetic analysis showed that the sequences formed two distinctive clades, the top clade was represented by 11 DyP-type peroxidases from

Streptomyces species (Figure 4.1), while the bottom clade was represented by 15 DyP-type peroxidases mostly mined from non-streptomycete genomes (Figure 4.2). Detailed information on the nucleotide sequences exhibiting the highest sequence similarities to the DyP-type peroxidases identified in this study are summarised in Tables 4.1 and 4.2.

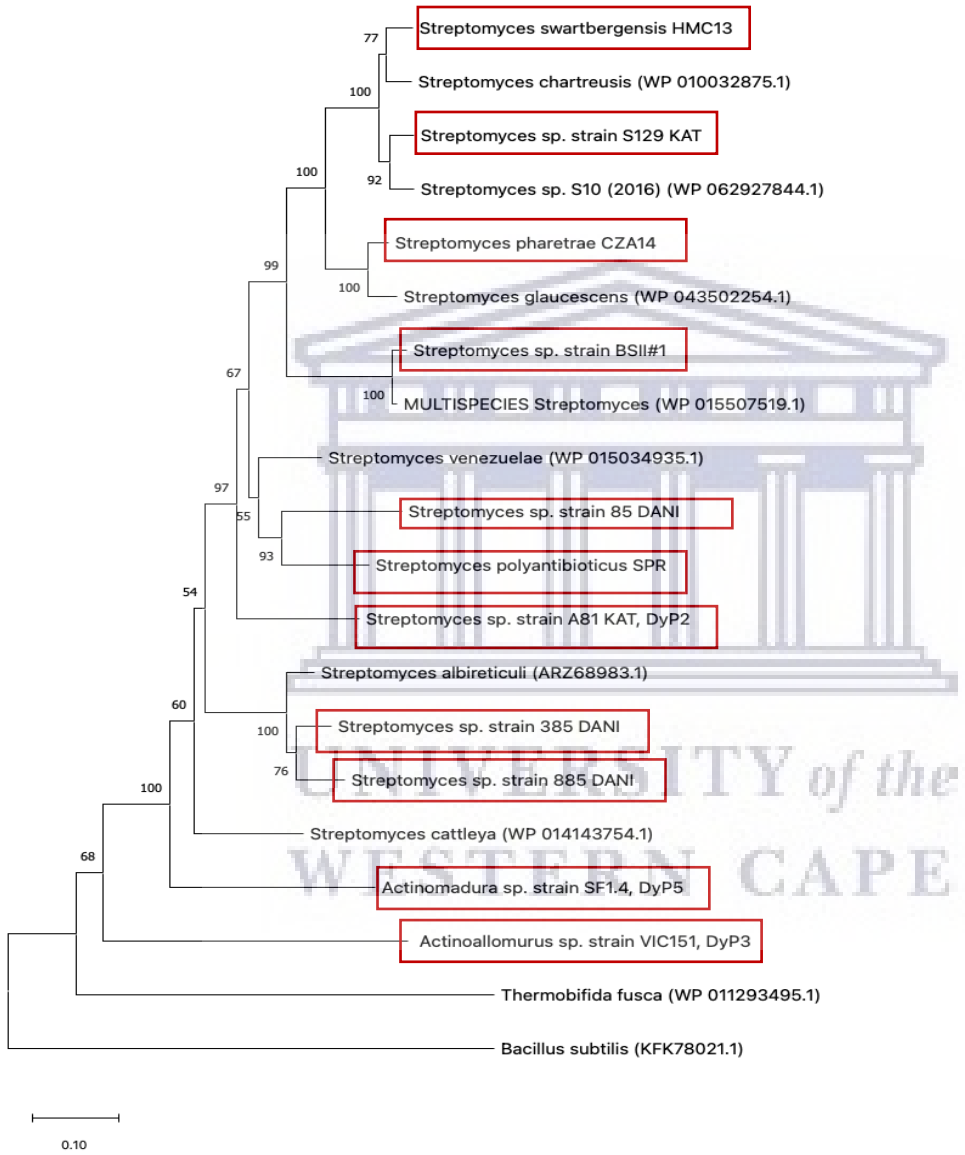

Figure 4.1: Phylogenetic tree of 11 DyP-type peroxidase sequences aligned to *Thermobifida fusca* DyP-type peroxidase (accession no. NC_007333.1) forming the top clade of the main phylogenetic tree. The tree was generated using the Neighbour Joining method. Sequences identified in this study are highlighted in red.

Table 4.1: Nucleotide sequences with the highest predicted sequence similarity to the DyP-type peroxidases presented in Figure 4.1. The presence of a signal peptide and predicted amino acid sequence length of the genome-mined sequences are also indicated.

Source of DyP-type peroxidase (this study)	Top BLAST hit	Accession No.	% sequence identity	Signal peptide present in predicted amino acid sequence (this study)	Predicted amino acid sequence length (this study)
HMC13	*Streptomyces chartreusis* NRRL 3882	LT963352.1	100	Tat signal peptide predicted. Reliability score: 0.992	429
S129	*Streptomyces* sp. S10(2016), complete genome	CP015098.1	100	Tat signal peptide predicted Reliability score: 0.994	432
CZA14	*Streptomyces glaucescens* strain GLA.O, complete genome	CP009438.1	100	Tat signal peptide predicted Reliability score: 0.969	431
BSII#1	*Streptomyces albus* J1074, complete genome	CP004370.1	100	Tat signal peptide Reliability score: 0.994	425
385	*Streptomyces venezuelae* ATCC 10712 complete genome	FR845719.1	100	Tat signal peptide predicted Reliability score: 1.000	443

Source of DyP-type peroxidase (this study)	Top BLAST hit	Accession No.	% sequence identity	Signal peptide present in predicted amino acid sequence (this study)	Predicted amino acid sequence length (this study)
SPR^{T}	*Streptomyces venezuelae* ATCC 10712 complete genome	FR845719.1	100	Tat signal peptide predicted Reliability score: 0.999	427
A81 DyP 2	*Streptomyces violaceoruber* strain S21, complete genome	CP020570.1	100	Tat signal peptide predicted Reliability score: 0.992	441

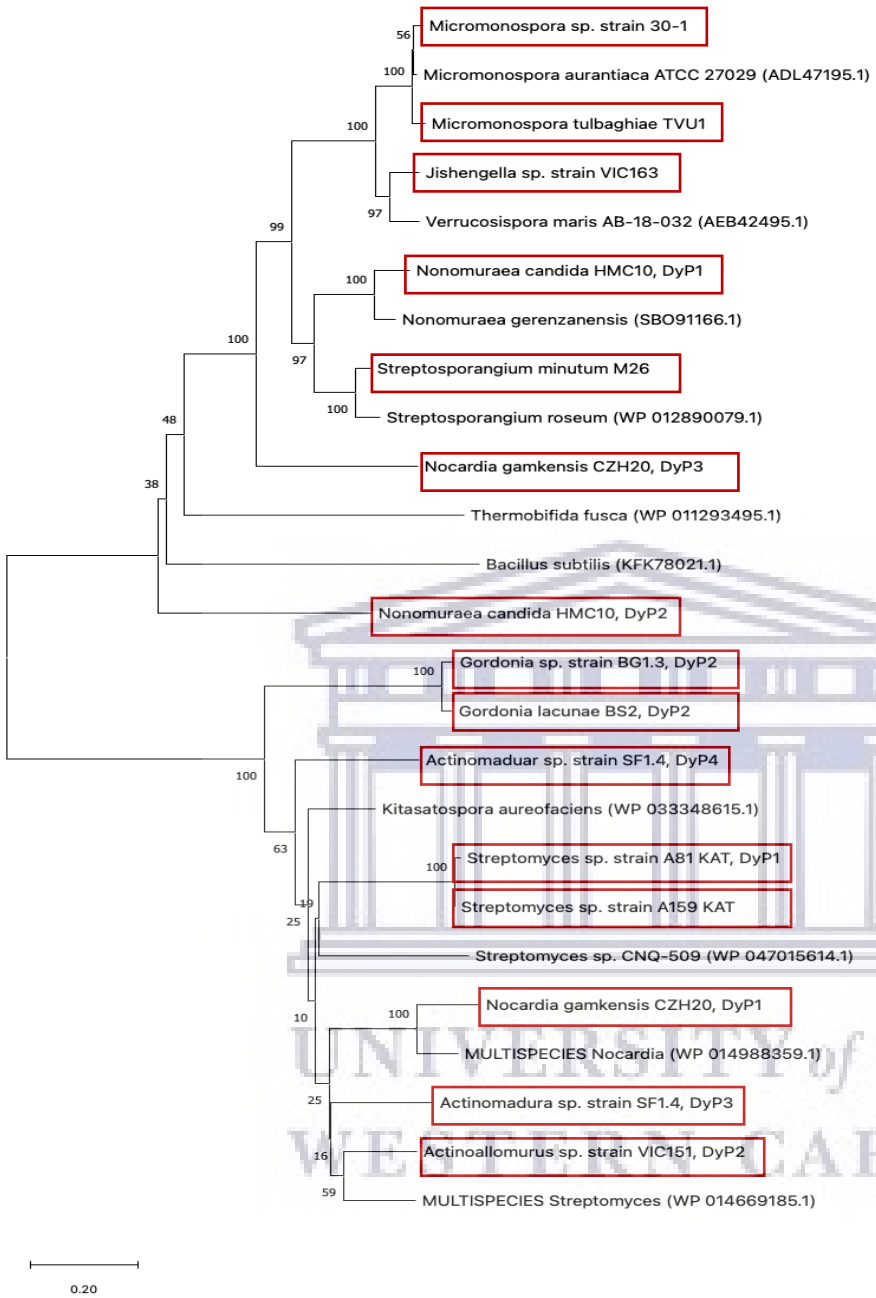

Figure 4.2: Phylogenetic tree of 15 DyP-type peroxidase sequences aligned to *Thermobifida fusca* DyP (accession no. NC_007333.1) forming the bottom, predominantly non-streptomycete clade of the main phylogenetic tree. The tree was obtained using the neighbour joining method. Sequences identified in this study are highlighted in red.

Table 4.2: Nucleotide sequences with the highest predicted sequence similarity to the DyP-type peroxidases presented in Figure 4.2. The presence of a signal peptide and predicted amino acid sequence length of the genome-mined sequences are also indicated.

Source of DyP-type peroxidase (this study)	Top BLAST hit	Accession No.	% sequence identity	Signal peptide present in predicted amino acid sequence (this study)	Predicted amino acid sequence length (this study)
151 Dyp 2	*Streptomyces hygroscopicus* subsp. *jinggangensis* TL01	CP003720.1	100	No signal peptide predicted. Reliability score: 0.251	360
CZH20^{T} DyP 1	*Nocardia brasiliensis* ATCC 700358, complete genome	CP003876.1	100	No signal peptide predicted. Reliability score: 0.709	353
SF 1.4 DyP 2	*Kitasatospora aureofaciens* strain DM-1 chromosome, complete genome	CP020567.1	100	Sec signal peptide predicted. Reliability score: 0.685	353
SF 1.4 DyP 4	*Streptomyces* sp. CNQ-509, complete genome	CP011492.1	100	No signal peptide predicted. Reliability score: 0.341	352

Source of DyP-type peroxidase (this study)	Top BLAST hit	Accession No.	% sequence identity	Signal peptide present in predicted amino acid sequence (this study)	Predicted amino acid sequence length (this study)
BG 1.3 DyP 2	*Gordonia* sp. KTR9	CP002907.1	100	No signal peptide predicted. Reliability score: 0.690	337
BS2 DyP 2	*Gordonia terrae* strain 3612 chromosome	CP016594.1	100	No signal peptide predicted. Reliability score: 0.552	334
A81 DyP 1	*Streptomyces violaceoruber* strain S21, complete genome	CP020570.1	100	No signal peptide predicted. Reliability score: 0.692	348
A159	*Streptomyces violaceoruber* strain S21	CP020570.1	100	No signal peptide predicted. Reliability score: 0.646	320
HMC10^{T} DyP 2	*Nocardia farcinica* IFM 10152 DNA, complete genome	AP006618.1	100	Tat signal peptide predicted	459

Source of DyP-type peroxidase (this study)	Top BLAST hit	Accession No.	% sequence identity	Signal peptide present in predicted amino acid sequence (this study)	Predicted amino acid sequence length (this study)
				Reliability score: 0.980	
CZH20^{T} DyP 3	*Nocardia brasiliensis* strain FDAARGOS_352 chromosome	CP022088.1	100	Tat signal peptide predicted. Reliability score: 0.979	403
HMC10^{T} DyP 1	*Nonomuraea* sp. ATCC 39727 isolate nono1 genome assembly, chromosome: I	LT559118.1	100	Tat signal peptide predicted Reliability score: 0.971	376
M26	*Streptosporangium roseum* DSM 43021, complete genome	CP001814.1	100	No signal peptide predicted. Reliability score: 0.744	316
163	*Verrucosispora maris* AB-18-032, complete genome	CP002638.1	100	Tat signal peptide predicted. Reliability score: 0.997	404

Source of DyP-type peroxidase (this study)	Top BLAST hit	Accession No.	% sequence identity	Signal peptide present in predicted amino acid sequence (this study)	Predicted amino acid sequence length (this study)
TVU1	*Micromonospora aurantiaca* ATCC 27029	CP002162.1	100	Tat signal peptide predicted. Reliability score: 0.964	408
30-1	*Micromonospora aurantiaca* ATCC 27029	CP002162.1	100	Tat signal peptide predicted. Reliability score: 0.973	405

The genome-mined sequences from the top clade (Figure 4.1) contained the majority of the class I DyP-type peroxidases. This is further confirmed by the PRED-TAT reliability score (Table 4.1). The PRED-TAT is a predictor tool used to predict the presence of TAT-signal peptides within enzymes. The most important features of this tool are that it is able to both predict Sec and TAT signal peptides, cleavage sites, as well as measure the reliability of its prediction, between a range of 0-1 (Melén *at al*., 2003). The higher the reliability measure, the higher the accuracy in identifying which signal peptide it is (Bagos *et al*., 2010).

For the bottom clade (Table 4.2), only a few sequences, namely HMC10^T DyP 1, HMC10^T DyP 2, CZH20^T DyP 3, 163, TVU1 and 30-1 are predicted to contain the TAT-signal peptide. Furthermore, the remaining sequences in Table 4.2 contain no signal peptides and their reliability measures ranged between 0.251 to 0.709 indicating a very low accuracy in the

signal peptide identification, as well as cleavage site confirmation. From this assessment eight sequences were selected for further study due to the presence of a TAT-pathway which is essential for the identification of class I (intermediate) DyP-type peroxidases (Table 4.3).

Table 4.3: Isolates selected for DyP-type peroxidase investigation in this study.

Isolate identification	TAT-pathway present
151 DyP3	✓
88S	✓
8S	✓
S129	✓
SPR^{T}	✓
HMC10^{T} DyP1	✓
CZH20^{T} DyP3	✓
30-1	✓

4.1.3 Genomic DNA isolation and 16S rRNA gene determination

Since the strains were obtained from various studies performed across two different laboratories, prior to the cloning of the DyP-type peroxidase genes of interest, the identity of the selected strains was confirmed through 16S rRNA gene sequence analysis. Edited sequences were submitted to BLAST and EzBioCloud for the determination of the closest phylogenetic neighbour (Table 4.4). The results confirmed the isolates cultivated were in agreement with the whole genome sequences provided by the NGS Facility, University of the Western Cape (Table 3.1).

Table 4.4: Identification of the eight strains selected for further study. Identification was based on the 16S rRNA gene sequence and results obtained from EzBiocloud and BLAST analyses.

Strain name	Identification based on 16S rRNA gene sequence analysis
151	*Streptomyces* sp.
88S	*Streptomyces* sp.
8S	*Streptomyces* sp.
S129	*Streptomyces* sp.
SPR^T	*Streptomyces polyantibioticus* SPR^T
HMC10^T	*Nonomureae candida* HMC10^T
CZH20^T	*Nocardia gamkensis* CZH20^T
30-1	*Micromonospora* sp. strain 30-1

4.2 Enzyme Production

4.2.1 Gene cloning

Primers for the amplification of the DyP-type peroxidases were designed in-house following the method described by Abd-Elsalam (2003) using the sequences annotated by RAST as templates (Table 3.2). Further evaluation of primer design was performed using DNA-MAN (Loenen, 2014) to identify whether the restriction enzymes used, *Nde*I and *Xho*I (New England BioLabs), were compatible for double digestion with the plasmid pET20b(+) (Ota *et al.,* 2007). DNA-MAN was also used to identify the optimal melting temperature for each DyP-type peroxidase primer pair designed (Table 4.5). Detailed information can be found in Supplementary Sheet A.

Table 4.5: The strains, identification of restriction enzymes, *Nde*I and *Xho*I, compatibility for double digestion and optimal annealing temperature (T_m) for amplification of genes annotated as DyP-type peroxidases.

DyP Strain identification	Restriction enzymes compatible (*Nde*I and *XhoI*)	Optimal annealing temperature (T_m in °C)
151_DyP3	✓	62
88S	✓	58
8S	✓	67
S129	✓	61
SPR^T	✓	60
HMC10^T_DyP1	✓	61
CZH20^T_DyP3	✓	65
30-1	✓	65

With the DyP-type peroxidase primers designed and the theoretical optimal annealing temperatures determined, a gradient PCR was conducted using the KAPA Taq ReadyMix Kit to test each primer set. Initially, a small-scale colony PCR (25 µL) reaction volume was used consisting of the components as described in the methodology section. The annealing temperature for the DyP-type peroxidase primers ranged from 56-72 °C. The samples were amplified and visualised on a 1% (w/v) agarose gel. Amplified DyP-type peroxidase genes for strains SPR^T, 30-1, and CZH20^T are highlighted in red, with the boxed area indicating the expected amplicon size (Figure 4.3).

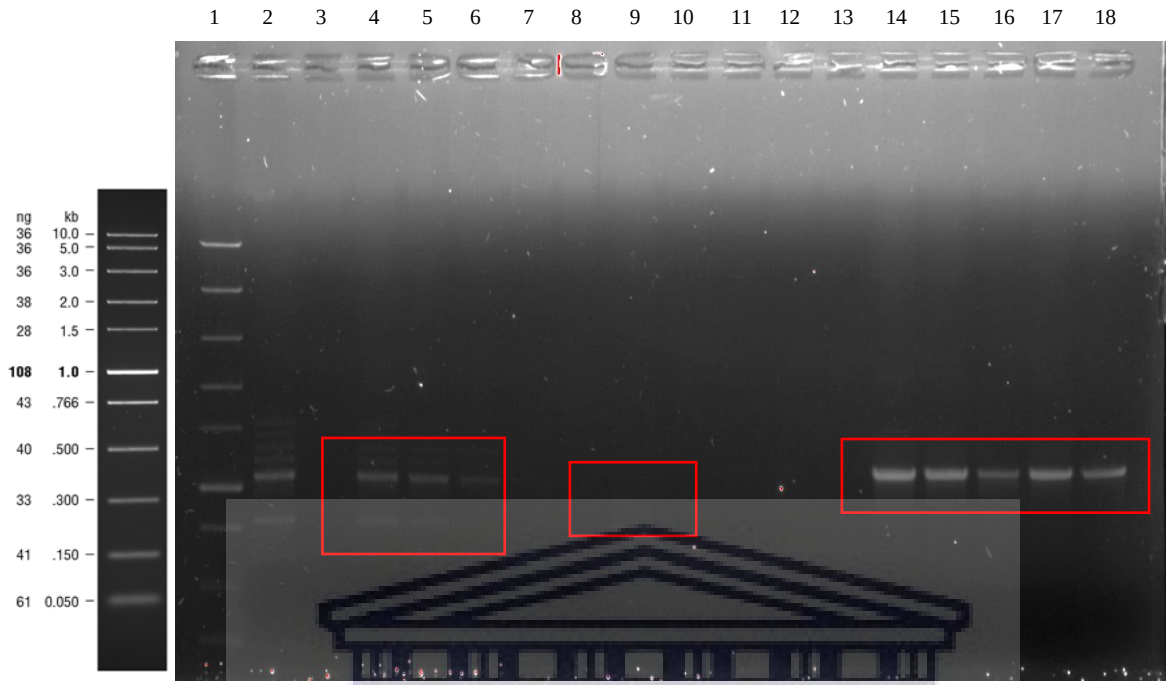

Figure 4.3: A gradient PCR (56-72 °C) for the amplification of the annotated DyP-type peroxidase genes of actinobacterial strains SPR^T, 30-1, and CZH20^T.

Lane 1: FAST DNA Ladder (New England Bio Labs®); Lane 2: Positive Control SPR^T – confirmed from a previous study at BTB Labs (60 °C); Lane 3: Negative Control; Lane 4: SPR^T (60 °C); Lane 5: SPR^T (60.9 °C); Lane 6: SPR^T (62.4 °C); Lane 7: SPR^T (64.5 °C); Lane 8: SPR^T (67.2 °C); Lane 9: 30-1 (64.5 °C); Lane 10: 30-1 (67.2 °C); Lane 11: 30-1 (69.0 °C); Lane 12: 30-1 (71.1 °C); Lane 13: 30-1 (72.0 °C); Lane 14: CZH20^T (64.5 °C); Lane 15: CZH20^T (67.2 °C); Lane 16: CZH20^T (69.6 °C); Lane 17: CZH20^T (71.1 °C); Lane 18: CZH20^T (72.0 °C).

Strains 885, HMC10^T and 85 were selected for the DyP-type peroxidase gradient PCR and visualised on a 1% (w/v) agarose gel. Amplified DyP-type peroxidase genes are highlighted in red, with the boxed area indicating the expected amplicon size (Figure 4.4 and Figure 4.5). Sample S129 showed no amplification and therefore only the seven samples were selected for gene cloning.

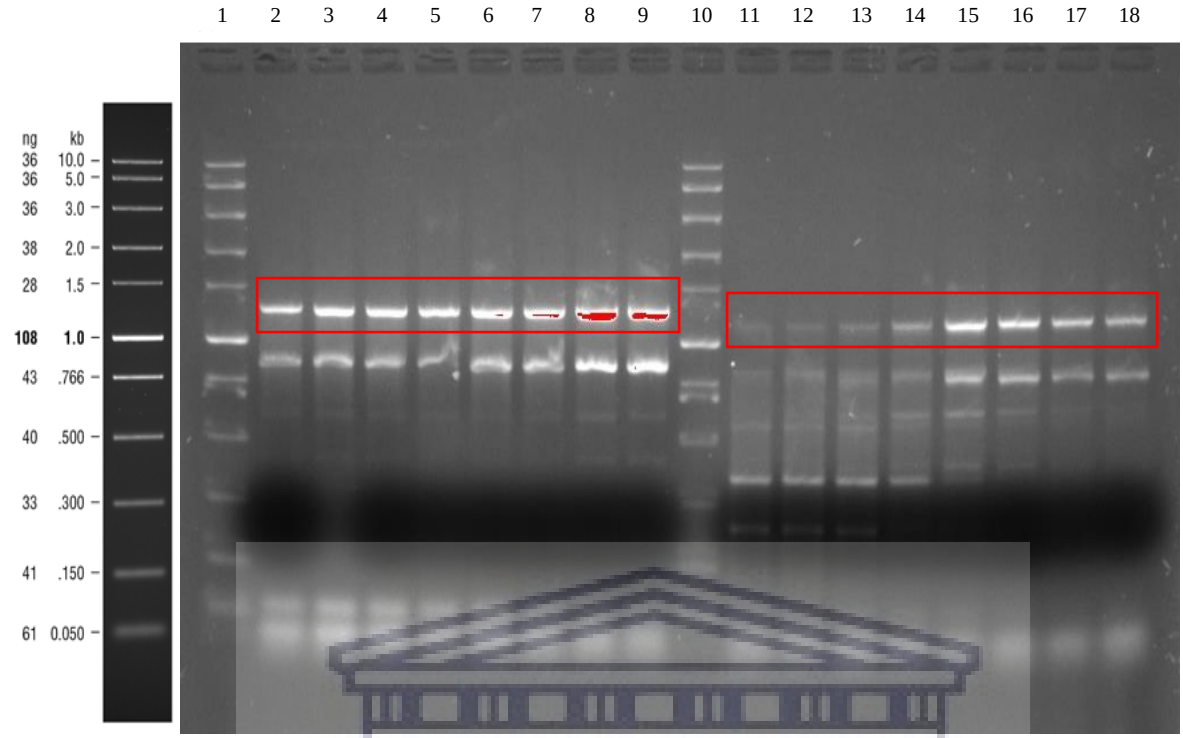

Figure 4.4: A gradient PCR (58-72 °C) for the amplification of the annotated DyP-type peroxidase genes of actinobacterial strains 885 and HMC10^{T}.

Lane 1: FAST DNA Ladder (New England Bio Labs®); Lane 2: 88S (58.0 °C); Lane 3: 88S (59.1 °C); Lane 4: 88S (61.5 °C); Lane 5: 88S (62.6 °C); Lane 6: 88S (63.9 °C); Lane 7: 88S (65.0 °C); Lane 8: 88S (66.1 °C); Lane 9: 88S (67.2 °C); Lane 10: FAST DNA Ladder (New England Bio Labs®); Lane 11: HMC10^{T} (58.0 °C); Lane 12: HMC10^{T} (59.1 °C); Lane 13: HMC10^{T} (61.5 °C); Lane 14: HMC10^{T} (62.6 °C); Lane 15: HMC10^{T} (63.9 °C); Lane 16: HMC10^{T} (65.0 °C); Lane 17: HMC10^{T} (66.1 °C); Lane 18: HMC10^{T} (67.2 °C).

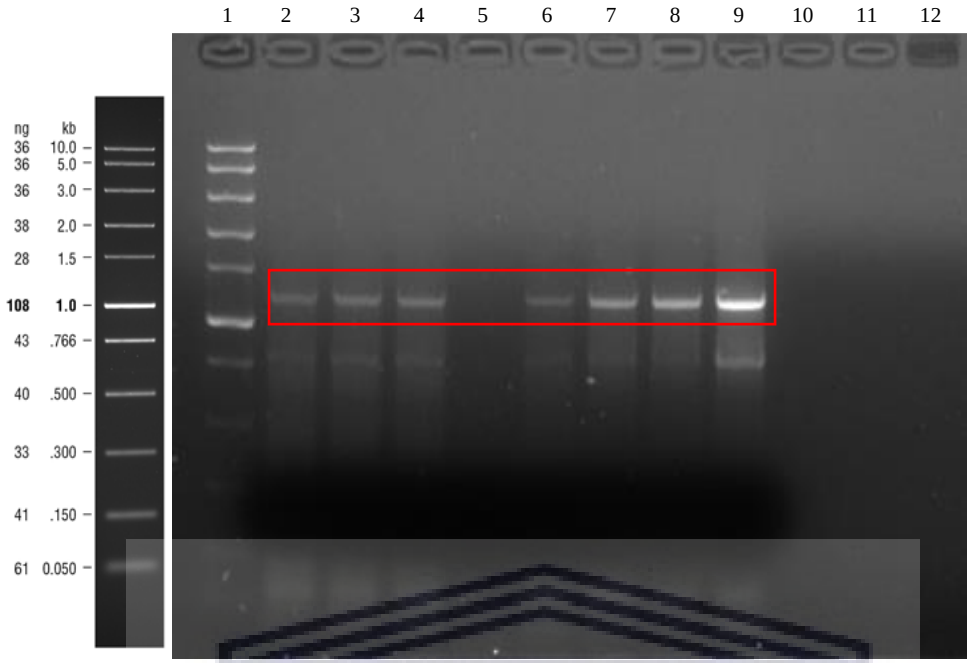

Figure 4.5: A gradient PCR (58-72 °C) for the amplification of the annotated DyP-type peroxidase genes of actinobacterial strain 85.

Lane 1: FAST DNA Ladder (New England Bio Labs®); Lane 2: 88S (58.0 °C); Lane 3: 88S (59.1 °C); Lane 4: 88S (61.5 °C); Lane 5: 88S (62.6 °C); Lane 6: 88S (63.9 °C); Lane 7: 88S (65.0 °C); Lane 8: 88S (66.1 °C); Lane 9: 88S (67.2 °C).

All successfully amplified actinobacterial DyP-type peroxidase amplicons were excised from the 1% (w/v) agarose gel and purified using the MSB® Spin PCRapace kit according to the manufacturer's instructions. Thereafter, the purified DNA was subjected to restriction digests.

4.2.2 Double digestion of DyP-type peroxidase amplicons

DyP-type peroxidase amplicons and pET20b(+) were double digested using the restriction enzymes *Nde*I and *Xho*I (New England BioLabs (NEB), (method described in section 3.2). Figure 4.6 shows that the amplicons for CZH20^T and 30-1 were successfully digested (bands highlighted in red).

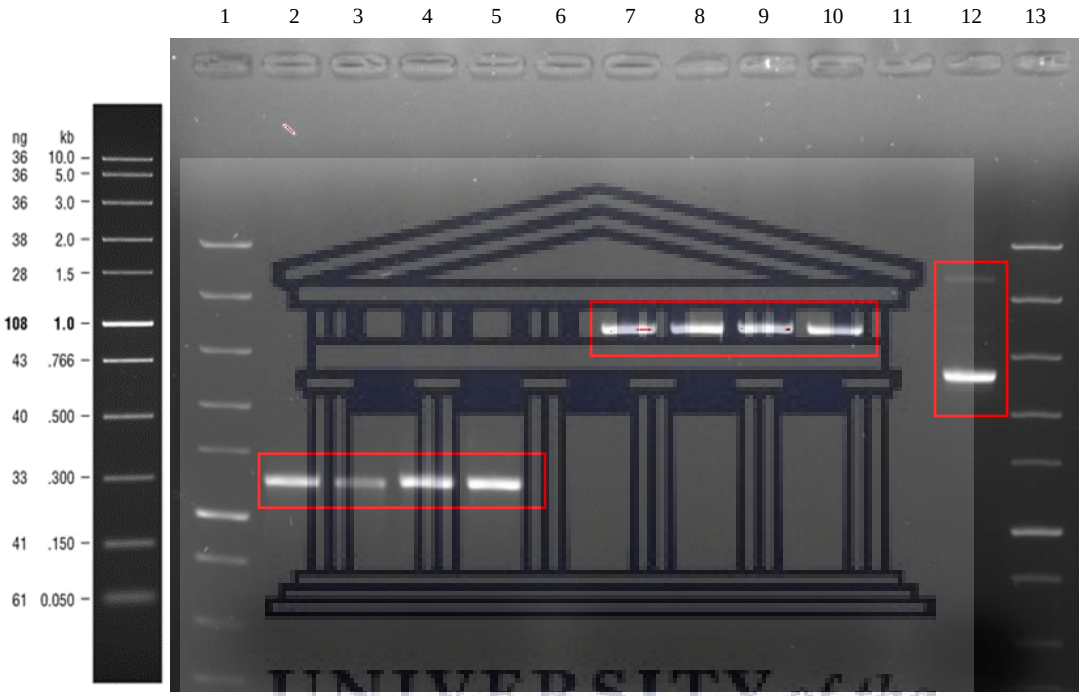

Figure 4.6: A double digest of CZH20^T and 30-1 amplified DyP-type peroxidase genes, pET20b(+) and undigested pET20b(+).

Lane 1: FAST DNA Ladder (New England Bio Labs®); Lane 2: Digested CZH20^T Lane 3: Digested CZH20^T; Lane 4: Digested 30-1; Lane 5: Digested 30-1; Lane 6: Digested 30-1; Lane 7: Digest pET20b(+); Lane 8: Digest pET20b(+); Lane 9: Digested pET20b(+); Lane 10: Digested pET20b(+); Lane 11: Negative control; Lane 12: Undigested pET20b(+); Lane 13: FAST DNA Ladder (New England Bio Labs®).

Similarly, the DyP-type peroxidase amplicons for 885, HMC10^T and 85 were subjected to digestion, which was also successful (Figure 4.7). Upon further investigation it was later identified that the primers designed for sample SPR^T was not of a DyP-type peroxidase but rather that of a catalase/peroxidase, thus SPR^T was not selected for further study.

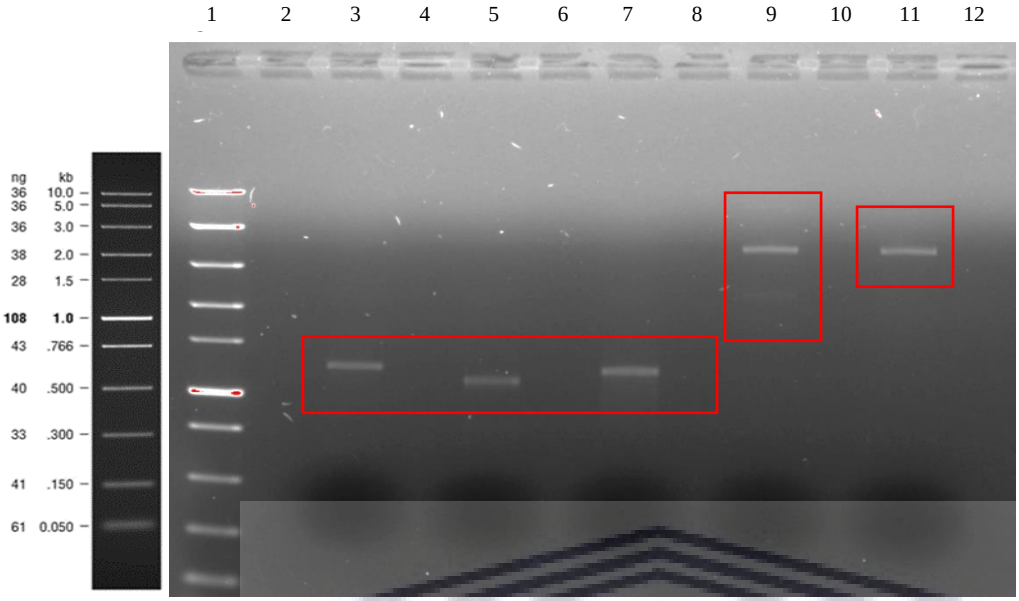

Figure 4.7: A double digest of 885, HMC10^{T} and 85 amplified DyP-type peroxidase genes, pET20b(+) and undigested pET20b(+).

Lane 1: FAST DNA Ladder (New England Bio Labs®); Lane 2: Blank Lane 3: Digested 885; Lane 4: Blank; Lane 5: Digested HMC10^{T}; Lane 6: Blank; Lane 7: Digested 85; Lane 8: Blank; Lane 9: Undigested pET20b(+); Lane 10: Blank; Lane 11: Digested pET20b(+); Lane 12: Blank.

4.2.3 Ligation and transformation

The six successfully amplified and digested DyP-type peroxidase amplicons were ligated to digested pET20b(+) using the LigaFast™ Rapid DNA Ligation System (New England Biolabs) and thereafter transformed into chemically-competent *E. coli* JM109 (Promega). Transformants were picked and subjected to a colony PCR with the primers designed for each specific DyP-type peroxidase and visualised on a 1% (w/v) agarose gel (Figure 4.8).

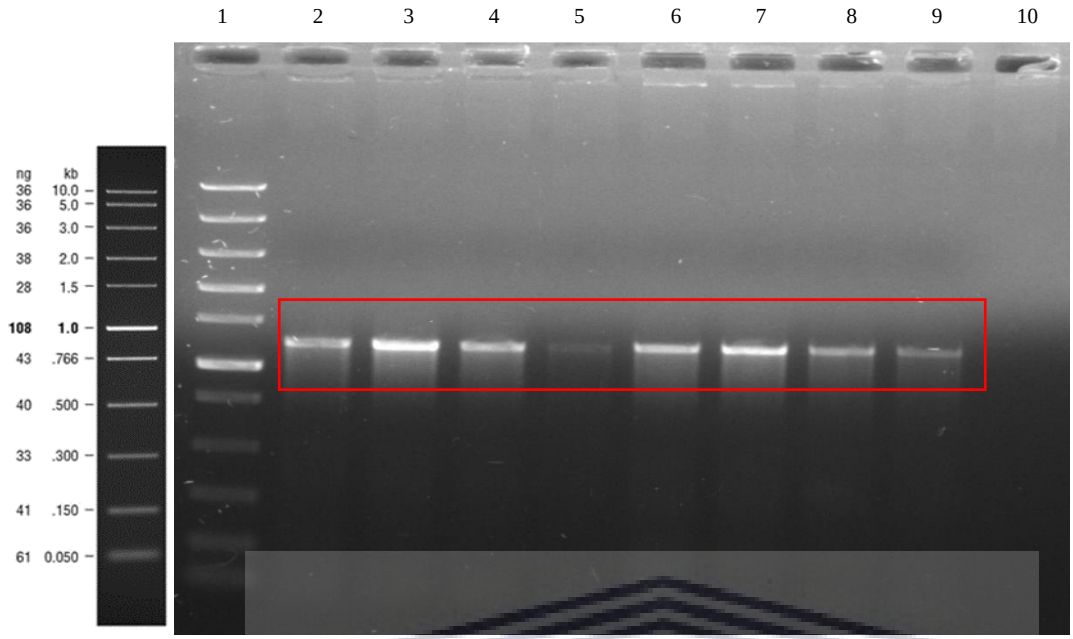

Figure 4.8: A DyP-type peroxidase colony PCR of the transformed *E. coli* JM109_30-1 and *E. coli* JM109_CZH20^{T}.

Lane 1: FAST DNA Ladder (New England Bio Labs®); Lane 2: *E.coli* JM109_30-1^{T} Replicate 1; Lane 3: *E.coli* JM109_30-1^{T} Replicate 2; Lane 4: *E.coli* JM109_30-1^{T} Replicate 3; Lane 5: *E.coli* JM109_30-1^{T} Replicate 4; Lane 6: *E.coli* JM109_CZH20^{T} Replicate 1; Lane 7: *E.coli* JM109_CZH20^{T} Replicate 2; Lane 8: *E.coli* JM109_CZH20^{T} Replicate 3; Lane 9: *E.coli* JM109_CZH20^{T} Replicate 4.

Colony PCRs for 885, HMC10^{T} and 85 gave no positive bands for each of these samples and the process was repeated with no success. The colony PCR of *E. coli* JM109_CZH20^{T} and *E. coli* JM109_30-1 generated an amplicon of the correct size, 1212 bp and 1218 bp, highlighted in red in Figure 4.8. Due to time limitations, it was decided that for the remainder of the study, only *E. coli* JM109_CZH20^{T} and *E. coli* JM109_30-1 would be analysed. Plasmids purified from these strains were further transformed into protein expression hosts *E. coli* BL21 (DE3) (Novagen™), Rosetta™ (DE3) PLysS (Novagen™), SHuffle® T7 (NEB), and ArcticExpress RP (Agilent). Colony PCR confirmed the presence of the genes of interest (Figure 4.9).

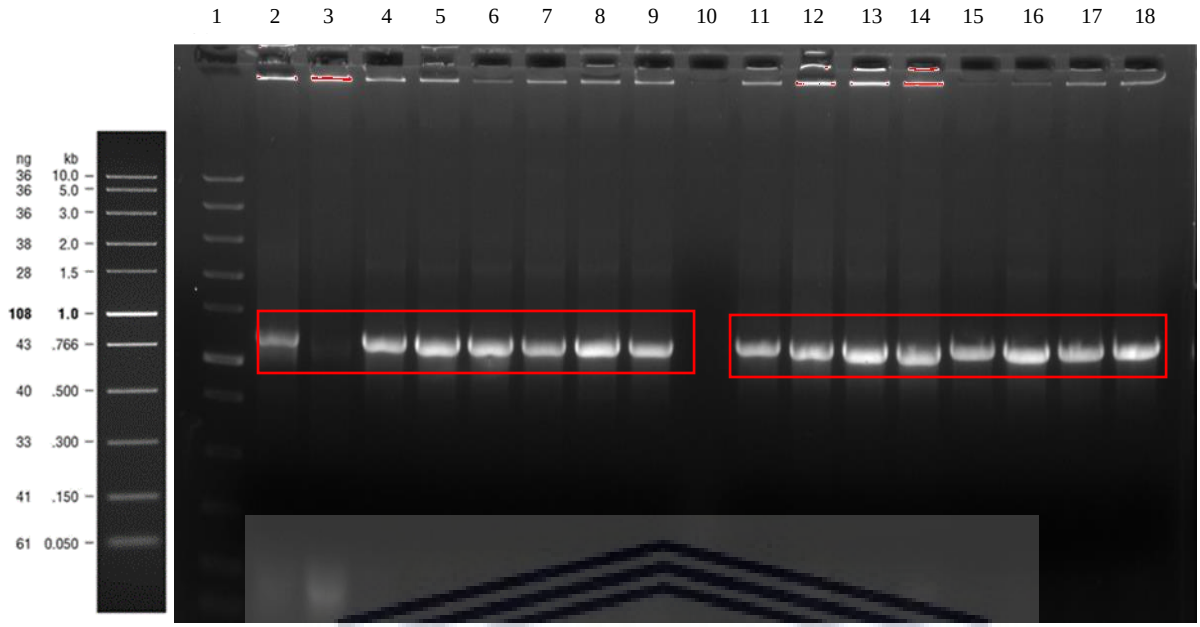

Figure 4.9: A colony PCR of pET_DyP_30-1 and pET_DyP_CZH20^T transformed into *E. coli* BL21 (DE3) (Novagen™), Rosetta™ (DE3) PLysS (Novagen™), SHuffle® T7 (NEB), and ArcticExpress RP (Agilent).

Lane 1: FAST DNA Ladder (New England Bio Labs®); Lane 2: pET_DyP_*E. coli* BL21_(DE3)_30-1 Replicate 1; Lane 3: pET_DyP *E. coli* BL21_(DE3)_30-1 Replicate 2; Lane 4: pET_DyP_Rosetta™_(DE3)_PLysS_30-1 Replicate 1; Lane 5: pET_DyP_Rosetta™_(DE3)_PLysS_30-1 Replicate2; Lane 6: pET_DyP_SHuffle®_T7_30-1 Replicate 1; Lane 7: pET_DyP_SHuffle®_T7_30-1 Replicate 2; Lane 8: pET_DyP_ArcticExpress_RP_30-1 Replicate 1; Lane 9 pET_DyP_ArcticExpress_RP_30-1 Replicate 2; Lane 10: Blank; Lane 11: pET_DyP_*E. coli* BL21_(DE3)_CZH20^T Replicate 1; Lane 12: pET_DyP_*E.coli*_BL21_(DE3)_CZH20^T Replicate 2; Lane 13: pET_DyP_Rosetta™_(DE3)_PLysS_CZH20^T Replicate 1; Lane 14: pET_DyP_Rosetta™_(DE3)_PLysS_CZH20^T Replicate 2; Lane 15: pET_DyP_SHuffle®_T7_CZH20^T Replicate 1; Lane 16: pET_DyP_SHuffle®_T7_CZH20^T Replicate 2; Lane 17: pET_DyP_ArcticExpress_RP_CZH20^T Replicate 1; Lane 18: pET_DyP_ArcticExpress_RP_CZH20^T Replicate 2.

Prior to protein expression, the two samples pET_DyP_ArcticExpress_RP_CZH20^T and pET_DyP_ArcticExpress_RP_30-1, were PCR-amplified with T7 primers (NEB) (Supplementary Sheet B) and Sanger sequenced to confirm the nucleotide sequences of the target DyP-type peroxidase genes. The predicted amino acid sequences were analysed on Uniprot (https://www.uniprot.org/help/uniprotkb - Accessed on 28 September 2020). The analyses revealed that the predicted 44.138 kDa CZH20^T DyP showed highest sequence similarity to the *Nocardia tenerifensis* DyP-type peroxidase (96%), while the predicted

41.317 kDa 30-1 DyP showed highest sequence similarity to the *Micromonospora aurantiaca* ATCC 27029 DyP-type peroxidase (98%).

4.2.4 Production of DyP-type peroxidases on small scale

The two constructs were subjected to protein expression on small scale (25 mL). Protein expression was conducted with four different hosts and four different expression media: Luria Bertani (LB) broth, 2× YT, Terrific Broth, and Auto Induction media (Appendix D). These preliminary small scale non-optimised expressions were visualised on SDS-PAGE gels (Figures 4.10 to 4.13)

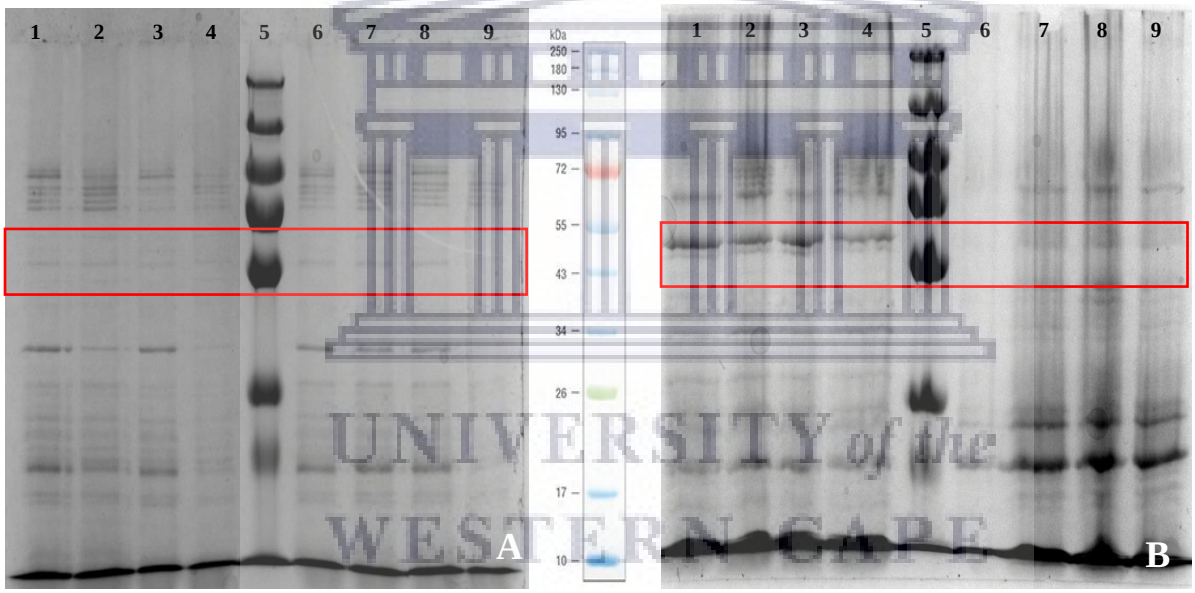

Figure 4.10: SDS-PAGE gels of CZH20^{T}_DyP_BL21; 30-1_DyP_BL21; CZH20^{T}_DyP_R; 30-1_DyP_R **(A)** CZH20^{T}_DyP_ST7; 30-1_DyP_ST7; CZH20^{T}_DyP_AE; 30-1_DyP_AE **(B)** expressed in LB broth (expected sizes 44 kDa for CZH20_DyP and 41 kDa for 30-1_DyP).

SDS-PAGE GEL A: Lane 1: CZH20^{T}_DyP_BL21 insoluble fraction; Lane 2: CZH20^{T}_DyP_BL21 soluble fraction; Lane 3: 30-1_DyP_BL21 insoluble fraction; Lane 4: 30-1_DyP_BL21 soluble fraction; Lane 5: Molecular Weight Marker (NEB); Lane 6: CZH20^{T}_DyP_R insoluble fraction; Lane 7: CZH20^{T}_DyP_R soluble fraction; Lane 8: 30-1_DyP_R insoluble fraction; Lane 9: _30-1_DyP_R soluble fraction (all expressed in LB broth).

SDS-PAGE GEL B: Lane 1: CZH20^{T}_DyP_ST7 insoluble fraction; Lane 2: CZH20^{T} _DyP_ST7 soluble fraction; Lane 3: 30-1_DyP_ST7 insoluble fraction; Lane 4: 30-1_DyP_ST7 soluble fraction; Lane 5: Molecular Weight Marker (NEB); Lane 6: CZH20^{T}_DyP_AE insoluble fraction; Lane 7: CZH20^{T}_DyP_AE soluble

fraction; Lane 8: 30-1_DyPAE insoluble fraction; Lane 9: 30-1_DyP_AE soluble fraction (all expressed in LB broth).

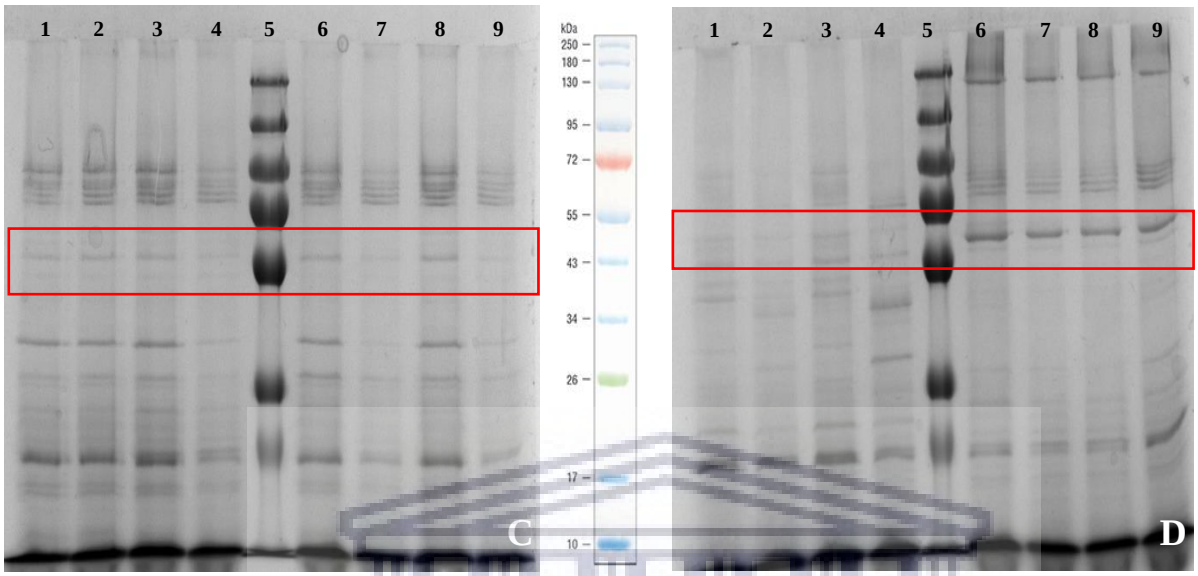

Figure 4.11: Figure 4.10: SDS-PAGE gels of CZH20^{T}_DyP_BL21; 30-1_DyP_BL21; CZH20^{T}_DyP_R; 30-1_DyP_R **(C)** CZH20^{T}_DyP_ST7; 30-1_DyP_ST7; CZH20^{T}_DyP_AE; 30-1_DyP_AE **(D)** expressed in 2x YT (expected sizes 44 kDa for CZH20_DyP and 41 kDa for 30-1_DyP).

SDS-PAGE GEL C: Lane 1: CZH20^{T}_DyP_BL21 insoluble fraction; Lane 2: CZH20^{T}_DyP_BL21 soluble fraction; Lane 3: 30-1_DyP_BL21 insoluble fraction; Lane 4: 30-1_DyP_BL21 soluble fraction; Lane 5: Molecular Weight Marker (NEB); Lane 6: CZH20^{T}_DyP_R insoluble fraction; Lane 7: CZH20^{T}_DyP_R soluble fraction; Lane 8: 30-1_DyP_R insoluble fraction; Lane 9: _30-1_DyP_R soluble fraction (all expressed in 2x YT).

SDS-PAGE GEL D: Lane 1: CZH20^{T}_DyP_ST7 insoluble fraction; Lane 2: CZH20^{T} _DyP_ST7 soluble fraction; Lane 3: 30-1_DyP_ST7 insoluble fraction; Lane 4: 30-1_DyP_ST7 soluble fraction; Lane 5: Molecular Weight Marker (NEB); Lane 6: CZH20^{T}_DyP_AE insoluble fraction; Lane 7: CZH20^{T}_DyP_AE soluble fraction; Lane 8: 30-1_DyPAE insoluble fraction; Lane 9: 30-1_DyP_AE soluble fraction (all expressed in 2x YT).

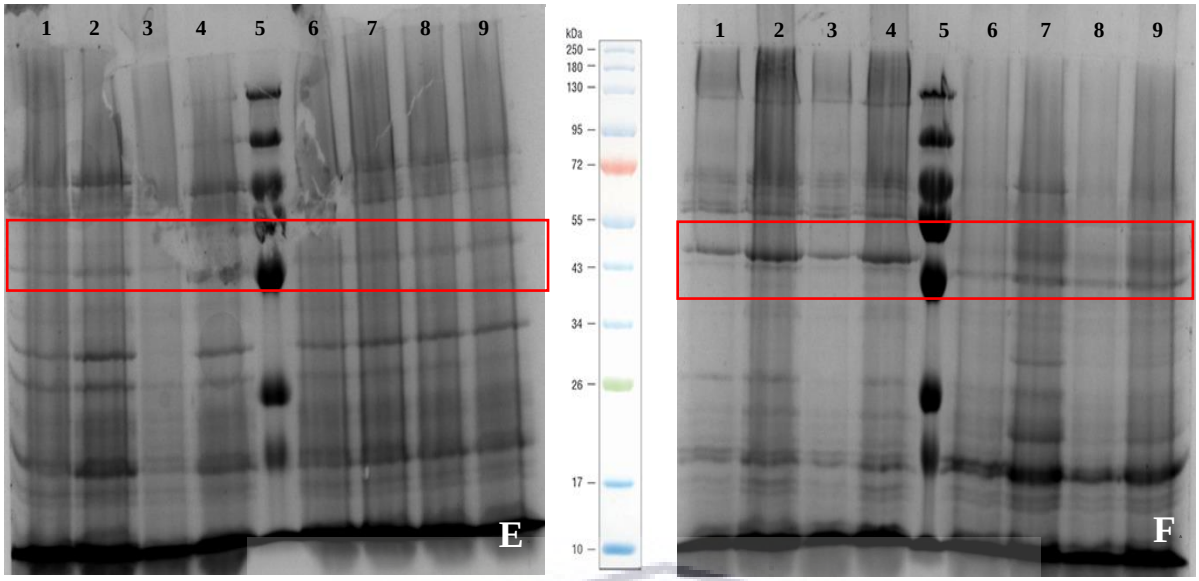

Figure 4.12: Figure 4.10: SDS-PAGE gels of CZH20^{T}_DyP_BL21; 30-1_DyP_BL21; CZH20^{T}_DyP_R; 30-1_DyP_R **(E)** CZH20^{T}_DyP_ST7; 30-1_DyP_ST7; CZH20^{T}_DyP_AE; 30-1_DyP_AE **(F)** expressed in Terrific Broth (expected sizes 44 kDa for CZH20_DyP and 41 kDa for 30-1_DyP).

SDS-PAGE GEL E: Lane 1: CZH20^{T}_DyP_BL21 insoluble fraction; Lane 2: CZH20^{T}_DyP_BL21 soluble fraction; Lane 3: 30-1_DyP_BL21 insoluble fraction; Lane 4: 30-1_DyP_BL21 soluble fraction; Lane 5: Molecular Weight Marker (NEB); Lane 6: CZH20^{T}_DyP_R insoluble fraction; Lane 7: CZH20^{T}_DyP_R soluble fraction; Lane 8: 30-1_DyP_R insoluble fraction; Lane 9: _30-1_DyP_R soluble fraction (all expressed in Terrific Broth).

SDS-PAGE GEL F: : CZH20^{T}_DyP_ST7 insoluble fraction; Lane 2: CZH20^{T} _DyP_ST7 soluble fraction; Lane 3: 30-1_DyP_ST7 insoluble fraction; Lane 4: 30-1_DyP_ST7 soluble fraction; Lane 5: Molecular Weight Marker (NEB); Lane 6: CZH20^{T}_DyP_AE insoluble fraction; Lane 7: CZH20^{T}_DyP_AE soluble fraction; Lane 8: 30-1_DyPAE insoluble fraction; Lane 9: 30-1_DyP_AE soluble fraction (all expressed in Terrific Broth).

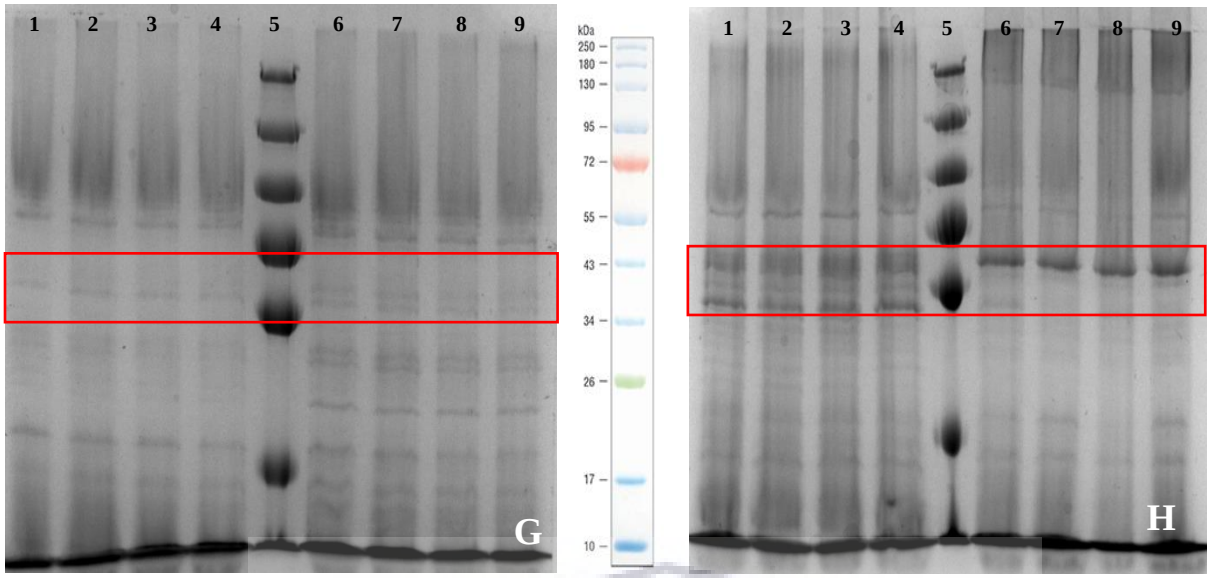

Figure 4.13: Figure 4.10: SDS-PAGE gels of CZH20^T_DyP_BL21; 30-1_DyP_BL21; CZH20^T_DyP_R; 30-1_DyP_R **(G)** CZH20^T_DyP_ST7; 30-1_DyP_ST7; CZH20^T_DyP_AE; 30-1_DyP_AE **(H)** expressed in Auto Induction media (expected sizes 44 kDa for CZH20_DyP and 41 kDa for 30-1_DyP).

SDS-PAGE GEL G: Lane 1: CZH20^T_DyP_BL21 insoluble fraction; Lane 2: CZH20^T_DyP_BL21 soluble fraction; Lane 3: 30-1_DyP_BL21 insoluble fraction; Lane 4: 30-1_DyP_BL21 soluble fraction; Lane 5: Molecular Weight Marker (NEB); Lane 6: CZH20^T_DyP_R insoluble fraction; Lane 7: CZH20^T_DyP_R soluble fraction; Lane 8: 30-1_DyP_R insoluble fraction; Lane 9: _30-1_DyP_R soluble fraction (all expressed in Auto Induction media).

SDS-PAGE GEL H: CZH20^T_DyP_ST7 insoluble fraction; Lane 2: CZH20^T _DyP_ST7 soluble fraction; Lane 3: 30-1_DyP_ST7 insoluble fraction; Lane 4: 30-1_DyP_ST7 soluble fraction; Lane 5: Molecular Weight Marker (NEB); Lane 6: CZH20^T_DyP_AE insoluble fraction; Lane 7: CZH20^T_DyP_AE soluble fraction; Lane 8: 30-1_DyPAE insoluble fraction; Lane 9: 30-1_DyP_AE soluble fraction (all expressed in Auto Induction media).

Based on the expression observed in the different media types-expression hosts combinations, it was found that CZH20^T_DyP_AE and 30-1_DyP_AE had the highest protein concentration, 0.124 mg/mL and 0.135 mg/mL, respectively (as determined by the Bradford's assay), when grown in Auto Induction medium. Therefore, when determining the optimal induction temperature only the two ArcticExpress transformants were tested over the temperature range 15 °C, 25 °C, 30 °C and 37 °C (Figure 4.14 and Figure 4.15).

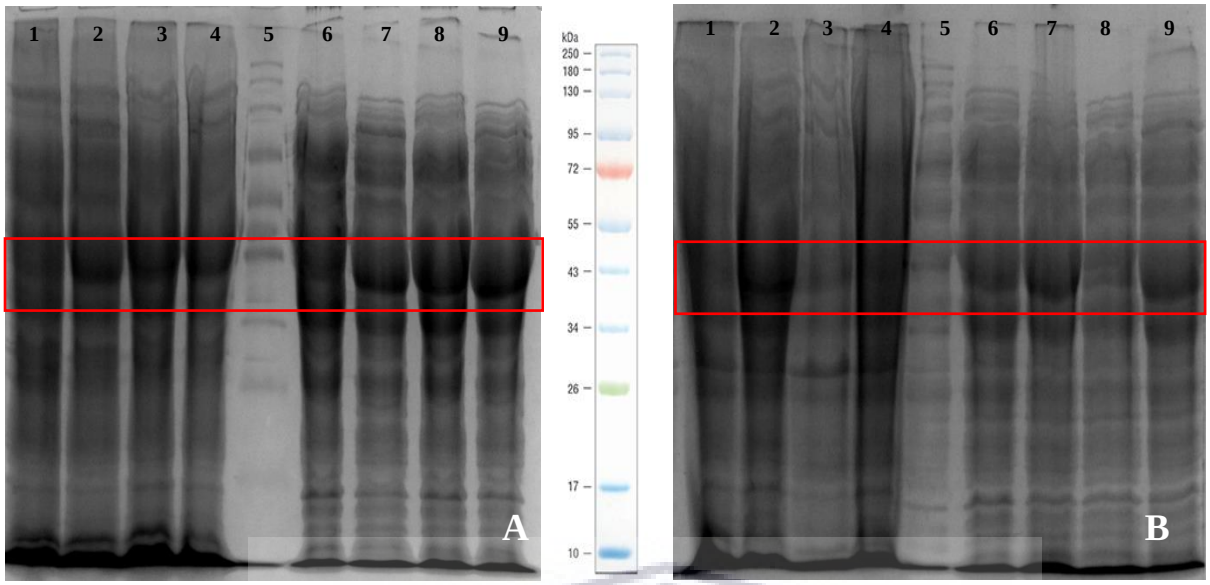

Figure 4.14: SDS-PAGE gels of CZH20^{T}_DyP_AE and 30-1_DyP_AE at 15 °C **(A)** and CZH20^{T}_DyP_AE and 30-1_DyP_AE at 25 °C **(B)** expressed in Auto Induction media (expected sizes 44 kDa for CZH20_DyP and 41 kDa for 30-1_DyP).

SDS-PAGE GEL A: Lane 1: CZH20^{T}_DyP_AE uninduced insoluble fraction; Lane 2: CZH20^{T}_DyP_AE uninduced soluble fraction; Lane 3: CZH20^{T}_DyP_AE induced insoluble fraction; Lane 4: CZH20^{T}_DyP_AE induced soluble fraction; Lane 5: Molecular Weight Marker (NEB); Lane 6: 30-1_DyP_AE uninduced insoluble fraction; Lane 7: 30-1_DyP_AE uninduced soluble fraction; Lane 8: 30-1_DyP_AE induced insoluble fraction; Lane 7: 30-1_DyP_AE induced soluble fraction (all expressed in Auto Induction media at 15 °C).

SDS-PAGE GEL B: Lane 1: CZH20^{T}_DyP_AE uninduced insoluble fraction; Lane 2: CZH20^{T}_DyP_AE uninduced soluble fraction; Lane 3: CZH20^{T}_DyP_AE induced insoluble fraction; Lane 4: CZH20^{T}_DyP_AE induced soluble fraction; Lane 5: Molecular Weight Marker (NEB); Lane 6: 30-1_DyP_AE uninduced insoluble fraction; Lane 7: 30-1_DyP_AE uninduced soluble fraction; Lane 8: 30-1_DyP_AE induced insoluble fraction; Lane 7: 30-1_DyP_AE induced soluble fraction (all expressed in Auto Induction media at 25 °C).

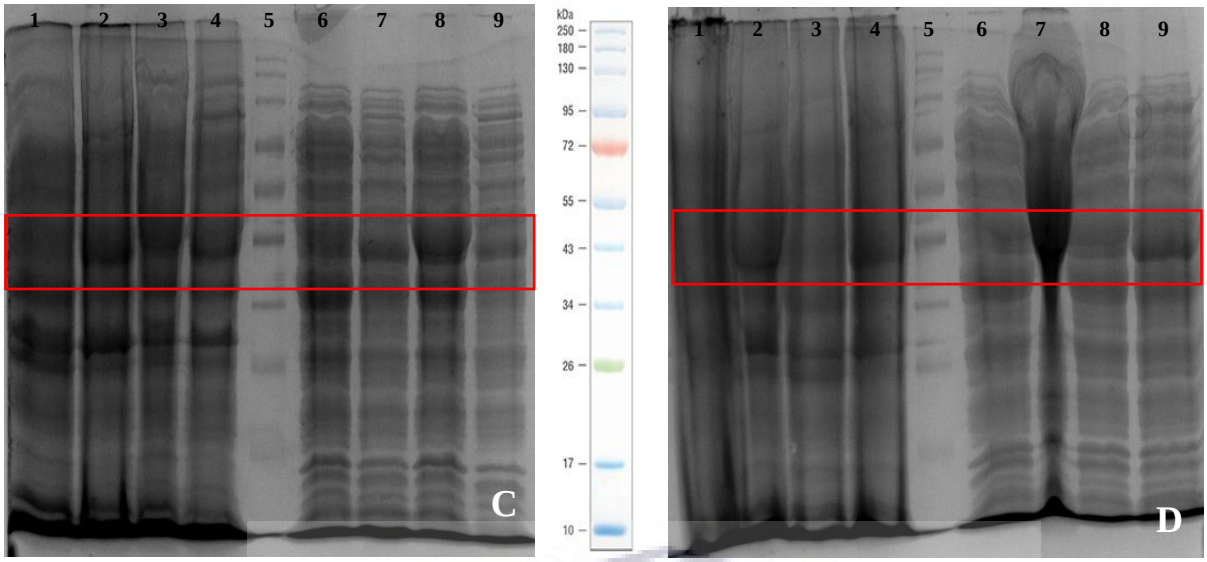

Figure 4.15: SDS-PAGE gels of CZH20^T_DyP_AE and 30-1_DyP_AE at 30°C **(C)** and CZH20^T_DyP_AE and 30-1_DyP_AE at 37 °C **(D)** expressed in Auto Induction media (expected sizes 44 kDa for CZH20_DyP and 41 kDa for 30-1_DyP).

SDS-PAGE GEL C: Lane 1: CZH20^T_DyP_AE uninduced insoluble fraction; Lane 2: CZH20^T_DyP_AE uninduced soluble fraction; Lane 3: CZH20^T_DyP_AE induced insoluble fraction; Lane 4: CZH20^T_DyP_AE induced soluble fraction; Lane 5: Molecular Weight Marker (NEB); Lane 6: 30-1_DyP_AE uninduced insoluble fraction; Lane 7: 30-1_DyP_AE uninduced soluble fraction; Lane 8: 30-1_DyP_AE induced insoluble fraction; Lane 7: 30-1_DyP_AE induced soluble fraction (all expressed in Auto Induction media at 30 °C)

SDS-PAGE GEL D: Lane 1: CZH20^T_DyP_AE uninduced insoluble fraction; Lane 2: CZH20^T_DyP_AE uninduced soluble fraction; Lane 3: CZH20^T_DyP_AE induced insoluble fraction; Lane 4: CZH20^T_DyP_AE induced soluble fraction; Lane 5: Molecular Weight Marker (NEB); Lane 6: 30-1_DyP_AE uninduced insoluble fraction; Lane 7: 30-1_DyP_AE uninduced soluble fraction; Lane 8: 30-1_DyP_AE induced insoluble fraction; Lane 7: 30-1_DyP_AE induced soluble fraction (all expressed in Auto Induction media at 37 °C)

A Bradford's assay was conducted to determine the protein concentration of the CZH20^T_DyP_AE and 30-1_DyP_AE expressed proteins at the various temperatures, and functional expression was confirmed with the 2,4-DCP assay. With the calculated specific activity, the optimal induction temperature could be selected (Supplementary Sheet C). A summarised version of the volumetric activity (U/mL), protein concentration (mg/mL) and highest specific activity (U/mg) at the varying temperatures was recorded (Table 4.6).

Table 4.6: Summary of the volumetric activity (U/mL), protein concentration (mg/mL) specific activity (U/mg) at varying temperatures of CZH20^{T}_DyP_AE and 30-1_DyP_AE in Auto Induction media. Standard deviations indicated are based on triplicate analyses.

Sample Name	Temperature (°C)	Volumetric Activity (U/mL)	Protein Concentration (mg/mL)	Specific Activity (U/mg)
CZH20^{T}_DyP_AE induced insoluble fraction	15	0.0650± 0.023	0.1165	0.7941±0.072
30-1_DyP_AE induced soluble fraction	15	0.10630±0.013	0.095	1.1220±0.066
CZH20^{T}_DyP_AE induced insoluble fraction	25	0.0650±0.084	0.1165	0.5577±0.029
30-1_DyP_AE induced soluble fraction	25	0.06801±0.051	0.1347	0.5049±0.071
CZH20^{T}_DyP_AE induced insoluble fraction	30	0.1478±0.054	0.1150	1.2851±0.082
30-1_DyP_AE induced soluble fraction	30	0.1117±0.028	0.1255	0.8905±0.045
CZH20^{T}_DyP_AE induced insoluble fraction	37	00993±0.063	0.1693	0.6133±0.087
30-1_DyP_AE induced soluble fraction	37	0.1625±0.091	0.1685	0.9639±0.054

It was identified that the most promising functional expression of CZH20^{T}_DyP_AE and 30-1_DyP_AE were in the induced samples, with most activity detected in the soluble fraction.

4.2.5 Production of DyP-type peroxidase on large scale

CZH20^{T}_DyP_AE and 30-1_DyP_AE was grown for protein expression at larger scale (200 mL) in Auto Induction medium at 30 °C. As can be seen from Figure 4.16, overexpression of both proteins was observed, with higher levels of production of for CZH20^{T} DyP. The induced samples contain the inducing sugar 50× 5052 and the uninduced samples do not contain this component, which served as control (Studier, 2005).

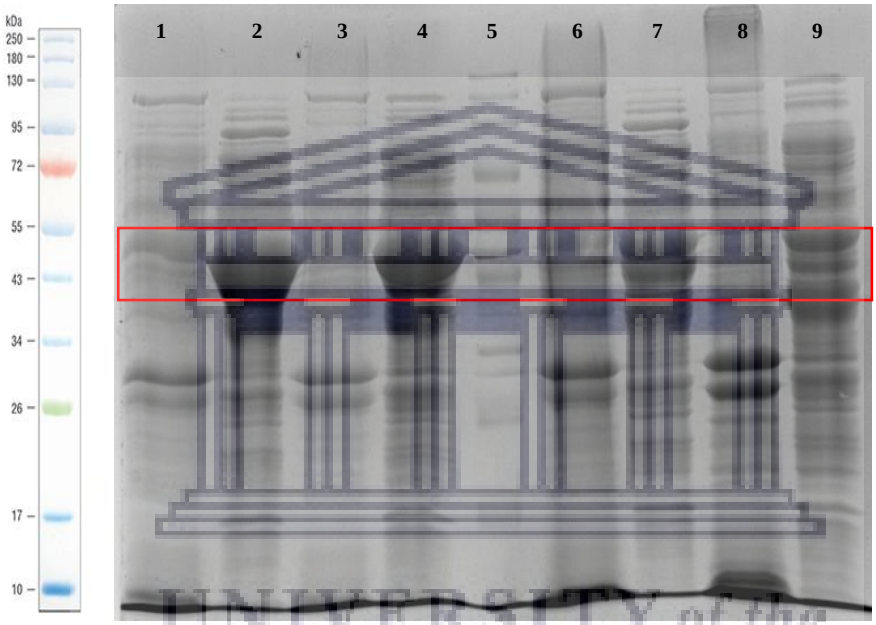

Figure 4.16: SDS-PAGE gels of CZH20^{T}_DyP_AE and 30-1_DyP_AE at 30 °C in 200 mL of Auto Induction media (expected sizes 44 kDa for CZH20_DyP and 41 kDa for 30-1_DyP).

Lane 1: Lane 1: CZH20^{T}_DyP_AE uninduced insoluble fraction; Lane 2: CZH20^{T}_DyP_AE uninduced soluble fraction; Lane 3: CZH20^{T}_DyP_AE induced insoluble fraction; Lane 4: CZH20^{T}_DyP_AE induced soluble fraction; Lane 5: Molecular Weight Marker (NEB); Lane 6: 30-1_DyP_AE uninduced insoluble fraction; Lane 7: 30-1_DyP_AE uninduced soluble fraction; Lane 8: 30-1_DyP_AE induce d insoluble fraction; Lane 7: 30-1_DyP_AE induced soluble fraction (all expressed 200 mL of Auto Induction media at 30 °C)

After the scale up of CZH20^{T}_DyP_AE and 30-1_DyP_AE at 30 °C, it was identified that the highest specific activity for both of these transformants was in the uninduced soluble fraction and the uninduced insoluble fraction with the values of 0.8514 U/mg and 0.5021 U/mg, respectively (Table 4.7).

Table 4.7: The volumetric activity (U/mL), protein concentration (mg/mL) and specific activity (U/mg) at 30 °C for CZH20^T_DyP_AE and 30-1_DyP_AE in 200 mL of Auto Induction media. Standard deviations indicated are based on triplicate analyses.

Sample Name	Volumetric Activity (U/mL)	Protein Concentration (mg/mL)	Specific Activity (U/mg)
CZH20^T_DyP_AE uninduced insoluble fraction	0.0418±0.047	0.1340	0.3125±0.059
CZH20^T_DyP_AE uninduced soluble fraction	0.1590±0.082	0.1868	0.8514±0.073
CZH20^T_DyP_AE induced insoluble fraction	0.0432±0.074	0.1289	0.3352±0.068
CZH20^T_DyP_AE induced soluble fraction	0.0562±0.065	0.1936	0.2901±0.034
30-1_DyP_AE uninduced insoluble fraction	0.0781±0.056	0.1556	0.5021±0.042
30-1_DyP_AE uninduced soluble fraction	0.0394±0.071	0.1869	0.2109±0.089
30-1_DyP_AE induced insoluble fraction	0.0069±0.082	0.1720	0.040±0.067
30-1_DyP_AE induced soluble fraction	0.0357±0.047	0.1855	0.1926±0.074

CZH20^T_DyP_AE uninduced soluble fraction had the highest volumetric activity of 0.1590 U/mL and a protein concentration of 0.1868 mg/mL, while for 30-1_DyP_AE the uninduced insoluble fraction showed the best volumetric activity of 0.0781 U/mL and a protein concentration of 0.1556 mg/mL. Overall, the results for the large-scale production differed from the findings of the small scale (25 mL) protein expression of these samples whereby the samples had higher specific activity in the induced samples.

4.3 Purification of DyP-type Peroxidases

Purification of the CZH20^{T}_DyP_AE uninduced soluble fraction and 30-1_DyP_AE uninduced soluble fraction in Auto Induction medium was performed via fast performance liquid chromatography (FPLC) using an AKTAprime™ system (Amersham-Biosciences). Initially 2 mL of the crude protein sample was filter-sterilised and applied to the column. Separation of the sample was performed at a flow rate of 1 mL/min with 50 mM potassium phosphate (KPO_4) buffer (pH 7.3). The purified sample was collected in 1 mL fractions. The chromatogram contained peaks (in milli-Absorbance units (mAU)) indicative of the intensity of the protein absorbance and is indicated by the dark blue line measuring the UV spectra. Peaks with high intensity are highlighted in red (Figure 4.17). The highest peak was observed at about 55 mAu. When a peak was observed, the fractions were subsequently collected and subjected SDS-PAGE analysis (Figure 4.18) to identify the level of purity of the protein of interest and to confirm that the protein sample collected contained proteins the size of the protein of interest. Thus the fractions that were selected were, 21-24 (collected about 38 minutes to 53 minutes when the initial sample was added to the column); 31-34 (collected about 59 minutes to 73 minutes after intial sample was added to the column); 42-45 (collected about 80 to 100 minutes after the initial sample was added to the column) and 52-55 (collected at about 102 to 122 minutes after the initial sample was added to the column).

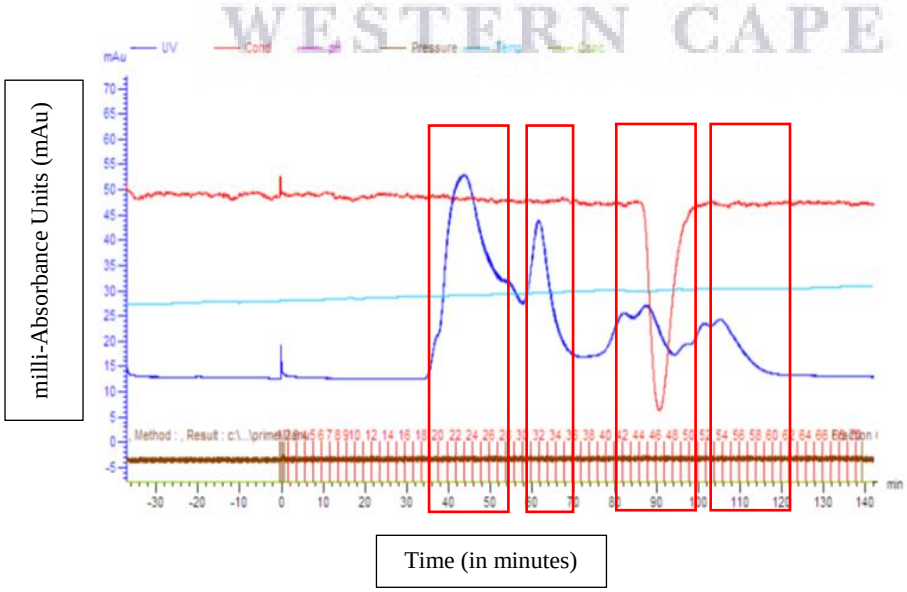

Figure 4.17: Chromatogram of the FPLC-purification of the CZH20^{T}_DyP detected in the CZH20^{T}_DyP_AE_Auto Induction media uninduced soluble fraction (50 mM potassium phosphate buffer (pH7.3) at a flow rate of 1 mL/min).

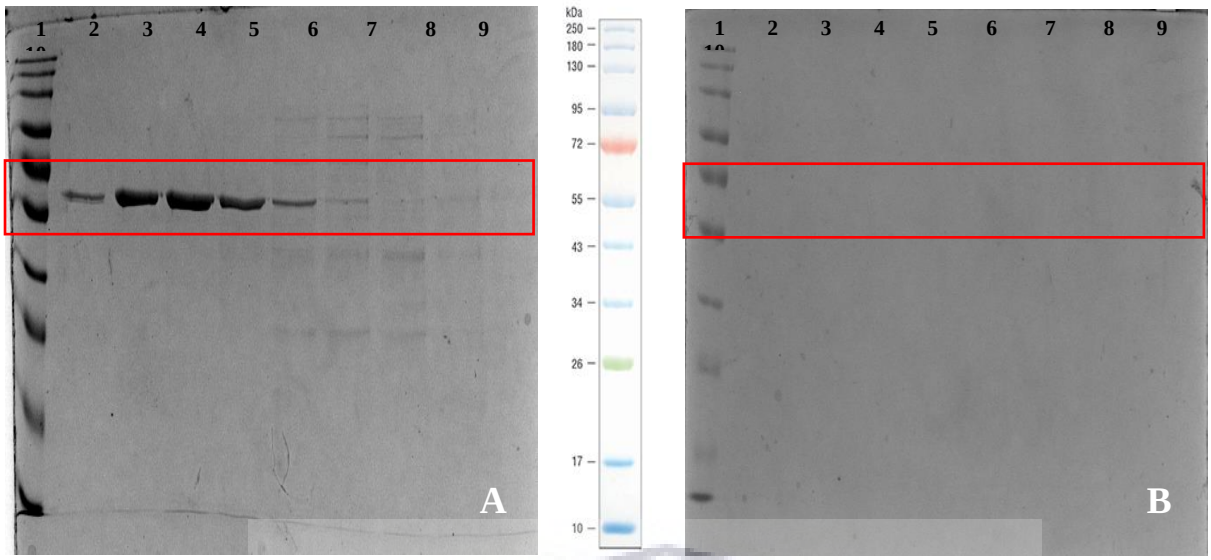

Figure 4.18: SDS-PAGE gels of FPLC-purified fractions of CZH20^T_DyP_AE_Auto Induction media uninduced soluble fraction eluted with 50 mM potassium phosphate buffer, pH7.3, at a flow rate of 1 mL/min (expected sizes 44 kDa for CZH20_DyP).

Gel A: Lane 1: Molecular Weight Marker (NEB); Lane 2: CZH20^T_DyP_AE uninduced soluble fraction 21; Lane 3: fraction 22; Lane 4: fraction 23; Lane 5: fraction 24; Lane 6: fraction 31; Lane 7: fraction 32; Lane 8: fraction 33; Lane 9: fraction 34; Lane 10: fraction 42

Gel B: Lane 1: Molecular Weight Marker (NEB); Lane 2: fraction 43; Lane 3: fraction 44; Lane 4: fraction 45; Lane 6: fraction 52; Lane 7: fraction 53; Lane 8: fraction 54; Lane 9: fraction 55

It was observed that the first two peaks, 45-55 mAu (Figure 4.17) contained purified and partially purified enzyme (Figure 4.18). The first four fractions (21-24) were subjected to a 2,4–DCP assay spot test to identify whether the DyP-type peroxidase was present. Unfortunately, no colour change was detected, which was hypothesized to be due to loss of a co-factor during purification. Therefore, these four fractions were pooled and incubated with 1 µM hemin at 4 °C for one hour. Distilled water was also incubated at 4 °C with the same concentration of hemin and served as a control in the peroxidase assay. A 2,4–DCP assay was conducted, and the results revealed that the hemin in dH_2O had a specific activity of 91.79 U/mg and the pooled purified fraction had a specific activity of 126.17 U/mg. As there was little difference between the control and the purified fraction the purification for this sample was subjected to further optimisation.

30-1_DyP_AE uninduced soluble fraction was subjected to the same analysis as above and the chromatogram revealed only two small peaks, highlighted in red (Figure 4.19). The

one mL fractions selected were, 8-12 (collected at about 11 minutes to 21 minutes after intial sample was added to the column) and 16-18 (collected at about 29 minutes to 39 minutes after intial sample was added to the column) and these were subjected to SDS-PAGE analysis (Figure 4.20).

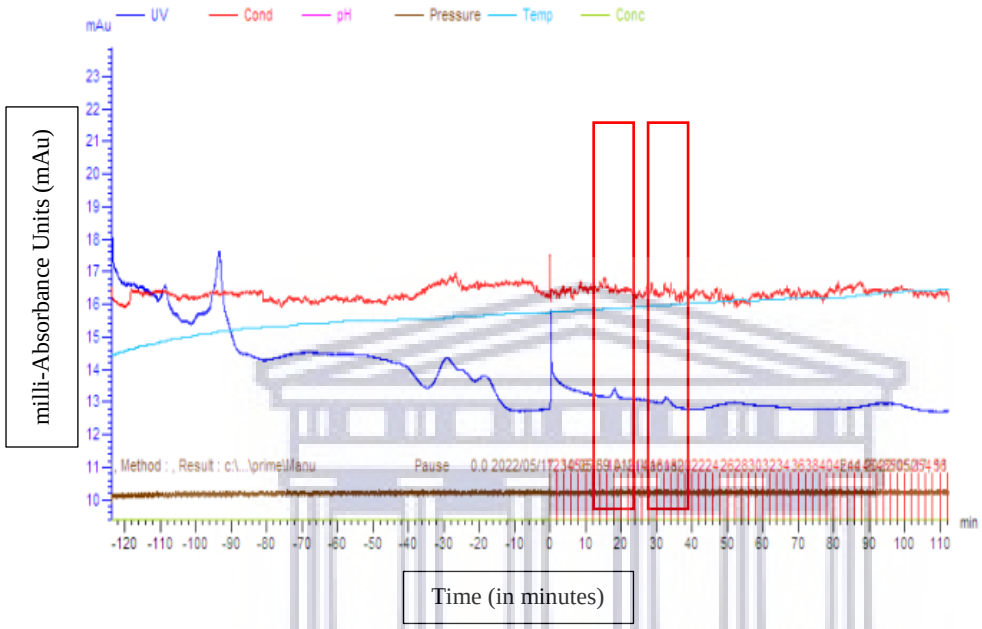

Figure 4.19: Chromatogram of the FPLC-purification of 30-1_DyP_AE_Auto Induction media uninduced soluble fraction with 50 mM potassium phosphate buffer, pH7.3 at a flow rate of 1 mL/min.

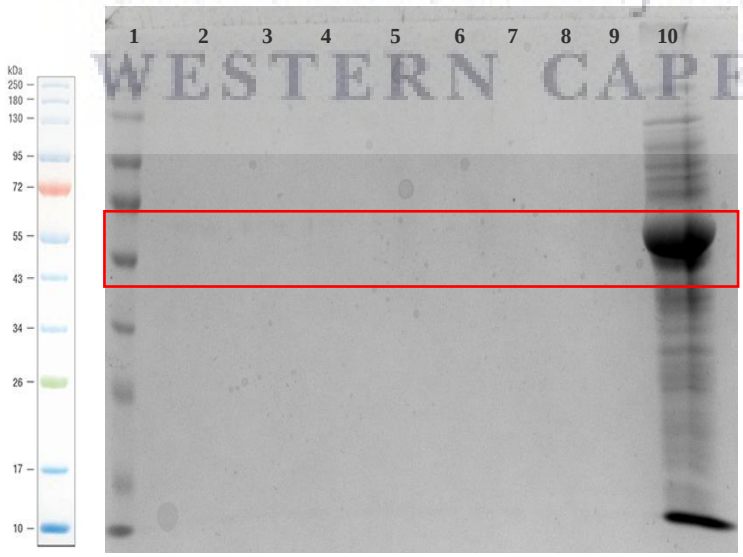

Figure 4.20: SDS-PAGE gel of FPLC-purified fractions of 30-1_DyP_AE_Auto Induction media uninduced soluble fraction with 50 mM potassium phosphate buffer, pH7.3 at a flow rate of 1 mL/min.

Lane 1: Molecular Weight Marker (NEB); Lane 2: 30-1_DyP_AE_Auto Induction media uninduced soluble fraction 8; Lane 3: fraction 9; Lane 4: fraction 10; Lane 5: fraction 11; Lane 6: fraction 12; Lane 7: fraction 16; Lane 8: fraction 17; Lane 9: fraction 18; Lane 10: 30-1-DyP_AE_Auto Induction media uninduced SNF (control).

As the observable peaks were lower for 30-1_DyP_AE (Figure 4.20) compared to CZH20^{T}_DyP_AE uninduced soluble fraction (Figure 4.17), an unpurified 30-1_DyP_AE uninduced soluble fraction was run with the selected purified fraction samples as a control (Figure 4.20). Due to the lack of purified proteins present in the SDS-PAGE analysis of 30-1_DyP_AE uninduced soluble fraction, only CZH20^{T}_DyP_AE was selected for purification optimisation and biochemical characterisation.

For optimisation, protein expression was repeated on large scale (200 mL) and subjected to protein purification using FPLC. Four mL of filter sterilised CZH20^{T}_DyP_AE uninduced soluble fraction was added and purified at a lower flow rate of 0.8 mL/min and 2 mL fractions were collected. According to the chromatogram, the purified protein was potentially in the first peak (Supplementary Sheet D, Table C1 – C4), therefore only these initial fractions were subjected to SDS-PAGE analysis. Purification was conducted with four biological repeats therefore fractions 5, 6 and 9, 10 were analysed on SDS-PAGE from each of the four purifications (Figure 4.21).

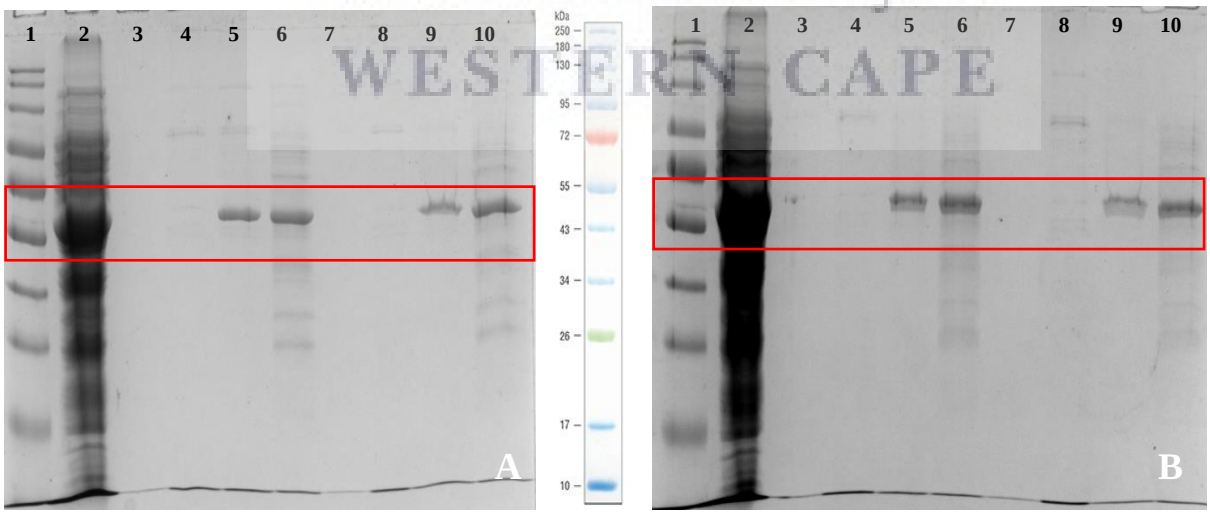

Figure 4.21: SDS-PAGE gels of FPLC-purified fractions of CZH20^{T}_DyP_AE_Auto Induction media uninduced soluble fraction 1-4 (elution with 50 mM potassium phosphate buffer, pH7.3, at a flow rate of 0.8 mL/min). Gel A and Gel B are from duplicate protein purifications.

Gel A: Lane 1: Molecular Weight Marker (NEB); Lane 2: Unpurified CZH20^T_DyP_AE_Auto Induction media uninduced soluble fraction 1 (control); Lane 3: fraction 5; Lane 4: fraction 6; Lane 5: fraction 7; Lane 6: fraction 8; Lane 7: SNF 2 fraction 5; Lane 8: fraction 6; Lane 9: fraction 7; Lane 10: fraction 8
Gel B: Lane 1: Molecular Weight Marker (NEB); Lane 2: Unpurified pET_DyP_ArcticExpress_RP_CZH20^T uninduced soluble fraction 1 (control); Lane 3: fraction 5; Lane 4: fraction 6; Lane 5: fraction 7; Lane 6: fraction 8; Lane 7: SNF 2 fraction 5; Lane 8: fraction 6; Lane 9: fraction 7; Lane 10: fraction 8

The reduced flow rate of 0.8 mL/min, resulted in the gradual separation of proteins into purified and partially purified proteins, Lane 5, 6, 9 and 10 respectively across both gels A and B (Figure 4.21). Purified and partially purified samples were pooled together and incubated with 1 mM trace salts at 4 °C overnight (for the trace salts g/100 mL: 0.1 $FeSO_4.7H_2O$, 0.1 $MnCl_2.4H_2O$, 0.1 $ZnSO_4.7H_2O$ was dissolved in dH_2O and filter sterilized before use). The protein concentrations of the purified and partially samples were assessed using a Bradford's assay and specific activity was determined by performing the 2,4–DCP assay (Table 4.8).

Table 4.8: The protein concentration (mg/mL) and specific activity (U/mL) of unpurified, purified and partially purified CZH20^T_DyP_AE. Standard deviations indicated are based on triplicate analyses.

Sample Name	Protein Concentration (mg/mL)	Specific Activity (U/mg)
CZH20^T_DyP_AE uninduced insoluble fraction 1	9.41	17.32±1.24
CZH20^T_DyP_AE uninduced soluble fraction 1	9.61	16.78±0.942
CZH20^T_DyP_AE uninduced insoluble fraction 2	10.49	18.60±0.243
CZH20^T_DyP_AE uninduced soluble fraction 2	9.57	16.62±0.078
Purified CZH20^T_DyP_AE uninduced soluble fraction	3.20	4.31±0.193
Partially Purified CZH20^T_DyP_AE uninduced soluble fraction	6.57	1.52±0.057

Since peroxidases have found application in both purified and partially purified forms, it was decided that the purified and partially purified CZH20^{T}_DyP_AE would be subjected to biochemical characterisation.

4.4 Biochemical Characterisation of CZH20^{T} DyP-type peroxidase

Biochemical characterisation of the CZH20^{T} DyP-type peroxidase was performed using the FPLC purified and partially purified samples. The assays were conducted using the SpectraMax-I3 and the SoftMax® Pro 7 Data Acquisition and Analysis Software (Molecular Devices). For the remainder of this study, purified and partially purified pET_DyP_ArcticExpress_RP_CZH20^{T} will be referred to as 'Purified CZH20_DyP' and 'Partially Purified CZH20_DyP'.

4.4.1 Optimum pH

The optimum pH for the oxidation of 2,4-DCP was determined from pH 3 to 9, in increments of 0.5 pH units for each buffer (50 mM) and tested at room temperature (25 ± 2 °C) for the purified and partially purified CZH20_DyP. The buffers that were used were *Legionella* Acid Buffer (KCl-HCl) pH 2.0, potassium dihydrogen phosphate-hydrochloric acid buffer (KH_2PO_4-HCl) pH 3.0, sodium acetate buffer pH 3.0-5.5, potassium phosphate buffer pH 6.0-7.5, and Tris-HCl buffer pH 8.0-9.0 (Figure 4.22).

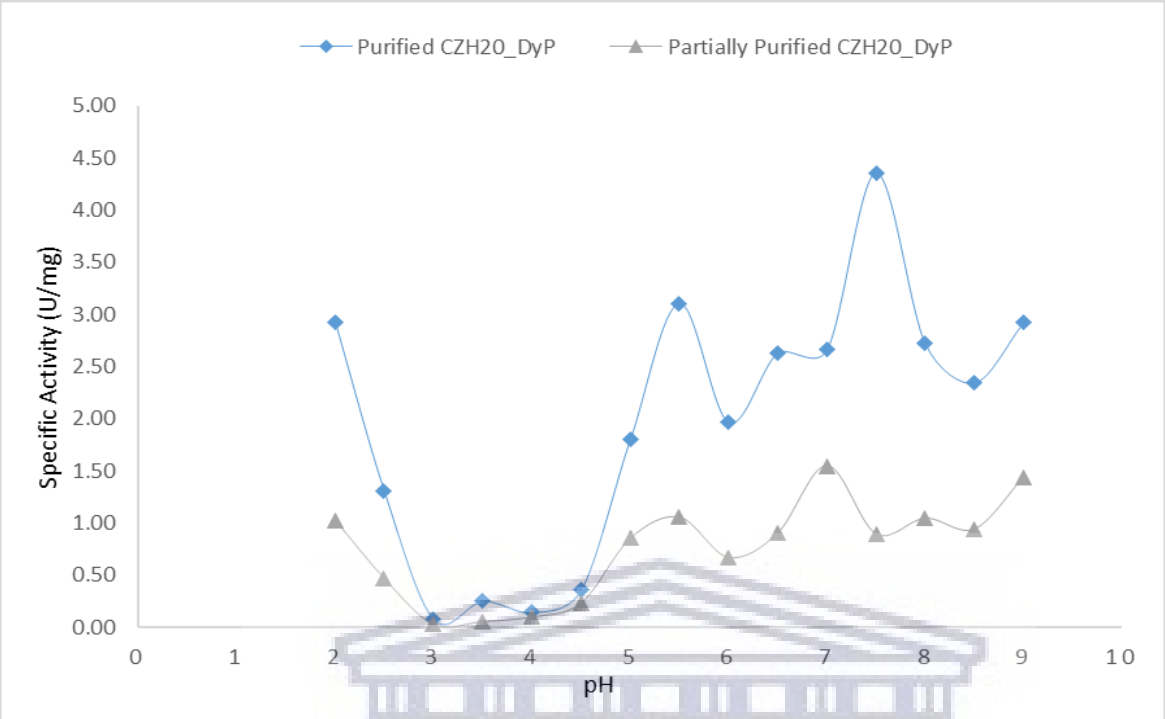

Figure 4.22: Optimum pH profiles for the DyP-type peroxidase from Purified CZH20_DyP and Partially Purified CZH20_DyP with 2,4-DCP as the substrate.

The specific activity for both the purified and partially purified DyP-type samples exhibit similar characteristics across the broad pH range (Figure 4.22). Both samples are capable of oxidising the substrate in *Legionella* Acid Buffer, as well as potassium dihydrogen phosphate-hydrochloric acid buffer. In this study distilled water was used as a control instead of supplementing the 2,4-DCP assay with the enzyme to identify DyP activity. Although several controls, other than that of dH_2O can be used such as, an enzyme that is not a peroxidase, Horseradish peroxidase (which is a well-characterised peroxidase) and supplementing the assay with no enzyme at all can serve as controls. Therefore, future work may be done to identify whether enzymatic or chemical hydrolysis is occurring. Furthermore, the oxidation of 2,4-DCP in sodium acetate buffer (pH 3.0-5.5) exhibit the lowest specific activity, over the broad substrate range, with the lowest specific activity for the purified and partially purified CZH20_DyP being at pH 3.0 with values of 0.08 U/mg and 0.03 U/mg. Furthermore, with the increase in pH of the potassium phosphate buffer (6.0-7.5) an increase in oxidation of the substrate occurred. The purified CZH20_DyP had the highest specific activity with the value of 4.36 U/mg at pH 7.5 (Figure 4.22). The partially purified CZH20_DyP had the highest specific activity with a value of 1.55 U/mg at pH 7.0. The data showed that the potassium phosphate buffer was the

optimal buffer for oxidation of 2,4-DCP which could be due to the fact that the enzyme was purified in 50 mM potassium phosphate buffer which was used to separate and purify the protein. Therefore, for further biochemical characterisation, 2,4-DCP assays for the purified CZH20_DyP were conducted with 50 mM potassium phosphate buffer pH 7.5 and for partially purified CZH20_DyP, 50 mM potassium phosphate buffer at pH 7.0.

4.4.2 Optimum Temperature

The optimum temperature for the oxidation of 2,4-DCP was determined by varying temperatures ranging from 25 °C to 45 °C in 5 °C intervals. The purified and partially purified CZH20-DyP samples were evaluated for the optimum temperature of 2,4-DCP oxidation in their respective optimum pH buffers (Figure 4.23).

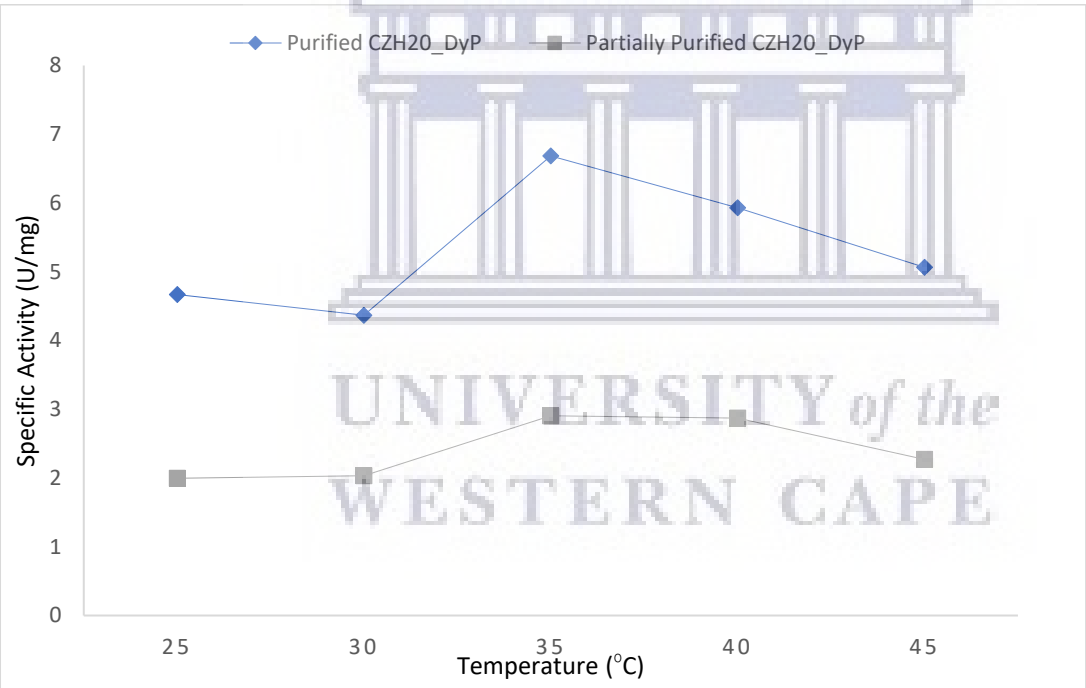

Figure 4.23: Temperature profiles for for the DyP-type peroxidase from purified CZH20_DyP and partially purified CZH20_DyP with 2,4-DCP as the substrate.

The temperature profiles for the purified and partially purified CZH20_DyP were assessed over a range of 25 °C to 45 °C. While both samples were active over the entire temperature range, purified and partially purified CZH20_DyP (at their optimal pH) had an optimal temperature for the oxidation of the 2,4 DCP at 35 °C (Figure 4.23).

4.4.3 Effect of Inhibitors, Reducing Agents, and Metal Ions

The effect of various concentrations of inhibitors, reducing agents and metal ions on purified and partially purified CZH20_DyP was determined after incubating the DyP-type peroxidase enzyme with the aforementioned for one hour at room temperature (25 ± 2 °C). The effect of inhibitors and reducing agents were identified by the complete inhibition of enzyme activity (Table 4.9). No inhibition of the purified and partially purified DyP-type peroxidase was observed at 50 mM NaCl, SDS, EDTA and sodium azide indicating that there were low levels of inhibition across the broad range (0.01- 50 mM) of concentrations of these inhibitors and reducing agents. L-cysteine and sodium metabisulphite had similar effects on the purified and partially purified DyP-type peroxidase with complete inhibition occurring at 0.1 mM and 0.2 mM, respectively. Although peroxidases catalyse the oxidation of a substrate, 2,4-DCP in this instance, with H_2O_2 as co-factor, incubation with different concentrations of hydrogen peroxide resulted in the most significant inhibition by all the inhibitors and reducing agents in this study. Complete inhibition of both the purified and partially purified DyP-type peroxidase occurred at 0.05 mM.

Table 4.9: Effect of enzyme inhibitors and reducing agents on the purified and partially purified CZH20_DyP.

Inhibitor or Reducing Agent	Sample	Complete inhibition (in mM)
Nacl	Purified CZH20_DyP	-
	Partially Purified CZH20_DyP	-
L-cysteine	Purified CZH20_DyP	0.1
	Partially Purified CZH20_DyP	0.2
Sodium dodecylsulphate (SDS)	Purified CZH20_DyP	-
	Partially Purified CZH20_DyP	-
Sodium metabisulphite	Purified CZH20_DyP	1.0
	Partially Purified CZH20_DyP	0.2
EDTA	Purified CZH20_DyP	-
	Partially Purified CZH20_DyP	-
L-ascorbic acid	Purified CZH20_DyP	-

	Partially Purified CZH20_DyP	-
Hydrogen peroxide (H_2O_2)	Purified CZH20_DyP	0.05
	Partially Purified CZH20_DyP	0.05
Sodium azide	Purified CZH20_DyP	5
	Partially Purified CZH20_DyP	-

The effects of various concentrations of metal ions on the purified CZH20_DyP (Figure 4.24) and partially purified CZH20_DyP (Figure 4.25) indicated that the metal ions had the same effect regardless of the purity of the enzyme. With the increase in concentration of manganese (0.1 mM to 5 mM), the highest degree of inhibition by all the metal ions for purified and partially purified DyP-type peroxidase was identified. In contrast, copper for both DyP-type peroxidases had an enhancing effect on both purified and partially purified DyP-type peroxidase. Magnesium and zinc, for both samples, exhibited low inhibition, but also enhanced enzyme activity as the concentration of the metal ion increased. The remaining metal ions, cobalt and iron, exhibited an enhancing effect from 0.1 mM to 1 mM, however inhibition by these ions increases as the concentration of the metal ion increases to 5 mM.

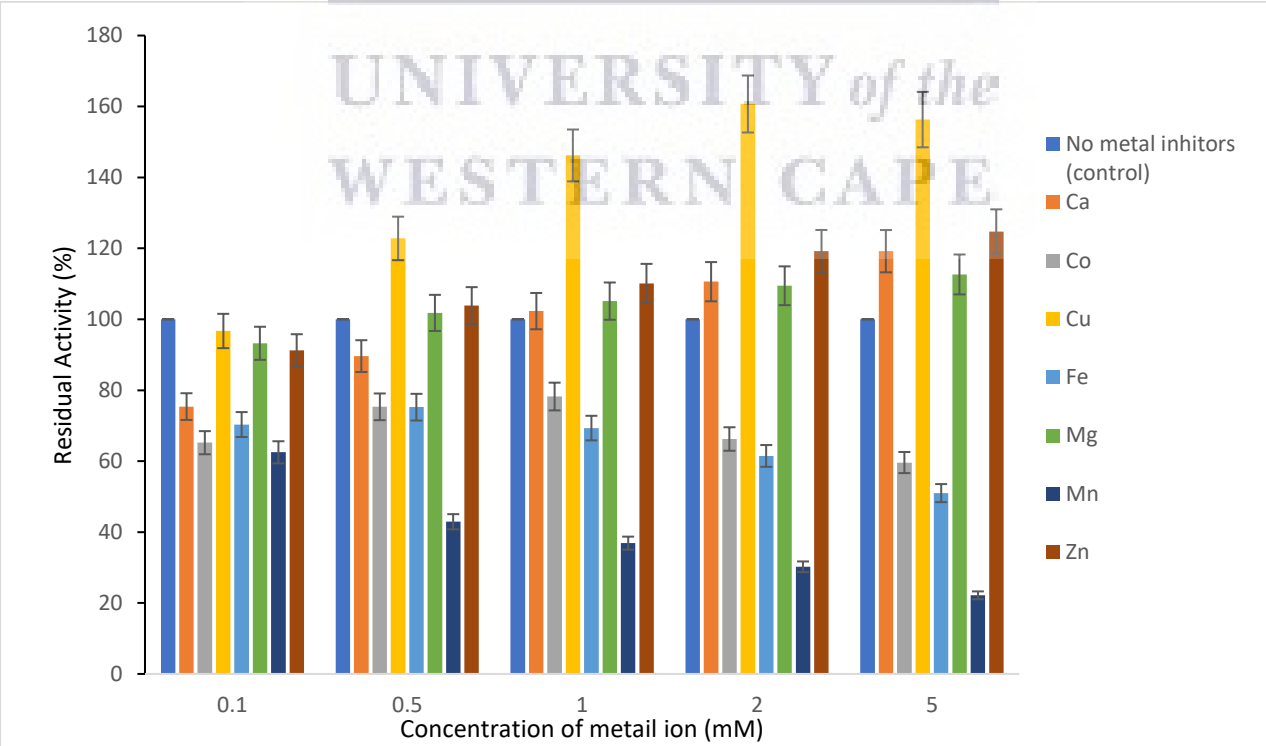

Figure 4.24: The effect of various concentrations of metal ions on the residual activity of Purified CZH20_DyP. Error bars represent the standard deviation of triplicate analyses.

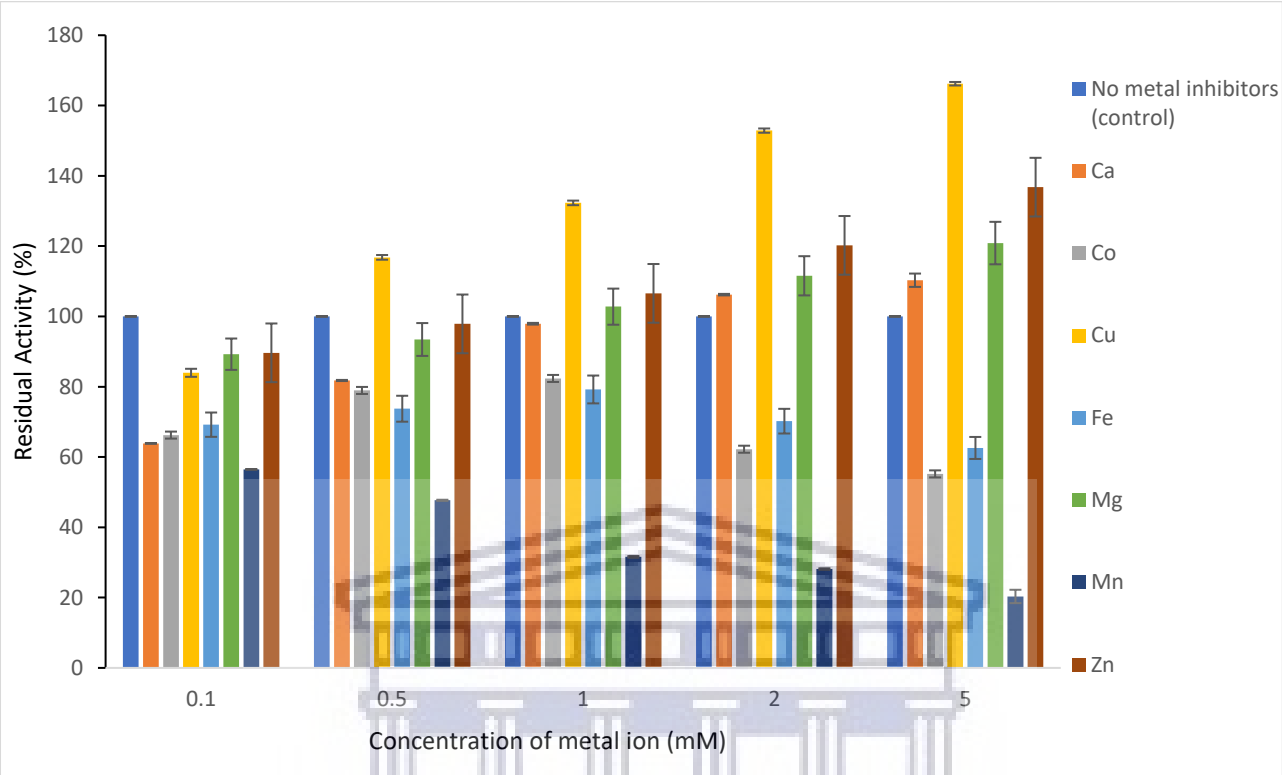

Figure 4.25: The effect of various concentrations of metal ions on the residual activity of partially purified CZH20_DyP. Error bars represent the standard deviation of triplicate analyses.

4.4.4 Effect of Organic Solvents on Enzyme Activity

The effect of various organic solvents on the oxidation of 2,4-DCP by the purified and partially purified DyP-type peroxidase was assessed at 10, 20, 30 and 40% (v/v) concentrations (Figure 4.26 and Figure 4.27). Over the incubation period of one hour and the varying concentrations, a decrease in enzyme activity was observed in both the purified (Figure 4.25) and partially purified CZH20_DyP (Figure 4.26) samples in relation to that of the control.

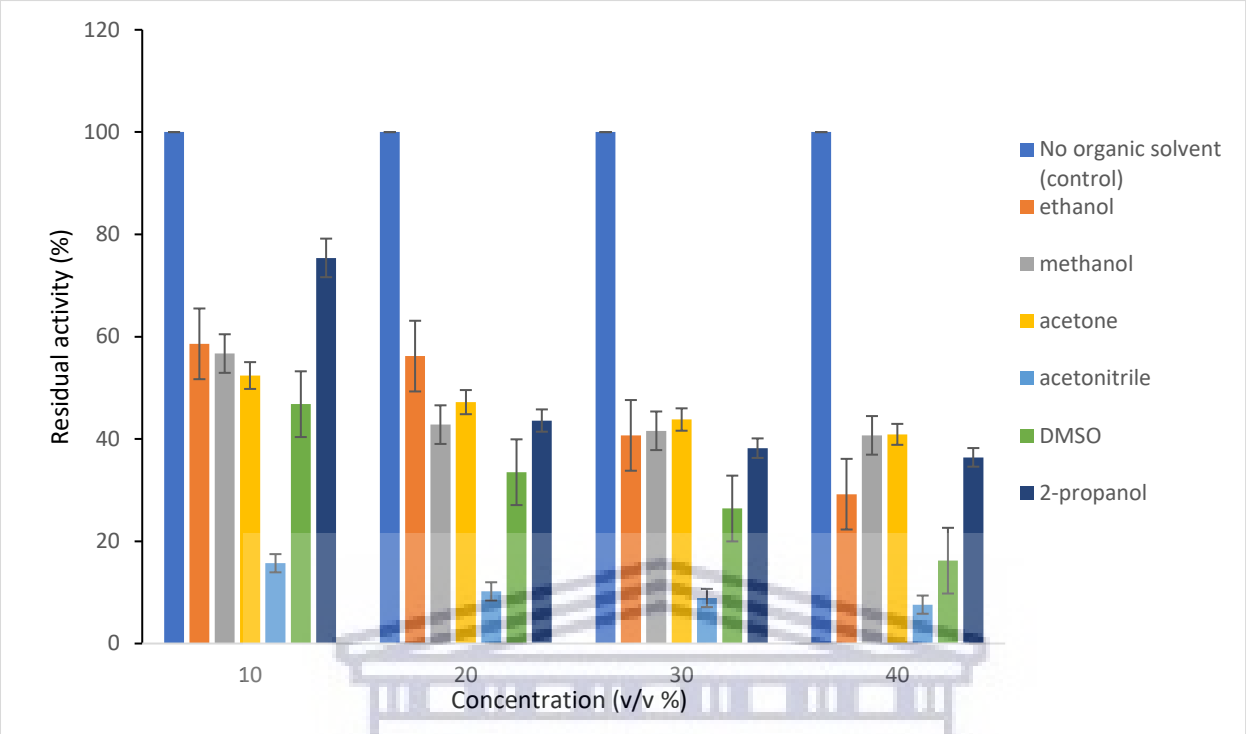

Figure 4.26: The residual activity of purified CZH20_DyP after incubation for 1 hour with different concentrations of organic solvents. Error bars represent the standard deviation of triplicate analyses.

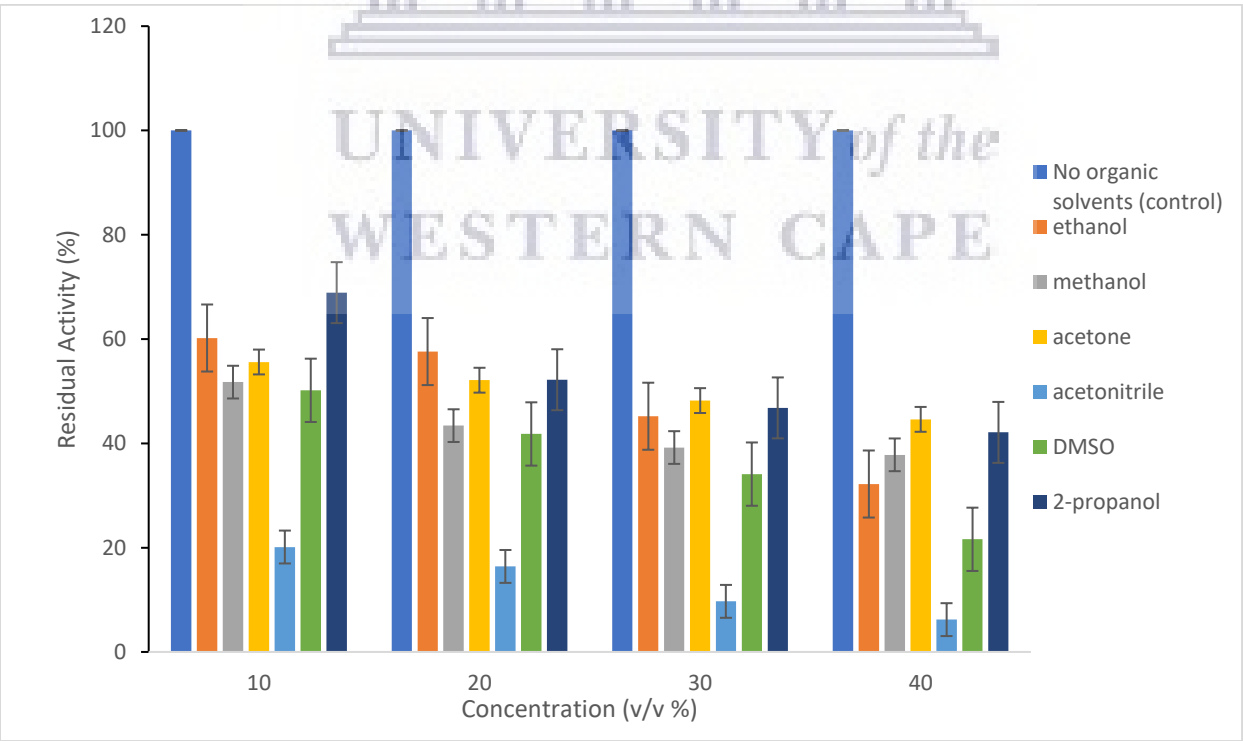

Figure 4.27: The residual activity of partially purified CZH20_DyP after incubation for 1 hour with different concentrations of organic solvents. Error bars represent the standard deviation of triplicate analyses.

4.4.5 Enzyme Kinetics

The kinetic parameters V_{max} and K_m were determined for the oxidation of 2,4-DCP by the use of non-linear regression analysis (Michaelis-Menton) (Table 4.10). Data was analysed using GraphPad version 10 for the purified and partially purified CZH20_DyP.

Table 4.10: The kinetic constants of the purified and partially purified CZH20_DyP.

Strain name	K_m (in mM)	V_{max} (in nmol/mg/protein.min)
Purified CZH20_DyP	29.17	142
		-
Partially Purified CZH20_DyP	36.44	155

4.4.6 Spectral Characteristics

A complete wavelength scan, 200 nm to 700 nm, of the purified and partially purified CZH20_DyP was performed. Literature states that a peak at approximately 400 nm corresponds to the Soret band typical of haem-containing peroxidases. Our data therefore indicates that the CZH20^T DyP-type peroxidase contains a haem moiety in its structure and is a haem peroxidase (Figure 4.28 and Figure 4.29).

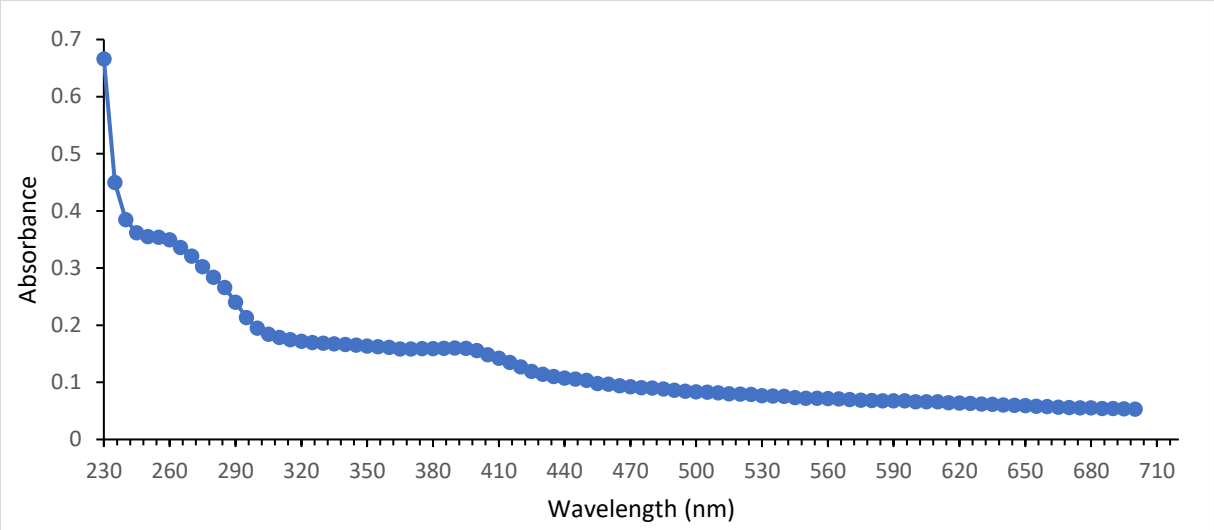

Figure 4.28: UV/VIS scan of the purified DyP-type peroxidase with a peak at approximately 400 nm of the Soret band.

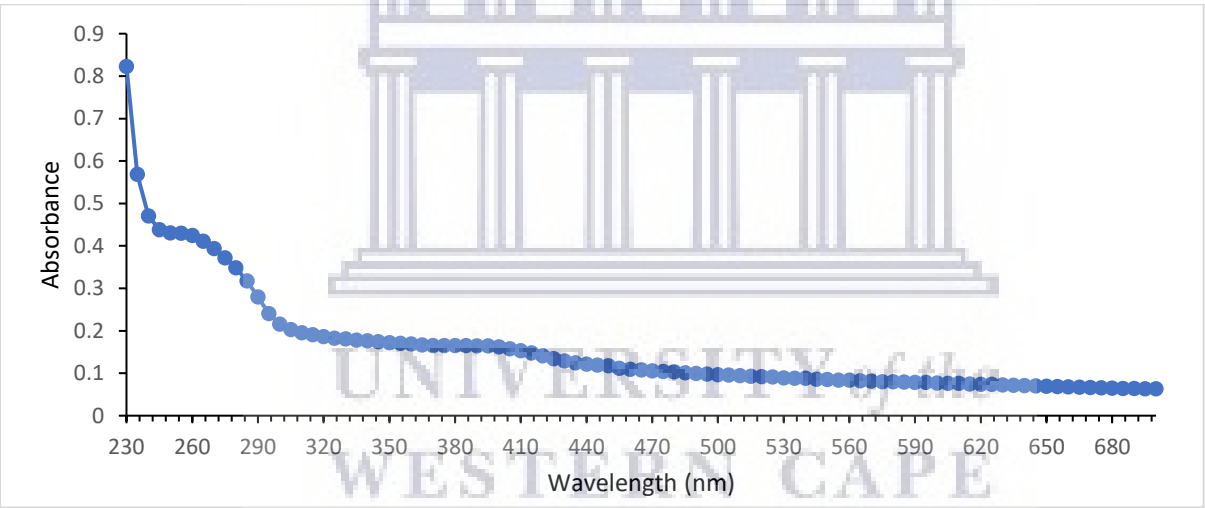

Figure 4.29: UV/VIS scan of the partially purified DyP-type peroxidase with a peak at approximately 400 nm of the Soret band.

4.4.7 Dye decolourisation assays

To identify the ability of the purified and partially purified CZH20_DyP to decolourise dyes, 100, 75, 25, 10 and 1 µM solutions of each dye were prepared in 50 mM sodium acetate buffer (pH 3.5), 50 mM sodium acetate buffer (pH 5.5), 50 mM potassium phosphate buffer (pH 7.5) and 50 mM Tris-HCl buffer (pH 9.5). Two hundred µL of the dye solution and 50 µL 50 mM H_2O_2 (prepared in respective buffers) were aliquoted into a 96 well microtitre plate in triplicate and 50 µL of a 1 U/mL enzyme solution was added

to each well. The decrease in absorbance was monitored over a 6-hour period, scanning at 30 minute increments, as well as after 24 hours of incubation at ambient temperature (25 ± 2 °C) whereby a graph was constructed based on the final 24 hour period of degradation. Oxidation of Reactive Blue 4 (anthraquinone dye) was monitored at 597 nm (ε = 4200 M^{-1} cm^{-1}), Reactive Black 5 (azo dye) at 598 nm (ε = 37 200 M^{-1} cm^{-1}), and Azure B (thiazine dye) at 605 nm (ε = 8700 M^{-1} cm^{-1}) (Figure 4.30 and Figure 4.31).

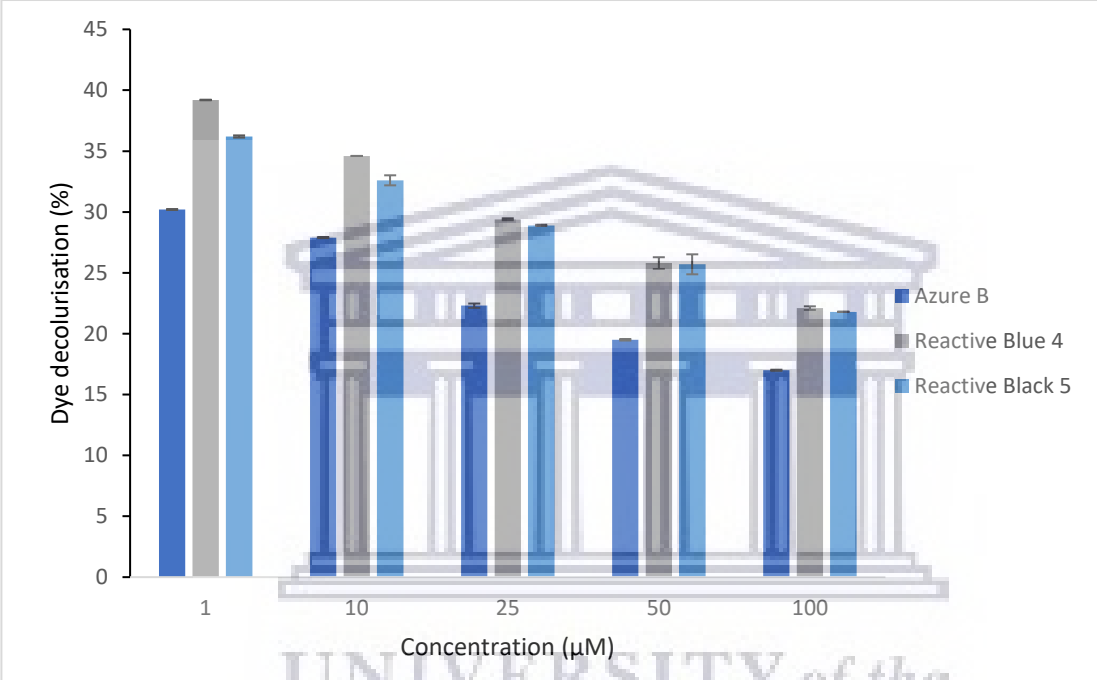

Figure 4.30: Dye decolourisation by the purified CZH20_DyP after 24 hours. All three dyes were tested at varying concentrations (1-100 µM). Graph was constructed based on the final 24-hour period. Error bars represent the standard deviation of triplicate analyses.

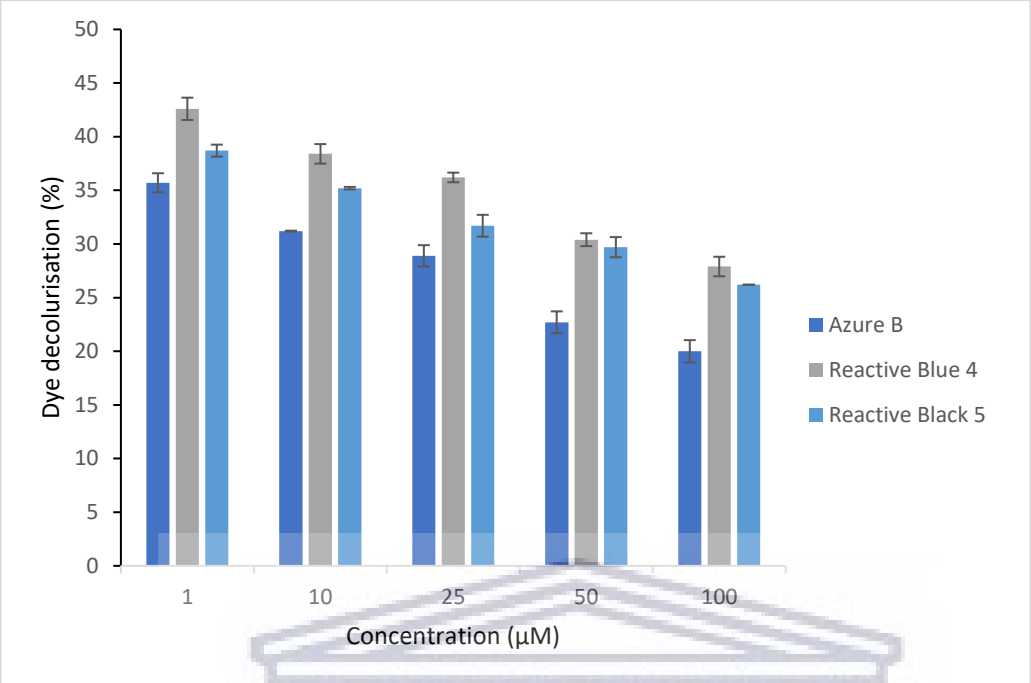

Figure 4.31: Dye decolourisation by the partially purified CZH20_DyP after 24 hours. All three dyes were tested at varying concentrations (1-100 µM). Graph was constructed based on the final 24-hour period. Error bars represent the standard deviation of triplicate analyses.

The findings of this study indicated that of the 26 DyP-type peroxidases identified from WGS, eight contained the PRED-TAT sequences conserved in DyPs. Primers were designed and seven sequences were successfully amplified. Two were cloned namely, CZH20_DyP and 30_1_DyP and expressed in Arctic Express in Auto Induction medium with optimal expression at 30 °C. These two samples were purified and only the CZH20_DyP, was selected for further biochemical charcaterisation. The next chapter will discuss the findings more in detail.

CHAPTER FIVE
DISCUSSION

Actinobacteria represent one of the most diverse bacterial phyla and have been extensively characterised and exploited for their potential over the years (Goodfellow, 2012). Actinobacteria occur in numerous and unique environments that have become hotspots for the discovery of novel biomolecules, such as enzymes and antibiotics, thus driving an active field of research and discovery. This group of bacteria are especially well recognised for their production of primary and secondary metabolites that have wide ranging applications in a variety of fields (Ranjani *et al.,* 2016). Additionally, actinobacteria are well known for their ability to produce extracellular enzymes that contribute to a range of applications, especially actinobacterial peroxidases that have shown industrial applications in the bioremediation of recalcitrant and toxic xenobiotics (Chen *et al.,* 2015a).

Peroxidases occur in nature across all areas of life and have the ability to oxidise a range of predominantly aromatic substrates using haem as their co-factor (Battistuzzi *et al.,* 2010). This study focused on a specific family of haem containing peroxidases, namely the dye-decolourising peroxidases (DyPs). The distinct feature of these enzymes is their potential in the bioremediation of recalcitrant dyes that are released into the environment as industrial waste (Bansal and Kanwar, 2013). DyP-type peroxidases potentially play a role in the degradation of anthraquinone compounds; however, their inherent function is still yet to be characterised (Sugawara *et al.,* 2019).

In this study, a genome mining approach was used to identify DyP-type peroxidase genes from the whole genome sequences of 21 actinobacterial strains isolated from various environments in South Africa and Zambia (Table 3.1). The genomes were assembled using the A5-miseq pipeline (Coil *et al.*, 2015) and annotated using the online server RAST (Rapid Annotations using Subsystems Technology) (Meyer *et al.*, 2008). The RAST output files contained thousands of predicted genes relating to the various functions of the annotated genome. Twenty-six DyP-type peroxidase genes were identified, and the relevant amino acid sequences were analysed using BLASTp analysis. BLASTp analysis

showed that all the predicted DyP-type sequences were homologous to DyP-type peroxidases present in whole genome sequences of actinobacterial strains with 100% sequence identity. The DyP-type gene sequences were derived from *Streptomyces* species, as well as non-streptomycete species, with the majority of sequences clustering within the *Streptomyces* DyP-type peroxidases clade.

Classification of the DyP-type peroxidases was based on the presence of the twin arginine translocation (TAT)-signal peptides, detected using PRED-TAT, which is a prediction model for signal peptides. The general secretion route, termed the Sec-pathway, is responsible for the transmembrane translocation of proteins in their unfolded conformation. As a result, they fold into their native structures at the trans-side of the membrane (Sturm *et al.,* 2006). However, in the TAT-pathway, the secretory proteins are translocated in their folded state (Natale *et al*., 2008). Despite the targeting signals that direct secretory proteins to these pathways showing high similarity, the translocation mechanisms and translocases involved are vastly different. For the DyP-type peroxidase class I (intermediate) the TAT-pathway is involved, which suggest that this class represents either periplasmic or extracellular proteins. The majority of the peroxidase genes identified by genome mining contained the TAT-signal belonging to class I (formerly class A) DyP-type peroxidases. PSORTb analysis was performed to determine whether the signal peptides were periplasmic or extracellular (Maibeche *et al.*, 2022).

Eight TAT-signals were identified from the 26 DyP-type peroxidase sequences with a reliability score as low as 0.956 and as high as 1.000 confirming the presence of the signal peptide. Class I DyP-type peroxidases are typically 395-455 amino acids in length. SnapGENE® Viewer was used to predict the amino acid length of all the DyP-type sequences. The derived amino acid lengths were between 300-500. This further supports the classification of these peroxidases as Class I DyP-type peroxidases. Phylogenetic analysis of these DyP-type sequences used in this study was aligned to a well-established DyP-type peroxidase from *Thermobifida fusca* (accession no. NC_007333.1) while the DyP-type peroxidase from *Bacillus subtilis* (accession no. KFK78021.1) was used as a non-actinobacterial enzyme. It is not surprising that the majority of the sequences derived from *Streptomyces* species aligned into one clade, whereas the non-steptomycete sequences predominantly formed their own (with a few streptomycete-derived

sequences). Analysis revealed that the majority of the TAT-signals were found in sequences that clustered in the *Streptomyces* DyPs clade.

Primers were designed to amplify the DyP-type peroxidase genes from eight actinobacterial strains. DNA-MAN was used to confirm several parameters, namely, primer binding site in the target gene, the optimal annealing temperature, the predicted amplicon size and compatibility with restriction enzymes (Supplementary Sheet A). All eight actinobacterial DyP-peroxidases amplified. However, the gene amplified from one strain, SPR^T, was identified as a catalase/peroxidase, and was therefore excluded from the study. Six DyP-type peroxidases were successfully digested using *Nde*I and *Xho*I, ligated into pET-20b(+) and transformed into *E. coli* JM109. Transformation of the S129 constructs, was unsuccessful, and was therefore excluded from the study. Colony PCR was used to confirm that the correct construct had been obtained. The cloned genes, CZH20-DyP and 30-1-DyP were amplified with DyP primers and sequenced to confirm their identity. BLAST analysis confirmed that the cloned DyP-type peroxidase 3 sequence from CZH20^T was identified as being most similar to the *Nocardia tenerifensis* (96% sequence similarity) DyP, while the 30-1 DyP revealed a sequence identity to the *Micromonospora aurantiaca* ATCC 27029 DyP (98% sequence identity).

Protein expression of dye decolourising peroxidase was first detected in the crude extracellular enzyme preparations of a fungal strain *Bjerkandera adusta* (Kim *et al.,* 1995). Subsequent studies on the purified protein found that it was a haem protein (60 kDa) with the ability to efficiently oxidise anthraquinone dyes (Kim and Shoda, 1999). In the present study, protein expression occurred in four expression hosts, at 25 mL scale with Arctic Express being the most successful, based on the protein concentration of the expressed proteins. It should be noted that due to time constraints only plasmids purified from *E. coli* JM109_CZH20^T and *E. coli* JM109_30-1 were transformed into the four expression hosts. The results revealed that the highest protein concentrations of 0.124 mg/mL for CZH20^T_DyP_AE with an expected protein size of ~44 kDa, and 0.135 mg/mL with an expected protein size of ~41kDa for 30-1_DyP_AE, was achieved in Auto Induction medium at 30 °C.

Multiple research projects have been conducted on the heterologous expression and purification of fungal and bacterial DyP proteins. However, no research has been published using the Arctic Express system for heterologous expression for bacterial DyPs as was selected for in this study. Most research using this expression system has been on fungal species. Studies performed by Kaplan *et al.* (2011) on heterologous expression of nitrilase from *Aspergillus niger* K10 used BL21(DE3), BL21-Gold(DE3), BL21-Gold(DE3)pLys, BL21-CodonPlus(DE3)-RIPL, BL21-CodonPlus(DE3)-RIL, Rosetta-gami 2 (DE3), ArcticExpress(DE3), ArcticExpress(DE3)-RP and ArcticExpress(DE3)-RIL for heterologous expression. They reported that the highest total activities was detected in BL21 and Rosetta-gami strains (65 and 230 U/L, respectively) compared to the Arctic Express strains (34-150 U/L). In this study, the four expression hosts were *E. coli* BL21 (DE3), Rosetta™ (DE3) PLysS, SHuffle® T7, and ArcticExpress RP. When expression was scaled up to 200 mL the CZH20^{T}_DyP_AE_Auto Induction medium of the uninduced insoluble fraction 2 had the highest protein concentration (10.49 mg/mL) (Table 4.8).

For enzyme purification of CZH20^{T}_DyP_AE_Auto Induction medium, the large scale (200 mL culture) crude protein preparation was successfully applied to the FPLC column in 4 mL increments and the resulting fractions analysed. Unfortunately, the purification resulted in a decrease in protein concentration as well as specific activity (protein purity). It was hypothesized that this could be due to the loss of the haem co-factor. Studies of recombinant haemoproteins suggest that it is necessary to supply sufficient haem for soluble and functional haemoprotein production (Graves *et al.,* 2008; Akhtar and Jones, 2014). Strategies have been developed to increase the solubility as well as stability of haemoproteins through the incorporation of increased levels of hemin and its precursor 5-aminolevulinic acid (ALA) in microbial culture media (Sudhamsu *et al.,* 2010; Varnado and Goodwin, 2004). Furthermore, if the levels of co-factors are low in the culture production this may result in reduced enzymatic activity (Krainer *et al.,* 2015; Jiang *et al.,* 2008). This suggests that for the optimisation of expression the increase in levels of haem may result in a higher expression of the protein of interest and through purification the co-factor may not decrease as observed in this study. However, with the detection of the Soret band for both the purified and partially purified CZH20-DyP at approximately 400 nm (Figures 4.28 and 4.29) gives an indication that a haem moiety is present within this enzyme structure, confirming its identification as a haem peroxidase.

Purified CHZ20-DyP and partially purified CZH20-DyP were subjected to biochemical characterisation through investigation of certain parameters. The ability for the two DyP-type protein preparations (purified and partially purified) to oxidise the substrate 2,4-DCP in different buffers (over the pH range 2.0 to 9.0) was determined after a 24-hour incubation at room temperature (25 ± 2 °C). The DyP-type protein from both samples was stable around pH 5.0 and pH 10.0, with maximum specific activity for the purified sample observed at pH 7.0 and the partially purified enzyme at pH 7.5 with an optimal range being observed between pH 5.0 and 9.0. There was a drastic loss of activity around pH 3.0 to pH 4.5 when incubated for one hour. It is interesting to note that the purified CZH20-DyP was stable in *Legionella* Acid Buffer (pH 2.0). As aforementioned, to identify whether chemical or enzymatic hydrolysis occurred future work would need to be conducted using a different enzyme, no enzyme at all or a well-characterised peroxidase (such as Horseradish peroxidase) to serve as a control. The optimal temperature for the two CZH20-DyP protein preparations for the oxidation of the substrate 2,4-DCP was investigated at temperatures ranging from 25 °C to 45 °C in 5 °C intervals. The optimal temperature for oxidation was observed at 35 °C for both. A study conducted by Elmetwalli *et al.* (2023) investigated the optimal pH of *Bacillus aryabhattai* B8W22 peroxidase which was found to be pH 8.0. Furthermore, Musengi *et al*. (2020) reported that the peroxidase from *Streptomyces albidoflavus* BSII#1 had an optimal pH between 5.0 and 10.0 and was stable at temperatures between 40 and 60 °C, similar to the observations made in this study. The higher temperature stability of the BSII#1 DyP was most probably related to the strain's isolation environment (hot springs), whereas *N. gamkensis* CZH20^T was isolated from the banks of the Gamka River, a more moderate environment. Future work would be to include a temperature stability assay as well to identify the most stable temperature and time period the DyP-type enzyme can remain active and stable at.

DyPs have the potential to be industrially viable and it remains critical to assess the tolerance of pH and temperature, as well the effects of various inhibitors, reducing agents, and metal ions. In this study, the CZH20-DyP was strongly inhibited by hydrogen peroxide with the lowest concentration tested showing complete inhibition of the protein (Table 3.10). Hydrogen peroxide is a co-factor of DyP-type peroxidases thus for the oxidation of

2,4-DCP as the substrate and hydrogen peroxide as the co-factor only the immediate results are defined over the assay period (5-minutes). The incubation of the DyP-type peroxidase with hydrogen peroxide, at varying concentrations, for 1 hour indicates that exposure for this time period causes rapid inhibition of the enzyme. Sodium chloride (NaCl), sodium dodecylsulphate (SDS), EDTA and sodium azide showed little to no inhibitory effects on the purified and partially purified DyP-type peroxidase preparations. Inhibition of purified and partially purified DyP-type peroxidase was similar in the presence of L-cysteine, sodium metabisulphite, L-ascorbic acid, and sodium azide over the concentration range of 0.1 mM to 5 mM. Of these inhibitors, sodium azide completely inhibited both DyP-type protein preparations. The inhibitory effect that sodium azide has on haem peroxidases, in particular horseradish peroxidase (HRP), is due to the production of azidyl from the interactions of HRP and sodium azide. The production of azidyl modifies a methionine residue near the haem or the group co-ordinated with the haem itself, resulting in loss of activity (Brill and Weinryb, 1967; Oritz de Montellano *et al.,* 1988). Since the absorption spectrum for the purified and partially purified CZH20-DyP showed a peak at 400nm (Soret band characteristic of haem peroxidases), it stands to reason that sodium azide would have an inhibitory effect on this peroxidase.

Various metal ions can also have a significant impact on DyP activity. Azevedo *et al.* (2003) investigated the effect of metal ions on DyP B, and they reported that calcium, manganese and zinc increased extracellular activity with zinc being the most proficient metal ion (Azevedo *et al.,* 2003). Some metal ions, such as mercury and iron, have a strong inhibitory effect on DyP and may destroy the hydrogen peroxide transfer mechanism. The most common heavy metals present in wastewater is lead, mercury, nickel, cadium, copper, arsenic, and chromium (Qasem *et al.,* 2021). The purified and partially purified CZH20-DyP produced in this study were inhibited by most of the metals, except for copper and zinc. The copper seemed to significantly increase activity of the samples with a residual activity of 160% for the purified CZH20-DyP at 2 mM and 166% for the partially purified CZH20-DyP at 5 mM after 1 hour incubation. There was negligible activity change for calcium across the concentration range tested (0.1 mM to 5 mM), however magnesium caused a great degree of inhibition with an increase in concentration for the two CZH20-DyP samples. Musengi *et al*. (2014) reported that they observed an increase in activity in the presence of copper. Furthermore, zinc was found to have no significant inhibitory

effect on their enzyme, whereas in the present study zinc enhanced enzyme activity with increase in concentration of the metal ion. It still remains difficult to characterise and associate inhibitory effects of metal ions, however it remains incredibly impactful to understand the effects especially in the context of potential industrial applications.

Enzymes are employed in a plethora of applications such as catalysts in chemical syntheses and industrial processes (Schmid *et al.,* 2001). A lot of research has focused on making enzymes active in organic solvents, however many of them remain inactivated or denatured in the presence of solvents (Carrea and Riva, 2000; Ogino and Ishikawa, 2001). The activities of the CZH20-DyP preparations were inhibited across the majority of concentrations of the various organic solvents tested, with acetonitrile showing the most inhibition (even at the lowest concentration tested, 10%, v/v). This is comparable to the study performed by Musengi *et al.* (2014). To circumvent the inhibitory effect of organic solvents, a modification of the active site would be necessary to maintain stability and activity in the presence of various concentrations of an organic solvent.

The kinetic properties of the two CZH20-DyP preparations were deduced using Graphpad. Graphpad analyses scientific data and performs statistical analysis to generate concise data. The K_m of the purified and partially purified CZH20-DyP was determined to be 29.17 mM and 36.44 mM, respectively. The V_{max} was 142 nmol/mgprotein/min and 155 nmol/mgprotein/min (Supplementary Sheet E). The comparison of the V_{max} of both CZH20-DyP preparations showed lower V_{max} than that of the DyP produced by *Streptomyces viridosporus* T7A (465.8 nmol/mgprotein/min; Yee and Wood, 1997) and the DyP produced by *Streptomyces* sp. AD 001 (529.7 nmol/mgprotein/min; Jeong-Ho *et al.,* 2002). To further assess the V_{max} value of the CZH20-DyP preparations, an increase of substrate concentrations from the original 1-10 mM to that of 1-40 mM should be applied in order to fully understand the kinetic activity of the enzyme.

One of the least understood properties of DyP-type peroxidases is their ability to degrade synthetic, azo and anthraquinone dyes, aromatic compounds and sulphides (Sugano *et al.,* 2007). In this study, Azure B (thiazine dye), Reactive Blue 4 (anthraquinone dye), and Reactive Black 5 (azo dye) were tested in dye decolourisation assays. The highest percentage of degradation for all dyes was at 1 µM dye concentration, which was the

lowest concentration evaluated. Reactive Blue 4 dye decolourisation was most proficient, with decolourisation values of 39% and 42% for the purified and partially purified CZH20-DyP, respectively. Overall, all the dyes were decolourised to various degrees which is in alignment with what was reported in previous studies (Strittmatter *et al.,* 2015, Musengi *et al*., 2014 and Xu *et al*., 2021).

CHAPTER SIX
CONCLUSION

In this study, annotated whole genome sequences of actinobacterial species were mined for the presence of DyP-type peroxidases. Twenty-six sequences of dye-decolourising peroxidases were identified in the 21 actinobacterial strains investigated. Bioinformatic analysis and phylogenetic screening deduced the presence of a TAT-signal peptide sequence which supported the identification of the sequences as belonging to class I (formerly class A) bacterial DyP-type peroxidases. Primers for DyPs were designed and the resulting amplicons were successfully cloned and expressed in four expression hosts. The peroxidase from *Nocardia gamkensis* sp. CZH20^T and *Micromonospora* sp. strain 30-1 was successfully homologously expressed in ArcticExpress RP at 30 °C, and the approximate molecular mass of the resulting proteins was determined to be 44 kDa and 41 kDa, respectively. Purification using fast performance liquid chromatography resulted in active DyP-type peroxidases in the purified and partially purified extracts from CZH20^T. Biochemical characterisation revealed a 'typical' actinobacterial DyP-type peroxidase that functioned over a wide range of pH and at a temperature optimum of 35 °C. The effect of inhibitors, reducing agents and metals were comparative to that of studies conducted with an unexpected tolerance to sodium azide, as well as zinc being observed. Residual enzyme activity across an increasing concentration range of organic solvents revealed 'typical' activity observed for bacterial DyP-type peroxidases (when compared to reports in literature), and the decolourisation of an anthraquinone, azo and thiazine dye was observed in which the most decolourisation occurred in the anthraquinone dye experimental work (as predicted in literature). Future studies will explore the ability of the enzyme to decolourise a wider range of dyes, to cross-link lignin model compounds, and its application in synergistic studies with other enzymes.

This study highlights that genome mining of whole genome sequences allows researches to access a wealth of previously untapped genetic potential. This is the first description of a DyP-type peroxidase from a *Nocardia* species, which warrants further investigation. The study objectives have been met however, with limitations in assessing all the DyP-type peroxidases selected, in particular for ligation, in future it would be best to vary the

molar ratio of vector to plasmid to successfully transform the plasmid-inserts and further transform them into all expression hosts. Additionally, testing the dye degradation on a wider range of dyes could enhance further understanding and characterisation of dye decolourising peroxidases. Biochemical characterisation of CZH20^{T}_DyP could lead to applications with potential industrial value.

REFERENCES

Abd-Elsalam, K.A. (2003) Bioinformatic tools and guideline for PCR primer design. *African Journal of Biotechnology,* 2(5): 91-95.

Adav, S.S., Ng, C.S., Arulmani, M., Sze, S.K. (2010) Quantitative iTRAQ secretome analysis of cellulolytic *Thermobifida fusca. J. Proteome Res.*, 9: 3016-3024.

Ahmad, M., Pataczek, L., Hilger, T.H., Zahir, Z.A., Hussain, A., Rasche, F., Schafleitner, R. and Solberg, S.Ø. (2018) Perspectives of Microbial Inoculation for Sustainable Development and Environmental Management. *Front. Microbiol.* 9:2992.

Ahmad, M., Roberts, J.N., Hardiman, E.M., Singh, R., Eltis, L.D., Bugg, T.D. (2011) Identification of DypB from *Rhodococcus jostii* RHA1 as a lignin peroxidase. *Biochem.,* 50: 5096-5107.

Akhtar, M.K. and Jones, P.R. (2014) Cofactor engineering for enhancing the flux of metabolic pathways. *Front Bioeng. Biotechnol.*, 2, 30.

Albarano, L., Esposito, R., Ruocco, N. and Costantini, M. (2020) Genome mining as new challenge in natural products discovery. *Mar. Drugs*, 18(4): 199-216.

Allison, S. D., and Martiny, J. B. H. (2008) Resistance, resilience, and redundancy in microbial communies. *Proc. Natl. Acad. Sci. U.S.A.*, 108, 11512–11519.

Allison, S. D. (2012) A trait-based approach for modeling microbial litter decomposition. *Ecol. Lett*. 15, 1058–1070.

Amann, R.I., Ludwig, W. and Schleifer, K.H. (1995) Phylogenetic identification and in situ detection of individual microbial cells without cultivation. *Microbiol. Rev.*, 59:143-169.

Anandan, R., Dhanasekaran, D., Manogaran, G.P. (2016) An Introduction to Actinobacteria, Actinobacteria – Basics and Biotechnological Applications, Dharumadurai Dhanasekaran and Yi Jiang, IntechOpen. Published online. [viewed 2020].

Asad, S., Amoozegar, M.A., Pourbabaee, A.A., Sarbolouki, M.N. and Dastgheib, S.M. (2007) Decolourization of textile dyes by newly isolated halophilic and halotolerant bacteria. *Biores. Tech.*, 98: 2082-2088.

Azevedo, A.M., Martins, V.C., Prazeres, D.M., Vojinović, V., Cabral, J.M., Fonseca, L.P. (2003) Horseradish peroxidase: A valuable tool in biotechnology. *Biotechnol. Annu. Rev*., 9: 199–247.

Aziz, R.K., Bartels, D., Best, A.A., DeJongh, M., Disz, T., Edwards, R.A., Formsma, K., Gerdes, S., Glass, E.M., Kubal, M., Meyer, F., Olsen, G.J., Olson, R., Osterman, A.L., Overbeek, R.A., McNeil, L.K., Paarman, D., Paczian, T., Parrello, B., Pusch, G.D., Reich, C., Stevens, R., Vassieva, O., Vonstein, V., Wilke, A., Zagnitko, O. (2008) The RAST server: rapid annotations using subsystems technology. *BMC Gen.*, (9):75.

Baban, A., Yediler, A., Ciliz, N.K. (2010) Integrated water management and CP implementation for wool and textile blend processes. *Clean,* 38(1): 84-90.

Babu, B.R., Parande, A.K., Kumar, S.A. and Bhanu, S.U. (2011) Treatment of dye effluent by electrochemical and biological processes. *Open J. Saf. Sci. Technol.,* 1: 12-18.

Bafana, A., Chakrabarti, T., Devi, S.S. (2008) Azoreductase and dye detoxification activities of *Bacillus velezensis* strain AB. *Appl. Microbiol. Biotechnol.,* 77: 1139-1144.

Bagos, P.G., Nikolaou, E.P., Liakopoulos, T.D., Tsirigos, K.D. (2010) Combined prediction of Tat and Sec signal peptides with hidden Markov models. *Bioinfor.*, 26(22): 2811-2817.

Banci, L. (1997) Structural properties of peroxdases. *J. Biotechnol.,* 53:253-263.

Barr, D.P. and Aust, S.D. (1994) Mechanisms white rot fungi use to degrade pollutants. *Environ. Sci. Technol.,* 28: 78-87.

Bansal, N. & Kanwar, S.S. (2013) Peroxidase(s) in environment protection. *Sci. World J.*, 714639, 9.

Battistuzzi, G., Bellei, M., Bortolotti, C.A., Sola, M. (2010) Redox properties of heme peroxidases. *Arc. of Biochem. and Biophy.*, 500(1), 21–36.

Bayoumi, M.N., Al-Wasify, R.S., Hamed, S.R. (2014) Bioremediation of Textile Wastewater Dyes using Local Bacterial Isolates. *Int. J. Curr. Microbiol. Appl. Sci.,* 3(12): 962-970.

Bell, J., Plumb, J.J., Buckley, C.A., Stuckey, D.C. (2000) Treatment and decolourization of dyes in an anaerobic baffled reactors. *J. Environ. Eng. Div.*, ABCE 126: 1026-1032.

Berradi, M., Hsissou, R., Khudhair, M., Assouag, M., Cherkaoui, O., El Bachiri, A., El Harfi, A. (2019) Textile finishing dyes and their impact on aquatic environs. *Heliy.*, 5(11): e02711.

Betancur, L.A., Naranjo-Gaybor, S.J., Vinchira-Villarraga, D.M., Moreno-Sarmiento, N.C., Maldonado, L.A., Suarez-Moreno, Z.A. (2017) Marine *Actinobacteria* as a source of compounds for phytopathogen control: An integrative metabolic-profiling/bioactivity and taxonomical approach. PLoS ONE 12(2): e0170148.

Bornscheuer, U.T., Huisman, G.W., Kazlauskas, R.J., Lutz, S., Moore, J.C., Robins, K. (2012) Engineering the third wave of biocatalysis. *Nat.,* 485: 185-194.

Brill, A.S., Weinryb, I. (1967) Reactions of horseradish peroxidase with azide. Evidence for a methionine residue at the active site. *Biochem.,*6: 3528-3535.

Brown, D., Hamburger, B. (1987) The degradation of dyestuffs, Part 111 – investigations of their ultimate degradability. *Chemo.*, 16: 1539-1553.

Burner, U., Krapfenbauer, G., Furtmuller, P.G., Regelsbeger, G., Obinger, C. (2000) Oxidation of hydroquinone, 2,3-dimethylhydroquinone and 2,3,5-trimethylhydroquinone by human myeloperoxidase. *Redox. Rep.,* 5: 185-190.

Carrea, G., Riva, S. (200) Properties and synthetic applications of enzymes in organic solvents. *Angew. Chem. Int. Ed. Engl.,* 39 (2000): 2227-2254.

Catucci, G., Valetti, F., Sadeghi, S.J. Gilardi, G. (2020) Biochemical features of dye-decolorizing peroxidases: current impact on lignin degradation. *Biotechnol. Appl. Biochem*. 67: 751–759.

Costa, R.B., O'Flaherty, V., Lens, P.N.L. (2020) Biological treatment of organic sulfate-rich wastewaters. In: Environmental Technologies To Treat Sulfur Pollution: Principles and Engineering, 2nd Edition, Piet N. Lens (Ed.).

Chander, M., Arora, D.S. (2007) Evaluation of some white-rot fungi for their potential to decolourise industrial dyes. *Dyes and Pig.*, 72(2): 192-198.

Chater, K.F., Biró, S., Lee, K.J., Palmer, T., Schrempf, H. (2010) The complex extracellular biology of *Streptomyces*. *FEMS Microbiol. Rev.*, 34(2): 171-198.

Chen, H. (2006) Recent advances in azo dye degrading enzyme research. *Curr. Prot. Pept. Sci.,* 7: 101-111.

Chen, C., Shrestha, R., Jia, K., Gao, P.F., Geisbrech, B.V., Bosmann, S.H., Shi, J., Li, P. (2015a) Characterization of dye-decolorizing peroxidase (DyP) from *Thermomonospora curvata* reveals unique catalytic properties of A-type DyPs. *J. Bio. Chem.*, 290(38), 23447–23463.

Chen, M., Xu, P., Zeng, G., Yang, C., Huang, D., Zhang, J. (2015b) Bioremediation of soils contaminated with polycyclic aromatic hydrocarbons, petroleum, pesticides, chlorophenols and heavy metals by composting: applications, microbes and future research needs. *Biotechnol. Adv.*, 33: 745-755.

Coil, D., Jospin, G., Darling, A.E (2015) A5-miseq: an updated pipeline to assemble microbial genomes from Illumina MiSeq data. *Bioinfor.*, 31: 587-589.

Colpa, D.I., Fraaije, M.W., van Bloois, E. (2014) DyP-type peroxidases: A promising and versatile class of enzymes. *J. Ind. Microbiol. Biotechnol.,* 41: 1-7.

Cook, A.E., Meyers, P.R. (2003) Rapid identification of filamentous actinomycetes to the genus level using genus-specific 16S rRNA gene restriction fragment patterns. *Int. J. Syst. Evol. Microbiol.,* 53(Pt 6): 1907-1915.

Cordas, C.M., Nguyen, G-S., Valério, G.N., Jønsson, M., Söllner, K., Aune, I.V., Wentzel, A., Moura, J.J.G. (2022) Discovery and characterization of a novel Dyp-type peroxidase from a marine actinobacterium isolated from Trondheim fjord, Norway. *J. Inorg. Biochem.,* 226:111651.

Cowan, D.A. (2000) Microbial genomes – the untapped resource. *Trends Biotechnol.*, 18: 14-16.

Cross, T. (1981) Aquatic actinomycetes: a critical survey of the occurrence, growth and role of actinomycetes in aquatic habitats. *J. Appl. Bacterriol.* 50(3): 397-423.

Das, M.P., Bhowmick, M., Reynolds, M. (2016) Biological decolourization of carcinogenic azo dye: an ecofriendly approach. *Int. J. Pharm. Bio. Sci.,* 7(3): 1164-1170.

Danford, H.B. (1999) Heme Peroxidases. Wiley-VCH, John Wiley and Sons: New York. 507pp.

Daniel, R. (2004) The soil metagenome – a rich resource for the discovery of novel natural products. *Curr. Opin. Biotechnol.,* 15: 199-204.

Davies, M.J., Hawkins, C.L., Pattison, D.I., Rees, M.D. (2008) Mammalian heme peroxidases: from molecular mechanisms to health implications. *Antioxidant. Red. Sig.,* 10: 1199-1234.

Dhanasekaran, S.S., Latha, S.S. (2013) *Nocardiopsis* sp. SD5: A potent feather degrading rare actinobacterium isolated from feather waste in Tamil Nadu, India. *J. Basic Microbiol.,* 53(7): 608-616.

Eaton, A.D., Clesceri, L.S. (1995) Greenberg A.E., eds. Standards and Methods for the Examination of Water and Wastewater.

Elmetwalli, A., Allam, N.G., Hassan, M.G., Albalawi, A.N., Shalaby, A., El-Said, K., Salama, A.F. (2023) Evaluation of *Bacillus aryabhattai* B8W22 peroxidase for phenol removal in wastewater effluents. *BMC Microbiol.,* 23: 19.

Faraco, V., Piscitelli, A., Sannia, G., Giardina, P. (2007) Identification of a new member of the dye-decolorizing peroxidase family from *Pleurotus ostreatus*, *World J. Microbiol. Biotechnol.* 23: 889–893.

Franzese, M., Iuliano, A. (2019) Hidden Markov Models. *Encyclo. Bioinf. Comp. Biol.*, 1: 753 – 762

Ferrer, M., Beloqui, A., Timmis, K.N., Golyshin, P.N. (2009) Metagenomics for mining new genetic resources of microbial communities. *J. Mol. Microbiol. Biotechnol*. 16:109–123.

Fraaije, M.W., van Bloois, E. (2012) DyP-type Peroxidases: A Promising and Versatile Class of Enzymes. *Enz. Eng.,* 1:2.

Goodfellow, M., Williams, S.T. (1983) Ecology of actinomycetes. *Annu. Rev. Microbiol.,* 37: 189-216.

Goodfellow, M (2012) Class I. Actinobacteria," in *Bergey's Manual of Systematic Bacteriology*, eds M. Goodfellow, P. Kampfer, H.-J. Busse, M. E. Trujillo, K.-I. Suzuki, W. Ludwig, and B. Whitman (New York, NY: Springer), 34–45.

Góngora-Castillo, E., López-Ocha, L.A., Apolinar-Hernández, M.M., Caamal, A.M., Contreras-de la Rosa, P.A., Quiroz-Moreno, A., Ramírez-Prado, J.H., O'Connor-Sánchez, A. (2020) Data mining of metagenomics to find novel enzymes: a non-computationally intensive method. 3 *Biotech.*, 10(2): 78.

Graves, P.E., Henderson, D.P., Horstman, M.J., Solomon, B.J., Olson, J.S. (2008) Enhancing stability and expression of recombinant human haemoglobin in *E. coli:* progress in the development of a recombinant HBOC source. *Biochim. Biophys. Acta.,* 1784, 1471-1479.

Handelsman, J., Rondon, M.R., Brady, S.F., Clardy, J., Goodman, R.M. (1998) Molecular biological access to the chemistry of unknown soil microbes: a new frontier for natural products. *Chem. & Biol.,* 5(10): R245-R249.

Healy, F.G., Ray, R.M., Aldrich, H.C., Wilkie, A.C., Ingram, L.O., Shanmugam, K.T. (1995) Direct isolation of functional genes encoding cellulases from the microbial consortia in a thermophilic, anaerobic digester maintained on lignocellulose. *Appl. Microbiol. Biotechnol.,* 43: 667-674.

Holt, J.G., Krieg, N.R., Sneath, P.H.A., Staley, J.T., Williams, S.T. (1994) Bergey's manual of determinative bacteriology (9th ed). Williams and Wilkins, Baltimore.

Hofrichter, M., Ulrich, R., Pecyna, M.J., Liers, C., Lundell, T. (2010) New and classic families of secreted fungal heme peroxidases. *Appl. Micro. Biotechnol.,* 87(3): 871-897.

Hong, K., Gao, A.H., Xie, Q.Y., Goa, H., Zhuang, L., Lin, H.P., Yu, H.P., Li, J., Yao, X.S., Goodfellow, M., Ruan, J.S. (2009) Actinomycetes for marine drug discovery isolated from mangrove soils and plants in China. *Mar. Drugs*, 7(4): 495-496.

Iqbal, H.A., Feng, Z., Brady, S.F. (2012) Biocatalysts and small molecule products from metagenomic studies. *Curr. Opin. Chem. Biol.,* 16: 109-116.

Jensen, P.R., Gontang, E., Mafnas, C., Mincer, T.J., Fenical, W. (2005) Culturable marine actinomycete diversity from tropical Pacific Ocean sediments. *Environ. Microbiol.,* 7(7): 1039-1048.

Jiang, F., Kongsaeree, P., Charron, R., Lajoie, H., Scott, G., Kelly, C. (2008) Production and separation of manganese peroxidase from heme amended yeast cultures. *Biotechnol.and Bioeng.,* 99(3): 540-549.

Johnson, A.R., Winding, A., Karlson, U., Roslev., P. (2002) Linking of microorganisms to phenanthrene metabolism in soil by analysis of 13C-labeled cell lipids. *Appl. Environ. Microbiol.,* 68(12): 6106-6113.

Jongbloed, J.D., Grieger, U., Antelmann, H., Hecker, M., Nijland, R. (2004) Two minimal Tat translocases in *Bacillus. Mol. Microbiol.,* 54: 1319-1325.

Kahramann, S., Yasilada, O. (2001) Industrial and agricultural wastes for laccase production by White Rot fungi. *Fol. Microbiol.,* 46: 133-136.

Kalyani, D.C., Telke, A.A., Dhanve, R.S., Jadhav, J.P. (2009) Ecofriendly Biodegradation and detoxification of Reactive Red 2 textile dye by newly isolated *Pseudomonas s*p. SUK1. *J. Hazard. Mater.,* 163(2-3): 735-742.

Kaplan, O., Bezouška, K., Plíhal, O., Ettrich, R., Kulik, N., Vaněk, O., Kavan, D., Benada, O., Malandra, A., Šveda, O., Veselá, A.B., Rinágelová, A., Slámová, K., Cantarella, M., Felsberg, J., J., Dušková, Dohnálek, J., Kotik, M., Křen, V., Martínková, L. (2008) Heterologous expression, purification and characterization of nitrilase from *Aspergillus niger*K10. *BMC Biotechnol.,* 11:2.

Kawabata, T. (2003) MATRAS: A program for protein 3D structure comparison. *Nuc. Acids Res.,* 31: 3367-3369.

Keegan, K.P., Glass, E.M., Meyer, F. (2016) MG-RAST, a metagenomics service for analysis of microbial community structure and function. *Meth. Mol. Biol.*, 1399: 207-233

Khadijah, O., Lee, K.K., Faiz, F. (2009) Isolation, screening and development of local bacterial consortia with azo dyes decolourising capability. *Malaysian J. Microbiol.,* 5(1): 25-32.

Khan, S., Ullah, M.W., Siddique, R., Nabi, G., Manan, S., Yousaf, M., Hou, H. (2016) Role of Recombinant DNA Technology to Improve Life. *Int. J. Genomics*. Published online. [Viewed 2020].

Kidd, P., Barcelo, J., Bernal, M.P., Navari-Izzo, F., Poschenrieder, C., Shilev, S., Clemente, R., Monterroso, C. (2009) Trace element behaviour at the root-soil interface: implications in phytoremediation. *Environ. Exp. Bot.*, 67: 243-259.

Kim, S.J., Ishikawa, M., Hirai, M., Shoda, M. (1995) Characterisitics of a newly isolated fungus, *Geotrichum candidum* Dec 1, which decolorizes various dyes. *J. Ferment. Bioeng.,* 79, 601-607.

Kim, S.J., Shoda, M. (1999) Purification and characterization of a novel peroxidase from *Geotrichum candidum* dec 1 involved in decolorization of dyes. *Appl. Environ. Microbiol.,* 65: 1029-1035.

Kimani, V., Ullrich, R., Büttner, E., Herzog, R., Kellner, H., Jehmlich, N., Hofrichter, M., Liers, C. (2021) First Dye-Decolorizing Peroxidase from an Ascomycetous Fungus Secreted *by Xylaria grammica. Biomol.*, 11(9): 1391.

Kong, L., Guo, D., Zhou, S., Yu, X., Hou, G., Li., R., Zhao, B. (2010) Cloning and expression of a toxin gene from *Pseudomonas fluorescens* GcM5-1A. *Arch. Microbiol.,* 192(7): 585-593.

Krainer, F.W., Capone, S., Jager, M., Vogl, T., Gerstmann, M., Glieder, A., Herwig, C., Spadiut, O. (2015) Optimizing cofactor availability for the production of recombinant heme peroxidase in *Pichia pastoris*. *Microbial Cell Fac.*, 14:4.

Kuberan, T., Anburaj, J., Sundaravadivelan, C., Kumar, P. (2011) Biodegradation of azo dye by *Listeria* sp. *Int. J. Environ. Sci.,* 1(7): 1760-1770.

Kurade, M.B., Waghmode, T.R., Govindwar, S.P. (2011) Preferential biodegradation of structurally dissimilar dyes from a mixture by *Brevibacillus laterosporus. J. Hazard. Mater.,* 192: 1746-1755.

Laemmli, U.K. (1970) Cleavage of structural proteins during the assembly of the head of the bacteriophage T4., *Nat*., 227(5259): 680-685.

Lawson, P.A. (2018) "The phylum actinobacteria," in *The Bifidobacteria and Related Organisms.* Biology, Taxonomy, Applications, eds P. Mattarelli, B. Biavati, W.H. Holzapfel, and B.J.B. Wood (London: Elsevier; Academic Press), 1-8.

Lee, H.S., Kwon, K.K., Kang, S.G., Cha, S.-S., Kim, S-J., Lee, J.-H. (2010) Approaches for novel enzyme discovery from marine environments. *Curr. Opin. Biotechnol*., 21:353–357, https://doi.org/10.1016/j.copbio.2010.01.015

Le-Roes-Hill, M., Khan, N., Burton, S.G. (2011) Actinobacterial Peroxidases: an Unexplored Resource for Bioactalysis. *Appl. Biochem. Biotechnol.,* 164: 681-713.

Li, J., Liu, C., Li, B., Yuan, H., Yang, J., Zheng, B. (2012) Identification and molecular characterization of a novel DyP-type peroxidase from *Pseudomonas aeruginosa* PKE117. *Appl. Biochem. Biotechnol.,* 166(3): 774-785.

Liers, C., Bobeth, C., Pecyna, M., Ullrich, R., Hofrichter, M. (2010) DyP-like peroxidases of the jelly fungus *Auricularia auricula-judae* oxidize nonphenolic lignin model compounds and high-redox potential dyes. *Appl. Microbiol. Biotechnol.,* 85: 1869-1879.

Liers, C., Pecyna, M.J., Kellner, H., Worrich, A., Zorn, H., Steffen, K.T., Hofrichter, M., Ulrich, R. (2013) Substrate oxidation by dye-decolorizing peroxidases (DyPs) from wood- and litter-degrading agaricomycetes compared to other fungal and plant heme-peroxidases. *Appl. Microbiol. Biotechnol.,* 97(13): 5839-5849.

Lima, R.N., Porto, A.L.M. (2016) Chapter eight – Recent advances in marine enzymes for biotechnological processes, in: S.-K. Kim, F. Toldrá (Eds.), *Adv. Food Nutr. Res*., Academic Press: 153–192.

Lindie, D., Ruiz-Duenas, F.J., Fernandez-Fueyo, E., Guallar, V., Hammel, K.E., Pogni, R., Martinez, A.T. (2015) Basidiomycete Dyps: Genomic diversity, structural-functional aspects, reaction mechanism and environmental significance. *Arch. Biochem. Biophys.,* 574: 66-74.

Lobb, B., Doxey, C. (2016) Novel function discovery through sequence and structural data mining. *Curr. Opin. Struct. Biol*., 38:53–61.

Lončar, N., Colpa, D.I., Fraaije, M.W. (2016) Exploring the biocatalytic potential of a DyP-type peroxidase by profiling the substrate acceptance of *Thermobifida fusca* DyP peroxidase. *Tet.,* 72: 7276-7281.

Lu, L., Zhao, M., Wang, T-N., Zhao, L-Y., Du, M-H, Li, T-L., Li, D-B (2012) Characterization and dye decolorization ability of an alkaline resistant and organic solvents tolerant laccase from Bacillus licheniformis LS04. *Biores. Technol.,* 115: 35-40. https://doi.org/10.1016/j.biortech.2011.07.111

Lui, X., Du, Q., Wang, Z., Zhu, D., Huang, Y., Li, N., Wei, T., Xu, S., Gu, L. (2011) Crystal structure and biochemical features of EfeB/YcdB from *Escherichia coli* O157: ASP235 plays divergent roles in different enzyme-catalyzed processes. *J. Biol. Chem.,* 286: 14922-14931.

Lundell, T.K., Mäkelä, M.R., Hildén, K. (2010) Lignin-modifying enzymes in filamentous basidiomycetes-ecological, functional and phylogenetic review. *J. Basic Microbiol.,* 50(1): 5-20.

Maibeche, R., Boucherba, N., Bendjeddou, K., Prins, A., Bouiche, C., Hamma, S., Benhoula, M., Azzouz, Z., Bettache, A., Benallaoua, Le Roes-Hill, M. (2022) Peroxidase-producing

actinobacteria from Algerian environments and insights from the genome sequence of peroxidase-producing *Streptomyces* sp. 19. *Intern.Microbiol.,* 25: 379-396.

Macagnan, D., Romeiro, R.D.S., de Sousa, J.T., Pomella, A.W.V. (2006) Isolation of actinomycetes and endospore-forming bacteria from the cacao pod surface and their antagonistic activity against the witches' broom and black pod pathogens. *Phytopara.,* 3: 122-132.

Mandel, M., Marmur, J. (1968) Use of ultraviolet absorbance-temperature profile for determining the guanine plus cytosine content of DNA, in: L. Grossman, K. Moldave (Eds.), Methods in Enzymology Vol. 12, Academic Press, New York, pp. 195 – 206.

Marco-Urrea, E., Reddy, C.A. (2012) Degradation of chloro-organic pollutants by white rot fungi microbial degradation of xenobiotics. *Environ. Sc. Engin.,* 2: 31-66.

Mason, M.G., Ball, A.S., Reeder, B.J., Silkstone, G., Nicholls, P., Wilson, M.T. (2001) Extracellular heme peroxidases in actinomycetes: a case of mistaken identity. *Appl. Environ. Microbiol.,* 67(10): 4512-4519.

Melén, K., Krogh, A., von Heijne, G. (2003) Reliability measures for membrane protein topology prediction algorithms. *J. Mol. Biol.,* 327(3): 735-744.

Mitchell, A.L., Scheremetjew, M., Denise, H., Potter, S., Tarkowska, A., Qureshi, M., Salazar, G.A., Pesset, S., Boland, M.A., Hunter, F.M.I., Ten Hoopen, P., Alako, B., Amid, C., Wilkinson, D.J., Curtis, T.P., Cochrane, G., Finn, R.D. (2018) EBI Metagenomics in 2017: enriching the analysis of microbial communities, from sequence reads to assemblies. *Nucleic Acids Res.,*46: D726–D735.

Mosjov, K.D., Andronikov, D., Janevski, A., Kuzelov, A., Gaber, S. (2016) The application of enzymes for the removal of dyes from textile effluents. *Adv. Technol.,* 5(1): 81-86.

Musengi, A., Khan, N., Le Roes-Hill, M., Pletschke, B.I., Burton, S.G. (2014) Increasing the scale of peroxidase production by *Streptomyces* sp. strain BSII#1. *J. Appl. Microbiol.,* 116:554–562.

Nagasawa, T., Shimizu, H., Yamada, H. (1993) The superiority of third-generation catalyst, *Rhodococcus rhodochrous* J1 nitrile hydratase, for industrial production of acrylamide. *Appl. Microbiol. Biotechnol.*, 40: 189-195.

Natale, P., Brüser, T., Driessen, A.J.M. (2008) Sec- and Tat-mediated protein secretion across the bacterial cytoplasmic membrane- - distinct translocases and mechanisms. *Biochem. Biophys. Acta.*, 1778(9): 1735-1756.

Nicell, J.A., Bewtra, J.K., Biswas, N., St. Pierre, C., Taylor, K.E. (1993) Enzyme catalysed polymerization and precipitation of aromatic compounds from aqueous solution. *Can. J. Civ. Eng.,* 20: 725-735.

Nikulina, G.L., Deveikis, D.N., Pyshnov, G. (1995) Toxicity dynamic of anionic dyes in air of the work place and long term effects after adsorption through the skin. *Med. Tr. Prom. Ekol.,* 6: 25-28.

Nzila, A., Razzak, S.A., Zhu, J. (2016) Bioaugmentation: an emerging strategy of industrial wastewater treatment for reuse and discharge. *Int. J. Environ. Res. Public Health*, 13: 846.

Okoro, C.K., Bull, A.T., Mutreja, A., Rong, X., Huang, Y., Goodfellow, M. (2010) *Lechevalieria atacamensis* sp. nov., *Lechevalieria deserti* sp. nov. and *Lechevalieria roselyniae* sp. nov. isolated from hyperarid soils. *Int. J. Sys. Evol.Microbiol.*, 60: 2.

Ogola, H.J., Kamiike, T., Hashimoto, N., Ashida, H., Ishikawa, T., Shibata, H., Sawa, Y. (2009) Molecular characterization of a novel peroxidase from the cyanobacterium *Anabaena* sp. strain PCC 7120. *Appl. Environ. Microbiol.,* 75: 7509-7518.

Ogino, H., Ishikawa, H. (2001) Enzymes which are stable in the presence of organic solvents. *J. Biosci. Bioeng.*, 91(2): 109-116.

Oritz de Montellano, P.R., David, S.K., Ator, M.A., Tew, D. (1988) Mechanism-based inactivation of horseradish peroxidase by sodium azide. Formation of meso-azidoprotoporphyrin IX. *Biochem.,* 27: 5470-5476.

Ota, M., Fukushima, H., Kulski, J.K., Inoko, H. (2007) Single nucleotide polymorphism detection by polymerase chain reaction-restriction fragment length polymorphism. *Nat.Prot.,* 2: 2857-2864.

Pagga, U., Brown, D. (1986) The Degradation of Dyestuff: Part II. Behaviour of Dye stuffs in Aerobic Biodegradation Tests. *Chemo.*, 15(4): 479-491.

Passardi, F., Cosio, C., Penel, C., Dunand, C. (2005) Peroxidases have more functions than a Swiss army knife. *Plant Cell Rep.,* 24: 255-265.

Priyadharsini, P., Dhanasekaran, D. (2015) Diversity of soil allelopathic Actinobacteria in Tiruchirappalli district, Tamilnadu, India. *J. Saud. Soci. Agri. Sci.,* 14(1): 54-60.

Puhse, M., Szweda, R.T., Ma, Y., Jeworreck, C. Winter, R., Zorn, H. (2009) *Marasmius scorodonius* extracellular dimeric peroxidase – exploring its temperature and pressure. *Biochim. Biophys. Acta.,* 1794(4): 1091-1098.

Qasem, N.A.A., Mohammed, R.H., Lawal, D.U. (2021) Removal of heavy metal ions from wastewater: a comprehensive and critical review. *npj Clean Water,* 4: 36.

Rahmanpour, R., Rea, D., Jamshidi, S., Fülöp, V., Bugg, T.D.H. (2016) *Structure of Thermobifida fusca* DyP-type peroxidase and activity towards Kraft lignin and lignin model compounds. *Arch. Biochem. Biophys*., 594: 54–60.

Ranjani, A., Dhanasekaran, D., Gopinath, P.M. (2016) An Introduction to Actinobacteria. Actinobacteria - Basics and Biotechnological Applications. InTech.

Reetz, M.T. (2010) Laboratory evolution of stereoselective enzymes: a prolific source of catalysts for asymmetric reactions. *Angew. Chem. Int. Ed. Engl.,* 50: 138-174.

Reetz, M.T. (2013) Biocatalysis in organic chemistry and biotechnology: past, present and future. *J. Am. Chem. Soc.,* 135: 12480-12496.

Regalado, C., García-Almendárez, B.E., Duarte-Vázquez, M.A. (2004) Biotechnological applications of peroxidases. *Pytochem. Rev.,* 3: 243-256.

Reszka, K.J., McCormick, M.L., Britigan, B.E. (2001) Peroxidase – and – nitrate dependent metabolism of the anthracycline anticancer agents daunorubicin and doxorubicin. *Biochem.,* 40: 15349-15361.

Reszka, K.J., Britigan, L.H., Britigan, B.E. (2005) Oxidation of anthracyclines by peroxidase metabolites of salicylic. *Aci. J. Pharmacol. Exp. Ther.,* 315: 283-290.

Robinson, T., McMullan, G., Marchant, R., Nigam, P. (2001) Remediation of dyes in textile effluent: a critical review on current treatment technologies with a proposed alternative. *Bioresour. Technol.,* 77: 247-255.

Rodriguez, E., Pickard, M.A., Duhalt, R.V. (1999) Industrial dye decolorization by laccasses from lignolytic fungi. *Curr. Microbiol.,* 38: 27-32.

Saha, S., Dhanasekaran, D., Shanmugapriya, S., Latha, S. (2013) *Nocardiopsis* sp. SD5: a potent feather degrading rare actinobacterium isolated from feather waste in Tamil Nadu, India. *J. Basic Microbiol.,* 53(7): 608-616.

Salvachua, D., Prieto, A., Martinez, A.T., Martinez, M.J. (2013) Characterisation of a novel dye-decolourising peroxidase (DyP)-type enzyme from *Irpex lacteus* and its application in enzymatic hydrolysis of wheat straw. *Appl. Environ. Microbiol.,* 79: 4316-4324.

Saratale, R.G., Saratale, G.D., Chang, J.S., Govindwar, S.P. (2011) Bacterial decolourization and degradation of azo dyes: A review. *J. Taiwan. Inst. Chem. Eng.,* 42: 138-157.

Savelli, B., Li, Q., Webber, M., Jemmat, A.M., Robitaille, A., Zamocky, M., Mathé, C., Dunand, C. (2019) RedoxiBase: a database for ROS homeostasis regulated proteins. *Redox Biol.,* 26: 101247

Schmeisser, C., Steele, H., Streit, W.R. (2007) Metagenomics, biotechnology with non-culturable microbes. *Appl. Microbiol. Biotechnol.*, 75:955-962.

Schmid, A., Dordick, J.S., Hauer, A., Kaener, M., Wubbolts, Witholt, B. (2001) Industrial biocatalysts today and tomorrow. *Nat.,* 49: 258-268.

Sharmin, S., Towhid Hossain, H.D., Anwar, M.N. (2005) Isolation and characterization of a protease producing bacteria *Bacillus amonvivorus* and optimization of some factors of culture conditions for protease production. *J. Biol. Sci.,* 5(3): 358-362.

Shendure, J., Balasubramanian, S., Church, G.M, Gilbert, W., Rogers, J., Schloss, J.A., Waterston, R.H. (2017) DNA sequencing at 40: past, present and future. *Nat.,* 550:345–353.

Simon. C., Daniel, R. (2009) Achievements and new knowledge unraveled by metagenomic approaches. *Appl. Microbiol. Biotechnol*., 85:265–276.

Singh, R., Grigg, J.C., Armstrong, Z., Murphy, M.E., Eltis, L.D. (2012) Distal heme pocket residues of B-type dye-decolorizing peroxidase: arginine but not aspartate is essential for peroxidase activity. *J. Biol. Chem.,* 287: 10623-10630.

Singh, R.P., Singh, P.K., Singh, R.L. (2014) Bacterial decolourization of textile azo dye Acid Orange by *Staphylococcus hominis* RMLRT03. *Toxicol. Int.,* 21(2): 160-166.

Singh, R.L., Singh, P.K., Singh, R.P. (2015a) Enzymatic Decolorization and Degradation of Azo Dyes – A Review. *Int. Biodeterior. Biodeg.,* 104: 21-31.

Singh, R.L., Gupta, R., Singh, R.P. (2015b) Microbial Degradation of Textile Dyes for Environmental Safety. In: Advances in Biodegradation and Bioremediation of Industrial Waste, R Chandra (Editor) CRC press, pp. 249-285.

Steele, H.L., Jaeger, K.E., Daniel, R., Streit, W.R. (2009) Advances in recovery of novel biocatalysts from metagenomes. *J. Mol. Microbiol. Biotechnol*., 16:25–37.

Stolz, A. (2001) Basic and applied aspects in the microbial degradation of azo dyes. *Appl. Microbiol. Biotechnol.,* 56: 69-80.

Strittmatter, E., Serrer, K., Liers, C., Ullrich, R., Hofrichter, M., Piontek, K., Schleicher, E., Plattner, D.A. (2015) The toolbox of *Auricularia auricular-judae* dye-decolorizing peroxidase – Identification of three new potential substrate-interaction sites. *Archives of Biochem. and Biophy.,* 574: 75-85.

Studier, F.W. (2005) Protein production by auto-induction in high density shaking cultures. *Prot. Exp. Pur.,* 41: 207-234.

Sturm, A., Schierhorn, A., Lindenstrauss, U., Lilie, H., Bruser, T. (2006) YcdB from *Escherichia coli* reveals a novel class of Tat-dependently translocated hemoproteins. *J. Biol. Chem.,* 281: 13972-13978.

Su, J.C., Horton, J.J. (1998) Allergic contact dermatitis from azo dyes. *Autralas. J. Dermatol.,* 39(1): 48-49.

Subramani, R., Aalbersberg, W. (2013) Culturable rare Actinomycetes: diversity, isolation and marine natural product discovery. *Appl. Microbiol. Biotechnol.,* 97: 9291-9321.

Subramaniyan, S., Prema, P. (2002) Biotechnology of Microbial Xylanases: Enzymology, Molecular Biology, and Application. *Crit. Rev. Biotechnol.,* 22(1): 33-64.

Sudhamsu, J., Kabir, M., Airola, M.V., Patel, B.A., Yeh, S.R., Rousseau, D.L., Crane, B.R. (2010) Co-expression of ferrochelatase allows for complete heme incorporation into recombinant proteins produced in *E. coli*. *Pro. Exp. and Purif.,* 73: 78-82.

Sugano, Y. (2009) DyP-type peroxidases compromise a novel heme peroxidase family. *Cell. Mol. Life Sci.,* 66: 1387-1403.

Sugano, Y., Muramatsu, R., Ichiyanagi, A., Sato., T., Shoda, M. (2007) DyP, a unique dye-decolorizing peroxidase, represents a novel heme peroxidase family: ASP171 replaces the distal histidine of classical peroxidases. *J. Biol. Chem.,* 286: 14922-14931.

Sugano, Y., Matsushima, Y., Tsuchiya, K., Aoki, H., Hirai, M., Shoda, M. (2009) Degradation pathway of an anthraquinone dye catalysed by a unique peroxidase DyP from *Thanatephorus cucumeris* Dec 1. *Biodeg.,* 3: 433-440.

Sugawara, K., Igeta, E., Amano, Y., Hyuga, M., Sugano, Y. (2019) Degradation of antifungal anthraquinone compounds is a probable physiological role of DyP secreted by *Bjerkandera adusta*. *AMB Exp.*, 9: 56.

Suriya, J., Bharathiraja, S., Manivasagan, P., Kim, S.-K. (2016) Enzymes from rare actinobacterial strains, in: *Adv. Food Nutr. Res.*, Elsevier: 67–98.

Tamura, K., Stecher, G., Peterson, D., Filipski, A., Kumar, S. (2013) MEGA6: Molecular Evolutionary Genetics Analysis Version 6.0. *Mol. Biol. Evol.,* 30(12): 2725-2729.

Tischler, D., van Berkel, W.J.H., Fraaije, M.W. (2019) Editorial: *Actinobacteria*, a Source of Biocatalytic Tools. *Front. Microbiol.* 10:800.

Tuffin, M., Anderson, D., Heath, C., Cowan, D.A. (2009) Metagenomic gene discovery: how far have we moved into novel sequence space? *Biotechnol. J.*, 4:1671–1683.

Twala, P.P., Mitema, A., Baburam, C., Feto, N.A. (2020) Breakthroughs in the discovery and use of different peroxidase isoforms of microbial origin. *AIMS Microbiol.,* 6(3): 330-349.

Uchiyama, T., Miyazaki, K. (2009) Functional metagenomics for enzyme discovery: challenges to efficient screening. *Curr. Opin. In Biotech.*, 20(6): 616-622.

van Bloois, E., Torres Pazmino, D.E., Winter, R.T., Fraaije, M.W. (2010) A robust and extracellular heme-containing peroxidase from *Thermobifida fusca* as prototype of a bacterial peroxidase superfamily. *Appl. Microbiol. Biotechnol.,* 86: 1419-1430.

Varnado, C.L., Goodwin, D.C. (2004) System for the expression of recombinant hemoproteins in *Escheria coli*. *Protein Expr. Purif.,* 35(1): 78-83.

Veitch, N.C. (2004) Horseradish peroxidase: a modern view of a classic enzyme. *Phytochem.,* 65: 249-259.

Venter, J.C., Remington, K., Heidelberg, J.F., Halpern, A.L., Rusch, D., Eisen, J.A., Wu, D., Paulsen, I., Nelson, K.E., Nelson, W., Fouts, D.E., Levy, S., Knap, A.H., Lomas, M.W., Nealson, K., White, O., Peterson, J., Hoffman, J., Parsons, R., Baden-Tillson, H., Pfannkoch, C., Rogers, Y.H., Smith, H.O. (2004) Environmental genome shotgun sequencing of the Sargasso sea. *Sci*., 304: 66-74.

Ventura, M., Canchaya, C., Tauch, A., Chandra, G., Fitzgerald, G.F., Chater, K.F., van Sinderen, D. (2007) Genomics of actinobacteria: tracing the evolutionary history of an ancient phylum. *Microbiol. Mol. Biol. Rev.,* 71: 495-548.

Wiltschi, B., Cernava, T., Dennig, A., Galindo Casas, M., Geier, M., Gruber, S., Haberbauer, M., Heidinger, P., Herrero Acero, E., Kratzer, R., Luley-Goedl, C., Müller, C. A., Pitzer, J., Ribitsch, Sauer M., Schmolzer, K., Schnitzhofer, W., Sensen, C. W., Soh, J., Steiner, K., Winkler, C.K., Winkler, M., Wriessnegger, T. (2020) Enzymes revolutionize the bioproduction of value-added compounds: from enzyme discovery to special applications. *Biotechnol. Adv.*, 40: 107520.

Xu, L., Sun, J., Qaria, M., Gao, L. Zhu, D. (2021) Dye decolorizing peroxidase structure, catalytic properties and applications: Current Advancement and Futurity. *Cat.*, 11(8): 995.

Yee, D.C., Wood, T.K. (1997) 2,4-dichlorophenol degradation using *Streptomyces viridosporus* T7A lignin peroxidase. *Biotechnol. Pro.*, 13:53-59.

Yoshida, T., Sugano, Y. (2015) A structural and functional perspective of DyP-type peroxidase family. *Arch. Biochem. Biophys.,* 574: 49-55.

Yoshida, T., Tsuge, H., Konno, H., Hisabori, T., Sugano, Y. (2011) The catalytic mechanism of dye-decolourizing peroxidase DyP may require the swinging movement of an aspartic acid residue. *FEBS J.,* 278: 2387-2394.

Yoshida, T., Tsuge, H., Hisabori, T., Sugano, Y. (2012) Crystal structures of dye-decolourizing peroxidase with ascorbic acid and 2,6-dimethoxyphenol. *FEBS J.,* 24: 4351-4356.

Yun, J., Ryu, S. (2005) Screening for novel enzymes from metagenome and SIGEX, as a way to improve it. *Microb. Cell Fact.*, 4(8).

Ziegenhagen, D., Hofrichter, M. (2000) A simple and rapid method to gain high amounts of manganese peroxidase with immobilized mycelium of the agric white-rot fungus *Clitocybula dusenii*. *Appl. Microbiol. Biotechnol.*, 53: 553-557.

Ziemert, N., Alanjary, M., Weber, T. (2016) The evolution of genome mining in microbes—A review. *Nat. Prod. Rep.,*33: 988–1005.

Zubieta, C., Joseph, R., Krishna, S.S., McMullan, D., Kapoor, M., Axelrod, H.L., Miller, M.D., Abdubek, P., Acosta, C., Astakhova, T., Carlton, D., Chiu, H.J., Clayton, T., Deller, M.C., Duan, L., Elias, Y., Elsliger, M.A., Feuerhelm, J., Grzechnik, S.K., Hale, J., Han, G.W., Jaroszewski, L., Jin, K.K., Klock, H.E., Knuth, M.W., Kozbial, P., Kumar, A., Marciano, D., Morse, A.T., Murphy, K.D., Nigoghossian, E., Okach, L., Oommachen, S., Reyes, R., Rife, C.L., Schimmel, P., Trout, C.V., van Bedem, H., Weekes, D., White, A., Xu, Q., Hodgson, K.O., Wooley, J., Deacon, A.M., Godzik, A., Lesley, S.A., Wilson, I.A. (2007a) Identification and structural characterization of heme binding in a novel dye-decolorizing peroxidase, TyrA. *Prot.*, 69(2): 234-243.

Zubieta, C., Joseph, R., Krishna, S.S., McMullan, D., Kapoor, M., Axelrod, H.L., Miller, M.D., Abdubek, P., Acosta, C., Astakhova, T., Carlton, D., Chiu, H.J., Clayton, T., Deller, M.C., Duan, L., Elias, Y., Elsliger, M.A., Feuerhelm, J., Grzechnik, S.K., Hale, J., Han, G.W., Jaroszewski, L., Jin, K.K., Klock, H.E., Knuth, M.W., Kozbial, P., Kumar, A., Marciano, D., Morse, A.T., Murphy, K.D., Nigoghossian, E., Okach, L., Oommachen, S., Reyes, R., Rife, C.L., Schimmel, P., Trout, C.V., van Bedem, H., Weekes, D., White, A., Xu, Q., Hodgson, K.O., Wooley, J., Deacon, A.M., Godzik, A., Lesley, S.A., Wilson, I.A. (2007b) Crystal structures of two novel dye-decolorizing peroxidases reveal a beta-barrel fold with a conserved heme-binding motif. *Prot.,* 69(2): 223-233.

APPENDIX

APPENDIX A

A1: Cell Suspension Buffer

In 90 mL distilled water, the following was combined:

1 mL	1 M Tris-HCl (pH 8.0)
0.2 mL	0.5 M Ethylenediaminetetraacetic acid (EDTA)
12 g	Sucrose

1 M Tris-HCl was made with Tris and the pH adjusted to 8.0 with HCl as well as the 0.5 M EDTA before combined to make the cell suspension buffer and made up to 100 mL.

A2: 2× Lysing solution

In 60 mL of distilled water, the following was combined:

10 mL	1 M Tris-HCl (pH 8.0)
8 mL	25%, w/v, Sodium dodecyl sulfate (SDS)
6 mL	5 M NaCl
4 mL	0.5 M EDTA
2 mL	β-mercaptoethanol
500 µL	Proteinase K (20 mg/mL)

All components were made prior and combined to 60 mL dH_2O before being made to a final volume of 100 mL.

APPENDIX B

B1: Super Optimal broth with Catabolite Repression (SOC) media:

In 90 mL of dH_2O, the following was combined:

1 mL	2 M Mg^{2+} stock solution
1 mL	2 M glucose, filter-sterilised
1 mL	1 M NaCl
0.25 mL	1 M KCl
2 g	Tryptone
0.5 g	Yeast Extract

All components, except the glucose, are combined and made up to a final volume of 99 mL and autoclaved. The glucose is added once the solution has cooled. Media can be stored at -20 °C in aliquots of 1 mL or 50 mL until required.

APPENDIX C

A 12.5% (w/v) resolving gel and 5% (w/v) stacking gel was used for the separation of the proteins of interest according to the Laemmli SDS-PAGE protocol (Laemmli, 1970). The reagents required were prepared as follows:

a. Resolving gel buffer (1.125 M Tris-HCl, pH 8.8 and 0.3%, w/v, SDS)
For 200 mL: 27.25 g Tris was dissolved in 150 mL distilled water, the pH adjusted to 8.8 with HCl, 0.6 g SDS was added and made up to 200 mL with water. The solution was autoclaved for 20 minutes, psi.

b. Stacking gel buffer (0.375 M Tris-HCl, pH 6.8 and 0.3%, w/v, SDS)
For 200 mL: 9.08 g Tris was dissolved in 150 mL distilled water, the pH adjusted to 6.8 with HCl, 0.6 g SDS was added and made up to 200 mL with water. The buffer was autoclaved for 20 minutes, 15 psi.

c. For the 12.5% (w/v) resolving gel, the following solutions were mixed prior to pouring the gel
4.17 mL acrylamide/bis-acrylamide (29.2 g:0.8 g), 2.5 mL resolving gel buffer, 3.33 mL distilled water, 50 µL 10% (w/v) ammonium persulphate and 15 µL TEMED. The resolving buffer was covered with a layer of isopropanol to allow the gel to set. Prior to pouring the stacking gel, the isopropanol layer was removed.

d. For the 5% (w/v) stacking gel, the following solutions were mixed and poured onto the resolving gel
1.34 mL acrylamide/bis-acrylamide mix (29.2 g:0.8 g), 2.0 mL stacking gel buffer, 4.6 mL distilled water, 60 µL 10% (w/v) ammonium persulphate and 15 µL TEMED. The comb was inserted into the stacking gel and the gel was allowed to set.

APPENDIX D

D1: Luria Bertini (LB) Broth

In 60 mL of dH_2O, the following components were combined:

1 g Tryptone

0.5 g Yeast Extract

1 g NaCl

The pH of the media is adjusted to 7 before being made up to a final volume of 100 mL.

D2: 2× YT

In 800 mL of dH_2O, the following components were combined:

16 g Tryptone

5 g Yeast Extract

5 g NaCl

The pH of the media is adjusted to 7 before being made up to a final volume of 1 L.

D3: Terrific Broth

In 900 mL of dH_2O, the following components were combined:

12 g Tryptone

24 g Yeast Extract

4 mL Glycerol

100 mL Potassium phosphate buffer (KPO_4)

The addition of the potassium phosphate buffer is comprised of 0.17 M KH_2PO_4 and 0.72 M K_2HPO_4. The following components are added and made up to a final volume of 1 L.

D4: Auto Induction Media

ZY:

In 900 mL of dH_2O, the following components were combined:

10 g Tryptone

5 g Yeast Extract

Once combined make up to a final volume of 1L.

20× NPS:

In 90 mL of dH_2O, the following components were combined:

6.6 g 0.5 M $(NH_4)SO_4$

13.6 g 1 M KH_2PO_4

14.2 g 1 M Na_2HPO_4

The pH of the media was adjusted to 6.75 and the final volume was made up to 100 mL.

50× 5052:

In 90 mL of dH_2O, the following components were combined:

25 g Glycerol

2.5 g Glucose

10 g Lactose

All the components are added together and made up to a final volume of 100 mL.

1 M $MgSO_4$:

In 90 mL of dH_2O, the following components were combined:

24.65 g $MgSO_4$

The final volume of this media was made up to 100 mL.

All components combined, 20× ZY, 20× NPS, 50× 5052, and 1 M $MgSO_4$ make up Auto Induction Media

APPENDIX E

Table 1E: Preparation of standards used in Bradford's Protein Assay.

Standard	Vol. 100 µg/mL BSA (µL)	Vol. Buffer (µL)	BSA conc. (µg/mL)
Blank	0	100	0
1	10	90	10
2	20	80	20
3	40	60	40
4	60	40	60
5	80	20	80
6	100	0	100

SUPPLEMENTARY SHEET

SUPPLEMENTARY SHEET A

Data generated by DNA-MAN for the analysis of primers designed to amplify the DyP-type peroxidase genes from isolates. Identifying self-complementary, restriction analysis, fragments generated for digestion as well as primer length, GC%, MW (kD) and melting temperatures (°C).

151 DyP3
Self-complementary – No complementary found
Two primers complementarity.
Max complementarity in continuous: 5 bp, free energy=-3.10 Kcal/mol
5'-CATATGATGGACCGTACGGTGAGCCGG-3'
|||||
3'-CCTGGAGTACCTCAGTGACACTAATGAGCTC-5'

Max complementarity in discontinuous: 11 bp
5'-CATATGATGGACCGTACGGTGAGCCGG-3'
||||| ||| | ||
3'-CCTGGAGTACCTCAGTGACACTAATGAGCTC-5'

Restriction analysis on 151_DyP_3
Methylation: dam-No dcm-No
Screened with 2 enzymes, 0 sites found
List by Site Order

Fragments generated by digestion (bp):
Linear DNA: 1209
Circular DNA:
Non-Cut Enzymes
*Nde*I *Xho*I

Forward Primer:
Length: 30
GC%: 53.3
MW (kD): 9.31
Melting Temperature (°C):
- Thermo: 75.6
- Hybrid: 61.8
- GC+AT: 92.0

Reverse Primer:
Length: 30
GC%: 53.6
MW (kD): 9.22
Melting Temperature (°C):
- Thermo: 73.5
- Hybrid: 61.8
- GC+AT: 92.0

88S
Self-complementary: No complementarity found.
Two primers complementarity.
Max complementarity in continuous: 5 bp, free energy=-3.40 Kcal/mol
5'-ATTCATATGATGGCTGAACAGACCGAGATGAC-3'
                |||||
3'-CTGTCGCAGACGACCTCCCGGAGCTCTTA-5'

Max complementarity in discontinuous: 11 bp
5'-ATTCATATGATGGCTGAACAGACCGAGATGAC-3'
   || || || |||||
3'-CTGTCGCAGACGACCTCCCGGAGCTCTTA-5'

Restriction analysis on 88S
Methylation: dam-No dcm-No
Screened with 2 enzymes, 0 sites found
List by Site Order

Fragments generated by digestion (bp):
 Linear DNA: 1239
 Circular DNA:
Non-Cut Enzymes
*Nde*I *Xho*I

Forward Primer:
Length: 32
GC%: 43.8
MW (kD): 9.91
Melting Temperature (°C):
- Thermo: 71.7
- Hybrid: 59.1
- GC+AT: 92.0

Reverse Primer:
Length:29
GC%: 62.1
MW (kD): 8.84
Melting Temperature (°C):
- Thermo: 77.9
- Hybrid: 64.7

GC+AT: 94.0

8S

Self-complementary: Max complementarity: 6 bp, dG= -2.20 Kcal/mol
Two primers complementarity.
Max complementarity in continuous: 6 bp, free energy=-9.50 Kcal/mol
5'-ATTCATATGATGAGCCGGCGGCGGCTCCTG-3'
|||||
3'-CTGTCGCCGACGACCTCCCCGAGCTCTTA-5'

Max complementarity in discontinuous: 11 bp
5'-ATTCATATGATGAGCCGGCGGCGGCTCCTG-3'
| | || |||||
3'-CTGTCGCCGACGACCTCCCCGAGCTCTTA-5'

Restriction analysis on 8S
Methylation: dam-No dcm-No
Screened with 2 enzymes, 0 sites found
List by Site Order

Fragments generated by digestion (bp):
Linear DNA: 1212
Circular DNA:
Non-Cut Enzymes
*Nde*I *Xho*I

Forward Primer:
Length: 30
GC%: 60.0
MW (kD): 9.27
Melting Temperature (°C):
- Thermo: 81.1
- Hybrid: 64.5
- GC+AT: 96.0

Reverse Primer:
Length: 29
GC%: 65.5

MW (kD): 8.78
Melting Temperature (°C):
- Thermo: 80.5
- Hybrid: 66.1

GC+AT: 96.0

S129
Self-complementary: No complementarity.
Two primers complementarity.
Max complementarity in continuous: 3 bp, free energy= 0.00 Kcal/mol
5'-ATTCATATGATGCCTGACCAGTCCCTTCC-3'
        |||
3'-CCGTCTTCAACGACCTCCCCGAGCTCTTA-5'

Max complementarity in discontinuous: 11 bp
5'-ATTCATATGATGCCTGACCAGTCCCTTCC-3'
   || | | ||| || | |
3'-CCGTCTTCAACGACCTCCCCGAGCTCTTA-5'

Restriction analysis on S129
Methylation: dam-No dcm-No
Screened with 2 enzymes, 0 sites found
List by Site Order

Fragments generated by digestion (bp):
Linear DNA: 1299
Circular DNA:
Non-Cut Enzymes
*Nde*I *Xho*I

Forward Primer:
Length: 29
GC%: 48.3
MW (kD): 8.79
Melting Temperature (°C):
- Thermo: 71.1
- Hybrid: 59.0
- GC+AT: 86.0

Reverse Primer:
Length: 29
GC%: 58.6
MW (kD): 8.74
Melting Temperature (°C):

- Thermo: 76.7
- Hybrid: 63.2
- GC+AT: 92.0

HMC10 DyP1
Self-complementary: No complementarity.
Two primers complementarity.
Max complementarity in continuous: 3 bp, free energy= 1.80 Kcal/mol
```
 5'-ATTCATATGATGATCACCCGCAGAGGGCTCT-3'
                  |||
3'-GCCCCTCAGCGACGACCGGGAGCTCTTA-5'
```

Max complementarity in discontinuous: 11 bp
```
5'-ATTCATATGATGATCACCCGCAGAGGGCTCT-3'
         |  | ||| |  ||| ||
       3'-GCCCCTCAGCGACGACCGGGAGCTCTTA-5'
```

Restriction analysis on HMC10_DyP_1
Methylation: dam-No dcm-No
Screened with 2 enzymes, 0 sites found
List by Site Order

Fragments generated by digestion (bp):
Linear DNA: 1131
Circular DNA:
Non-Cut Enzymes
*Nde*I *Xho*I

Forward Primer:
Length: 31
GC%: 48.4
MW (kD): 9.52
Melting Temperature (°C):
- Thermo: 74.2
- Hybrid: 60.4
- GC+AT: 92.0

Reverse Primer:
Length: 28
GC%: 67.9
MW (kD): 8.56
Melting Temperature (°C):
- Thermo: 81.2
- Hybrid: 66.3

- GC+AT: 94.0

CZH20 DyP3
Self-complementary: No self-complementary.
Two primers complementarity.
Max complementarity in continuous: 3 bp, free energy= 1.50 Kcal/mol
```
      5'-ATTCATATGGTGGCTGAGCGGAACGGACCG-3'
         |||
3'-CCCGTTAGTGACAAGCTCCGCGAGCTCTTA-5'
```

Max complementarity in discontinuous: 10 bp
```
5'-ATTCATATGGTGGCTGAGCGGAACGGACCG-3'
   ||   ||  ||| | ||
3'-CCCGTTAGTGACAAGCTCCGCGAGCTCTTA-5'
```

Restriction analysis on CZH20_DyP_3
Methylation: dam-No dcm-No
Screened with 2 enzymes, 0 sites found
List by Site Order

Fragments generated by digestion (bp):
Linear DNA: 1212
Circular DNA:
Non-Cut Enzymes
*Nde*I *Xho*I

Forward Primer:
Length: 30
GC%: 56.7
MW (kD): 9.34
Melting Temperature (°C):
- Thermo: 78.6
- Hybrid: 63.1
- GC+AT: 94.0

Reverse Primer:
Length: 30
GC%: 56.7
MW (kD): 9.17
Melting Temperature (°C):
- Thermo: 78.5
- Hybrid: 63.1
- GC+AT: 94.0

30-1
Self-complementary: No complementarity found.
Two primers complementarity.
Max complementarity in continuous: 4 bp, free energy=-4.80 Kcal/mol
```
 5'-ATTCATATGATGACCGGCAGGCGGGTGAGC-3'
           ||||
3'-AGCCGAGAGGTGACGAGCCGGAGCTCTTA-5'
```

Max complementarity in discontinuous: 9 bp
```
5'-ATTCATATGATGACCGGCAGGCGGGTGAGC-3'
   ||  |   || |  |||
 3'-AGCCGAGAGGTGACGAGCCGGAGCTCTTA-5'
```

Restriction analysis on 30-1
Methylation: dam-No dcm-No
Screened with 2 enzymes, 0 sites found
List by Site Order

Fragments generated by digestion (bp):
Linear DNA: 1218
Circular DNA:
Non-Cut Enzymes
*Nde*I *Xho*I

Forward Primer:
Length: 30
GC%: 56.7
MW (kD): 9.34
Melting Temperature (°C):
- Thermo: 78.6
- Hybrid: 63.1
- GC+AT: 94.0

Reverse Primer:
Length: 29
GC%: 62.1
MW (kD): 9.02
Melting Temperature (°C):
- Thermo: 79.6
- Hybrid: 64.7

GC+AT: 94.0

SUPPLEMENTARY SHEET B

Amplification of pET_DyP_ArticExpress_RP_CZH20^T and pET_DyP_ArticExpress_RP_30-1 using T7 primers.

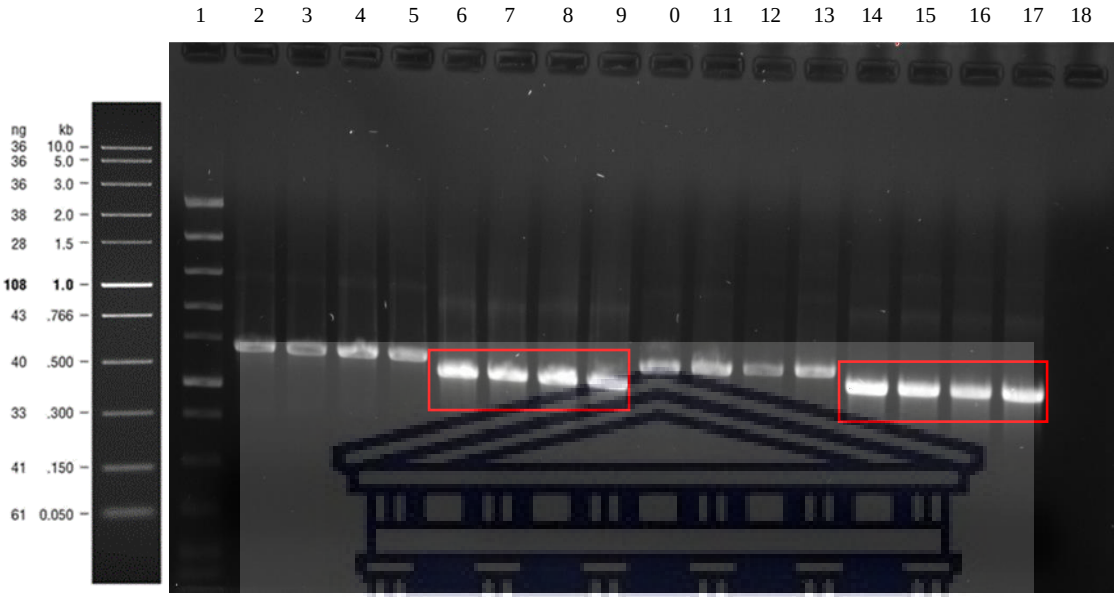

Figure B1: The amplification of pET_DyP_ArticExpress_RP_CZH20^T and pET_DyP_ArticExpress_RP_30-1 using T7 primers, highlighted in red.

Lane 1: Molecular FAST DNA Ladder (New England Bio Labs®); Lane 2-5: pET_DyP_ArcticExpress_RP_CZH20^T amplified with DyP-primers; Lane 5-9: pET_DyP_ArcticExpress_RP_CZH20^T amplified with T7-primers; Lane 10-13: pET_DyP_ArcticExpress_RP_30-1 amplified with DyP-primers; Lane 14-17: pET_DyP_ArcticExpress_RP_30-1 amplified with T7primers.

SUPPLEMENTARY SHEET C

Protein expression on small scale (25 mL) was optimised by testing the induction temperature at temperatures ranging from 15 °C, 25 °C, 30 °C and 37 °C of CZH20^{T}_DyP_AE and 30-1_DyP_AE in Auto Induction media. This was conducted to identify which temperature is the optimal for induction.

Table C1: The volumetric activity (U/mL); protein concentration (mg/mL) and the specific activity (U/mg) at 15 °C of CZH20^{T}_DyP_AE and 30-1_DyP_AE in Auto Induction media.

Sample Name	Volumetric Activity (U/mL)	Protein Concentration (mg/mL)	Specific Activity (U/mg)
CZH20^{T}_DyP_AE uninduced insoluble fraction	0.05867±0.0181	0.094	0.62216±0.075
CZH20^{T}_DyP_AE uninduced soluble fraction	0.03680±0.075	0.136	0.26371±0.047
CZH20^{T}_DyP_AE induced insoluble fraction	0.07001±0.042	0.088	0.79416±0.065
CZH20^{T}_DyP_AE induced soluble fraction	0.06067±0.062	0.130	0.46742±0.081
30-1_DyP_AE uninduced insoluble fraction	0.04433±0.098	0.092	0.48328±0.044
30-1_DyP_AE uninduced soluble fraction	0.03059±0.0116	0.135	0.22729±0.023
30-1_DyP_AE induced insoluble fraction	0.10630±0.054	0.095	1.1220±0.084
30-1_DyP_AE induced soluble fraction	0.52817±0.041	0.128	0.4120±0.091

Table C2: The volumetric activity (U/mL); protein concentration (mg/mL) and the specific activity (U/mg) at 25 °C of CZH20^{T}_DyP_AE and 30-1_DyP_AE in Auto Induction media.

Sample Name	Volumetric Activity (U/mL)	Protein Concentration (mg/mL)	Specific Activity (U/mg)
CZH20^{T}_DyP_AE uninduced insoluble fraction	0.0460±0.096	0.1133	0.4059±0.071
CZH20^{T}_DyP_AE uninduced soluble fraction	0.0261±0.075	0.1380	0.1893±0.078
CZH20^{T}_DyP_AE induced insoluble fraction	0.0650±0.041	0.1165	0.5577±0.022
CZH20^{T}_DyP_AE induced soluble fraction	0.02484±0.044	0.1327	0.1873±0.074
30-1_DyP_AE uninduced insoluble fraction	0.03418±0.077	0.1328	0.2573±0.041
30-1_DyP_AE uninduced soluble fraction	0.02951±0.089	0.122	0.2419±0.065
30-1_DyP_AE induced insoluble fraction	0.04942±0.061	0.1045	0.4729±0.089
30-1_DyP_AE induced soluble fraction	0.06801±0.022	0.1347	0.5049±0.064

Table C3: The volumetric activity (U/mL); protein concentration (mg/mL) and the specific activity (U/mg) at 30 °C of CZH20^{T}_DyP_AE and 30-1_DyP_AE in Auto Induction media.

Sample Name	Volumetric Activity (U/mL)	Protein Concentration (mg/mL)	Specific Activity (U/mg)
CZH20^{T}_DyP_AE uninduced insoluble fraction	0.0956±0.027	0.1579	0.6053±0.084
CZH20^{T}_DyP_AE uninduced soluble fraction	0.0990±0.041	0.1324	0.7480±0.076
CZH20^{T}_DyP_AE induced insoluble fraction	0.1263±0.025	0.1414	0.8933±0.061
CZH20^{T}_DyP_AE induced soluble fraction	0.1478±0.074	0.1150	1.2851±0.035
30-1_DyP_AE uninduced insoluble fraction	0.0562±0.056	0.1294	0.4339±0.047
30-1_DyP_AE uninduced soluble fraction	0.0422±0.011	0.1313	0.3215±0.084
30-1_DyP_AE induced insoluble fraction	0.1117±0.022	0.1255	0.8905±0.088
30-1_DyP_AE induced soluble fraction	0.1075±0.071	0.1213	0.8861±0.051

Table C4: The volumetric activity (U/mg); protein concentration (mg/mL) and the specific activity (U/mL) at 37 °C of CZH20^{T}_DyP_AE and 30-1_DyP_AE in Auto Induction media.

Sample Name	Volumetric Activity (U/mL)	Protein Concentration (mg/mL)	Specific Activity (U/mg)
CZH20^{T} _DyP_AE uninduced insoluble fraction	0.1102±0.087	0.1813	0.6077±0.084
CZH20^{T} _DyP_AE uninduced soluble fraction	0.0457±0.081	0.124	0.3684±0.077
CZH20^{T} _DyP_AE induced insoluble fraction	0.0993±0.045	0.1693	0.6133±0.036
CZH20^{T} _DyP_AE induced soluble fraction	0.0857±0.057	0.1446	0.5929±0.053
30-1_DyP_AE uninduced insoluble fraction	0.0956±0.062	0.1587	0.6026±0.061
30-1_DyP_AE uninduced soluble fraction	0.0435±0.055	0.1316	0.3309±0.047
30-1_DyP_AE induced insoluble fraction	0.1625±0.086	0.1685	0.9639±0.047
30-1_DyP_AE induced soluble fraction	0.1231±0.024	0.1358	0.9069±0.019

SUPPLEMENTARY SHEET D

All chromatograms in this section relates to the purification of pET_DyP_ArcticExpress_RP_CZH20^{T} uninduced SNF using the fast performance liquid chromatography (FPLC) using an AKTAprime™ system (Amersham-Biosciences). Purification was conducted with a flow rate at 0.8 mL/min and separated with 50 mM potassium phosphate buffer, pH 7.3. The peaks, highlighted in red, indicate the fractions that were subjected to SDS-PAGE analysis.

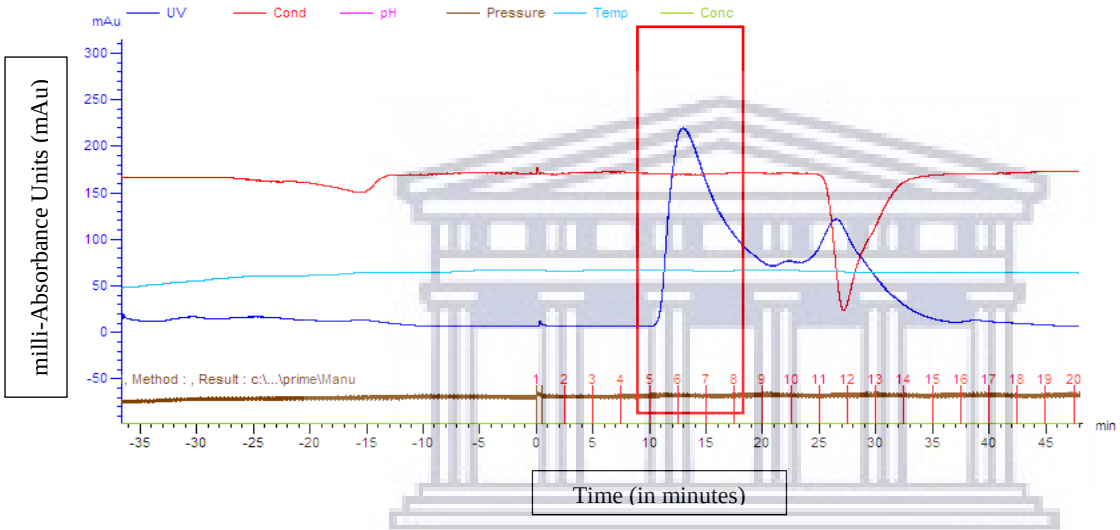

Figure D1: Chromatogram of the FPLC-purification of the CZH20^{T} DyP detected in the CZH20^{T}_DyP_AE_Auto Induction media soluble fraction (50 mM potassium phosphate buffer (pH 7.3) at a flow rate of 0.8 mL/min)

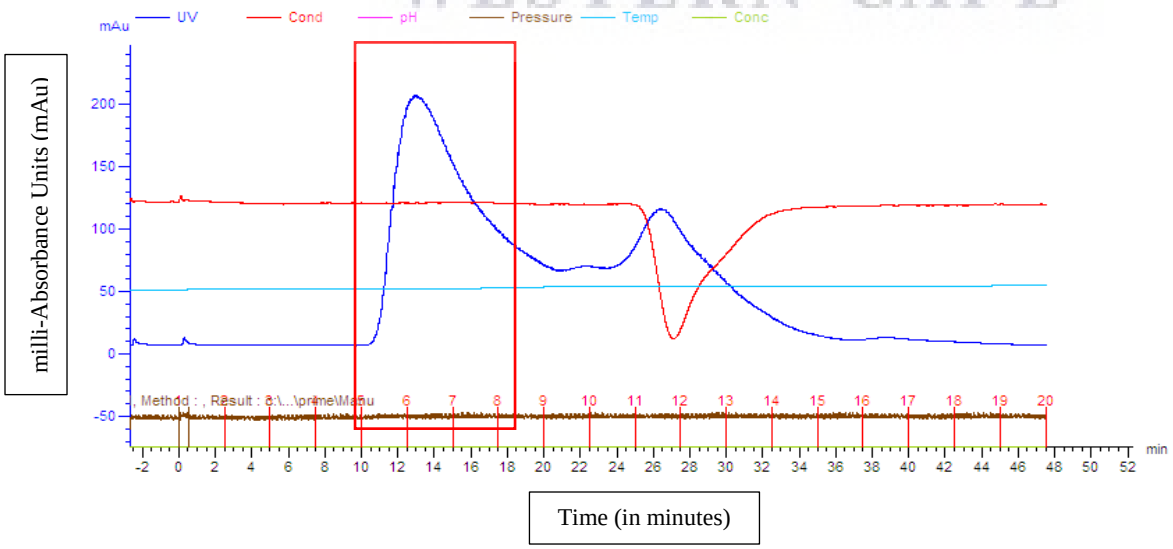

Figure D2: Chromatogram of the FPLC-purification of the CZH20^{T} DyP detected in the CZH20^{T}_DyP_AE_Auto Induction media soluble fraction (50 mM potassium phosphate buffer (pH 7.3) at a flow rate of 0.8 mL/min).

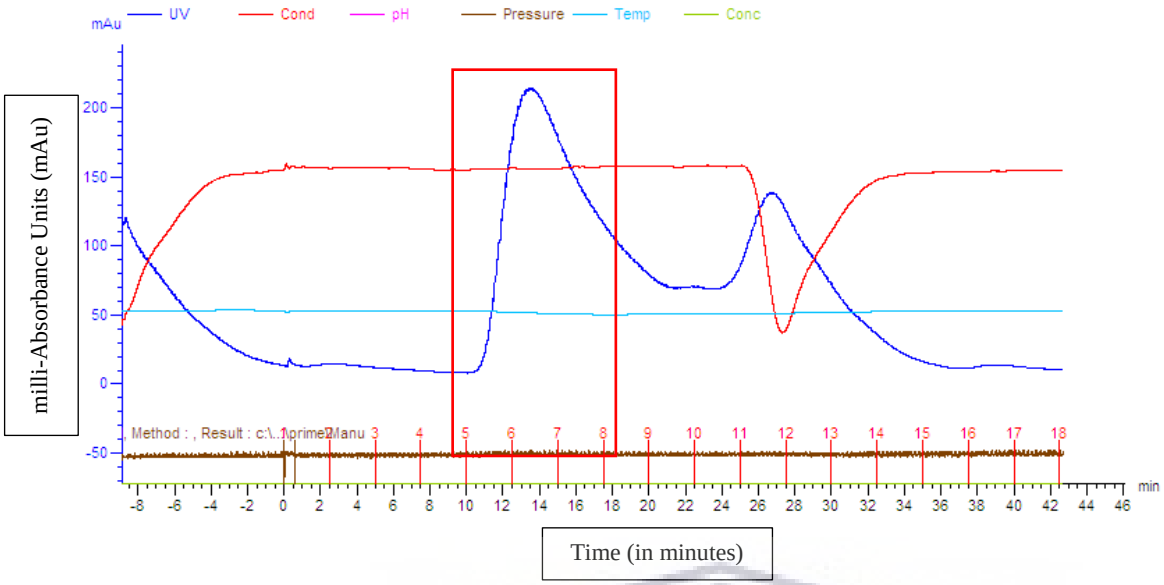

Figure D3: Chromatogram of the FPLC-purification of the CZH20^{T} DyP detected in the CZH20^{T}_DyP_AE_Auto Induction media soluble fraction (50 mM potassium phosphate buffer (pH 7.3) at a flow rate of 0.8 mL/min).

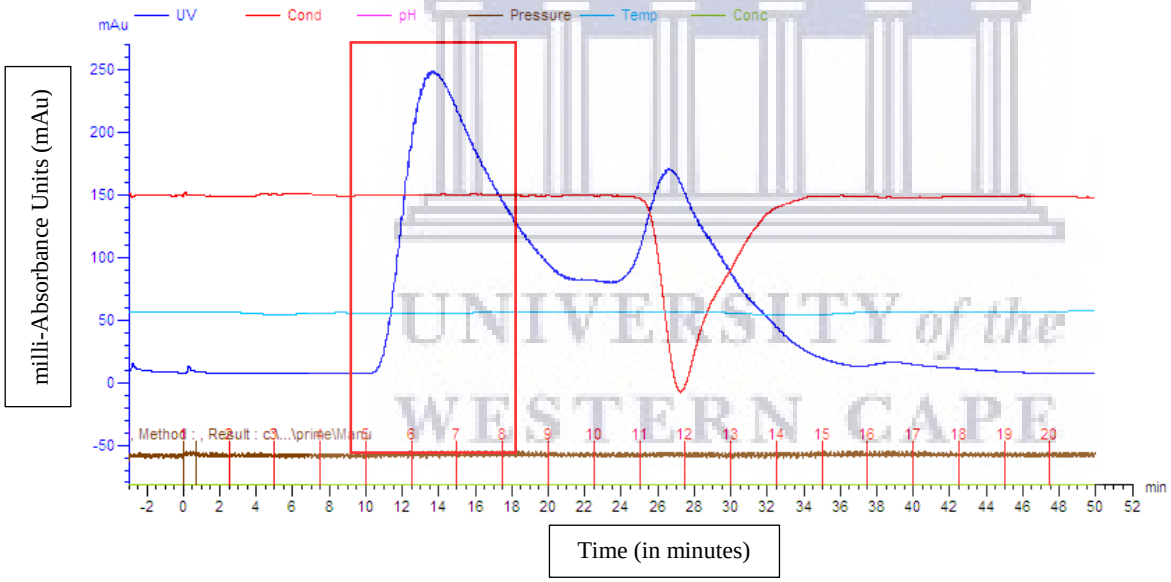

Figure D4: Chromatogram of the FPLC-purification of the CZH20^{T} DyP detected in the CZH20^{T}_DyP_AE_Auto Induction media soluble fraction (50 mM potassium phosphate buffer (pH 7.3) at a flow rate of 0.8 mL/min).